ASPECTS OF RETINAL AND OPTIC NERVE PATHOLOGY AFTER EXCITOTOXIC RETINAL INJURY

DR. SARABJIT KAUR SAGGU

Discipline of Ophthalmology and Visual Sciences
The University of Adelaide, South Australia

&

Division of Neuropathology
Institute of Medical and Veterinary Science
Adelaide, South Australia

A thesis submitted to the University of Adelaide in fulfilment of the requirements for the degree of Doctor of Philosophy

JUNE 2011

Chapter 1: INTRODUCTION

Excitotoxicity describes the process of neuronal death caused by excessive or prolonged activation of receptors for excitatory amino acid neurotransmitters. A large body of evidence supports the notion that excitotoxicity plays a role in the pathogenesis of certain neurological diseases, including central nervous system (CNS) ischaemia/stroke, Alzheimer's disease (AD), Huntington's disease, Parkinson's disease, Human Immuno-deficiency Virus [1] encephalopathy and motor neurone disease (MND).[2-12] Also, there is some evidence, albeit controversial, that excitotoxicity is involved in the pathogenesis of glaucoma, a chronic intraocular pressure (IOP)-sensitive optic neuropathy.[13, 14] Such neurological conditions are the leading causes of mortality and morbidity in the global population of 60 years of age and above.[15] In addition to the huge personal burden for individuals and families concerned, such diseases come at an immense economic cost to society. In Australia, in 2000-2001, conservative estimates for the combined direct costs of stroke, dementia and glaucoma totalled approximately 5 billion Australian Dollar (AUD).[16] Unchecked, these costs will escalate dramatically; hence, neurological diseases are a public health priority and effective treatments are urgently needed.

Most neuropathological conditions have traditionally been resistant to effective translational research but the recognition of excitotoxicity in the pathogenesis of severe debilitating CNS disorders has arguably provided one of the most successful strategies to date.[6, 9, 17-19] Clinical trials have shown that the low affinity, uncompetitive N-Methyl-D-Aspartate (NMDA) receptor antagonist, memantine, leads to functional improvement in AD patients with moderate to severe dementia.[19] Another anti-excitotoxic drug, riluzole has provided some clinical benefit to patients with MND.[17, 18]

Although an anti-excitotoxic treatment approach for CNS disorders has had some success, many aspects of excitotoxic injury still remain unclear. The mechanism of excitotoxicity in cell death has been widely studied.[20, 21] However, one aspect which has received little attention is the effect of perikaryal excitotoxic injury on the neuronal axon. Although the site of excitotoxic injury is principally at the level of the cell body (perikaryal), understanding the secondary effects on the neuronal axon is important because axonopathy is a documented early feature of these common neurological conditions; hence, an understanding of the pattern and mechanisms of secondary axonal degeneration after excitotoxic perikaryal injury could provide novel detection and treatment strategies in the early phase of neurological disease. The retina and optic nerve, as approachable regions of the CNS, provide a unique anatomical substrate to investigate the effect of perikaryal excitotoxic injury on the axon and associated glial tissue. The current study, therefore, focuses on various aspects of optic nerve pathology after excitotoxic injury to the retina.

The research aims primarily to explore the morphological and immunological changes in optic nerve axons secondary to intravitreal injection of NMDA into the rat eye. In this model, the neuronal cell bodies, retinal ganglion cells (RGCs), and the sites of toxic insult are physically isolated from the axons; hence, the observed axonal degeneration outside the eye is logically a consequence of the retinal injury. Because neuropathy models used so far have not made it clear where the primary site of insult is and what are the initial events in axon degeneration,[22-27] this NMDA model of RGC injury is well suited for providing information about the effect of perikaryal excitotoxic injury on axonal pathology.[28]

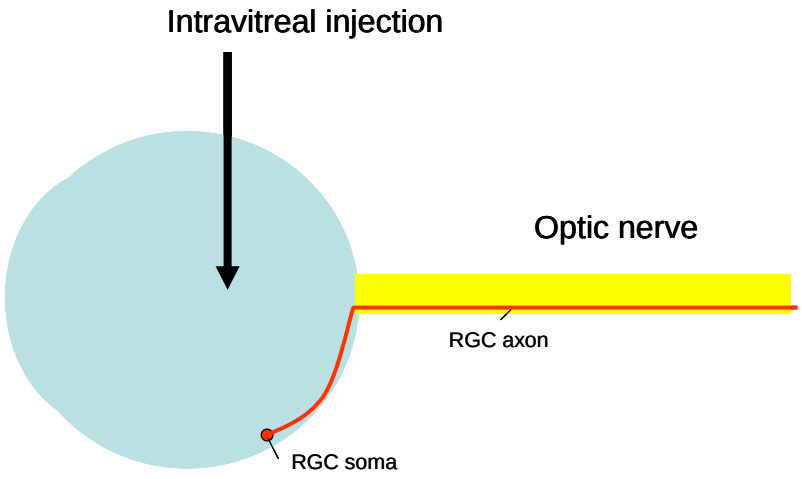

Figure 1. Schematic diagram of the excitotoxic injury model. Intravitreal injection of NMDA causes perikaryal RGC injury without primary injury to the axon.

During the study, damage to the optic nerve structure was examined by light microscopy (LM). This was followed by a detailed morphological assessment of nerve pathology under an electron microscope (EM). Changes in the axon transport system and glial cells were also revealed by immunohistochemistry. Pathological changes in the optic nerve were compared to the retinal damage. All methods used were easily reproducible and were based on the application of standard procedures with some modifications in a planned manner.

Results from this study will improve our understanding of the mechanism of optic nerve degeneration secondary to excitotoxic perikaryal RGC injury. As the study will elucidate aspects of axonal degeneration after exclusive excitotoxic insult to the perikaryon, this will potentially improve our understanding of all chronic neuropathological conditions of brain where excitotoxicity plays a major role.[8]

Subsequent chapters of the thesis will provide background information, aims and objectives of the study, and describe materials and methods used in this study. This will be followed by the

results, which are divided into different sections: light microscopy (LM), electron microscopy (EM), TUNEL staining of the retina, changes in axon transport and glial cells as revealed by immunohistochemistry. Each result section contains subsections describing changes in the retina and the optic nerve. Conclusions and future implications of this study are discussed.

Chapter 2: BACKGROUND RATIONALE

2.1 Definition of topic

'Nerve pathology' is defined as loss of functional activity and trophic degeneration of axons following destruction of their cells of origin (somagenic death) or interruption of their continuity with these cells (axogenic death). It characterizes neurodegenerative conditions. When applied to the optic nerve, this means functional and structural damage to the optic nerve axons following RGC injury or direct optic nerve damage.

'Optic nerve pathology' is a fairly common term used in the past in ophthalmologic glossary;[29, 30] however, it remains of much importance to clinical ophthalmologists, who define it as 'conditions involving retina and optic nerve, which result in partial or complete loss of vision'. In ophthalmic research, most studies are either widely based on less clinically relevant axotomy models, where the optic nerve is physically transacted [31, 32] or in eye conditions characterized by progressive RGC loss such as glaucoma.[33-36] It is quiet surprising that in all such studies, the so called optic nerve 'pathology' has never been thoroughly studied from pathological point of view. Because there are enough pointers to the role of excitotoxicity in RGC death in the common blinding condition, glaucoma,[13, 14] the current pathological study of optic nerve degeneration after excitotoxic retinal injury is justified. The concept can effectively be applied to any neurological condition that involves neuronal loss due to excitotoxicity.

2.2 Relevant Anatomy

2.2.1 Eyeball and Retina

During the visual process, light rays pass through the transparent cornea and optical media to fall on the light-sensitive sensory retina, which is situated on the inner surface of the posterior segment of the eye. The retina converts visual stimuli into electrical impulses, which then reach various centres in the brain through the optic nerve pathway. As retina is derived from the neural tube, like other parts of the CNS, it forms an ideal region of the brain to study CNS pathology.

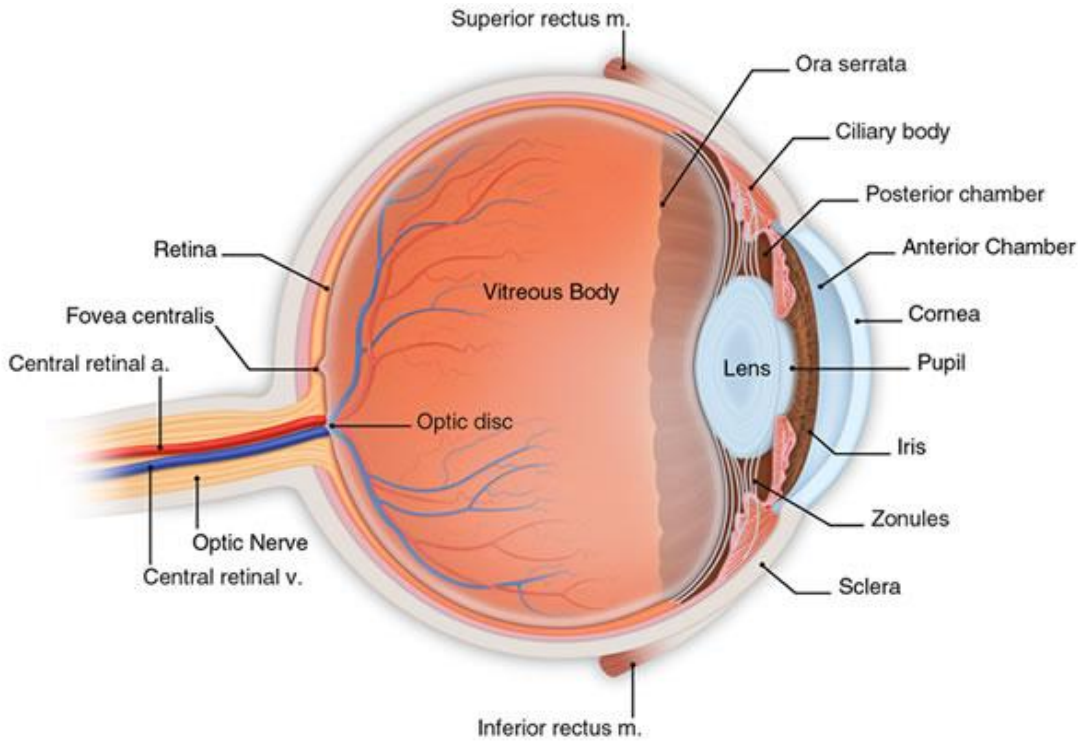

Figure 2. Sagittal section of the eyeball showing the main structures in the anterior and posterior segments.

2.2.1.1 Microscopic structure of the vertebrate retina

Observed under LM,[37] vertebrate retina is composed of the following ten layers: 1) *Pigment layer* separating the neural retina from choroid 2) *Photoreceptor layer* containing outer and inner segments of the photoreceptor cells 3) *Outer limiting membrane* (OLM) 4) *Outer nuclear layer* composed of the cell bodies of photoreceptor cells 5) *Outer plexiform layer* (OPL), formed by synapses between photoreceptor cells and nerve cell processes of cells located in the 6) *Inner nuclear layer* (INL), which contains horizontal, bipolar, amacrine and a few Müller cells *7) Inner plexiform layer* (IPL) convey the sensory input from the bipolar cells across the synapses to 8) *Ganglion cell layer* (GCL) containing ganglion cells and displaced amacrine cells 9) *Inner nerve fibre layer* (INFL) formed by axons of ganglion cells and finally, 10) *Inner limiting membrane* [38], which corresponds to the basal lamina formed by the Müller cells.

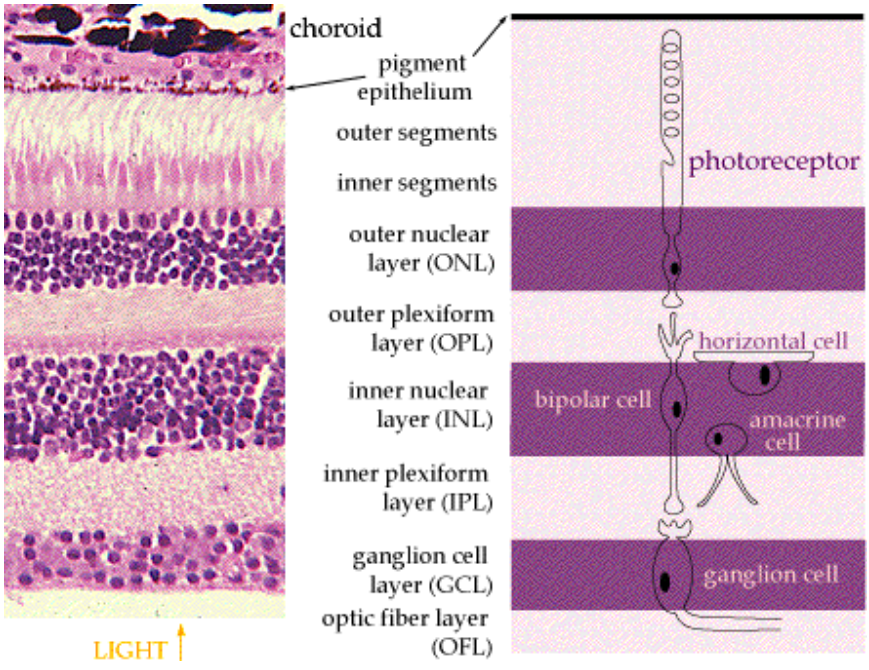

Figure 3. Histology of the normal retina. Section from the posterior pole of a normal retina (left) stained with Haematoxylin & Eosin (H&E). The corresponding diagram on the right shows the predominant cell type in each layer.

2.2.2 Optic Nerve

The optic nerve is the second cranial nerve formed by the collection of axons arising from the RGCs. It begins at the optic disc (optic nerve head), where the ganglion cell axons after running in the inner nerve fibre layer pass through a sieve-like structure in the posterior pole of the sclera called the lamina cribrosa. The nerve then runs backwards in the orbit surrounded by three meningeal layers, extraocular muscles and other retro-orbital tissue (intraorbital part) to enter the middle cranial fossa (intracranial part) passing through a small bony canal at the apex of the orbit (intracanalicular part).

Once inside the cranium, optic nerve fibres enter a cruciate structure called the optic chiasma. Here, fibres from the nasal half of the retina cross and run in the optic tract with the temporal fibres of the opposite side to end in the lateral geniculate body in different strata. Finally, optic radiations, which contain second order neurons arising from the lateral geniculate body relay in the visual cortex located in the occipital lobe.

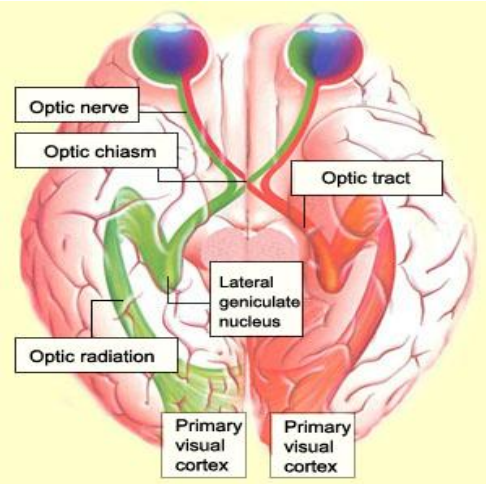

Figure 4. Schematic representation of the visual system. Diagram shows the course of optic nerve fibres as they emergne from the eyeball and run into the optic nerve, optic chiasm, optic tract to end in the lateral geniculate body. Second order order neurons from the lateral geniculate body ends in the primary visual cortex.

Histology of the optic nerve

Histologically, the optic nerve is surrounded by three meninges: dura, arachnoid and piamater. Septae arising from the innermost adherent piamater divide the nerve into fascicles or bundles, with each fascicle containing numerous nerve fibres supported by glial cells. These septae guide blood vessels to the nerve fibres. Although in anatomical continuity, the microscopic structure of the optic nerve fibres is quite different from that in axons running in the INFL. Intraretinal RGC axons are unmyelinated and show mitochondria-rich varicosities;[39] whereas the axons become heavily myelinated to become optic nerve fibres in the postlaminar region. Because the structure of the optic nerve consists of myelinated neurons and other neuroglial cells, further description of the histology needs elaboration of the basic structure of a myelinated neuron as well as neuroglial cells.

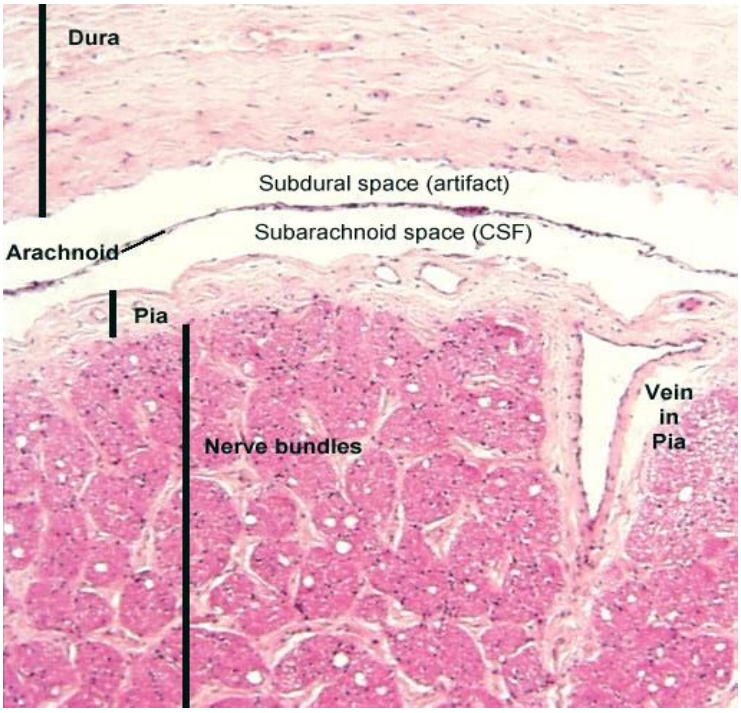

Figure 5. Histological appearance of transverse section of optic nerve.

2.2.3 Characteristic features of the albino rat visual system

The retina

Rat is a nocturnal animal with an effective and highly developed visual system. The GCL contains not only the ganglion cells, but also many displaced amacrine cells.[40] RGCs in GCL can be grouped according to their cell size; small (7-10μm diameter), medium (11-14μm diameter) and large (15-23μm diameter).[41] Huxlin and Goodchild also classified RGCs into three groups according to the cell and dendritic field size, with group A cells having large somata and large dendritic tree, group B cells having small somata and small dendritic tree and group C cells having small to medium somata and medium to large dendritic tree.[42]

The total number of RGCs in the retina is estimated to be approximately 10^5 with the density of cells varying between the central (near the optic disc) and periphery (near the ora serrata) retina.[41] This centro-peripheral distribution ratio (5:1) is seen in all rats after 11^{th} postnatal day.[43] The density of RGCs does not vary between different quadrants.[44]

The optic nerve

In the albino rat each optic nerve contains approximately 10^5 nerve fibres.[45, 46] More than 99.5% fibres are myelinated [47] and the mean diameter of the myelinated axons is reported as 0.59-0.65μm.[45, 46] Although the total cross-sectional area of the albino rat optic nerve is one-third of that of the pigmented rat, the fibre density is 1.4 times with each fiber having much thinner myelin sheath than them.[47] Based on the temporal degeneration in the fibres projecting in the lateral geniculate body, Lund et al suggested

the presence of three types of fibres in the optic nerve.[48] However, no characteristic features have yet been reported to differentiate them.

2.3 Morphology of the neuron

The neuron is the functional and morphological unit of the nervous system, specialized in receiving, integrating and transmitting information in the form of electrical impulses. Generally, a neuron consists of a cell body containing nucleus and numerous processes. Small tapering, twisting, and branching processes, called dendrites or cellulipetal processes, conduct impulses toward the cell body; whereas, the axon or somatifugal process, which is smooth and relatively straight, convey signals away from the cell body.[49] They do not usually branch or form synaptic contact before termination. They may or may not acquire myelin sheath, thereby, termed myelinated or unmyelinated. According to anatomical and functional characteristics of the cell processes, optic neurons are sensory neurons, with RGCs symbolizing the somata and the optic nerve fibres representing the myelinated axons.[50]

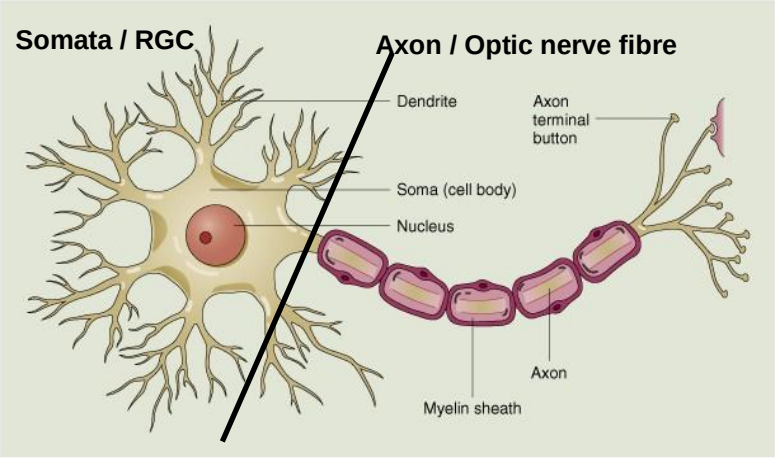

Figure 6. Schematic diagram of a typical myelinated neuron representing RGC system.

2.3.1 The neuronal cell body

The cell body or somata carries out all major biological processes in addition to supporting the specialized function of impulse transmission. Similar to other eukaryotic cells, a nerve cell body comprises a nucleus and the cytoplasm enclosed by a cell membrane.

2.3.1.1 Nucleus

Typically, neurons contain a large and spherical or slightly ovoid nucleus located centrally in the cell body. The nucleus is surrounded by a double membrane nuclear envelope, which separates the karyoplasm from the cytoplasm and control the movement of molecules across it. Although the structure of the nuclear envelope is believed to be similar to those of other cells, the karyoplasm of neurons is clear/ vesicular because of lack of chromatin particles. It contains one or more extremely dense, roughly spherical free nucleolus, carrying ribonucleoprotein in the form of tightly packed dense granules and fine filaments. The nucleus may contain intranuclear inclusions in the form of rods, small dense bodies and, sheath of filaments.[51]

2.3.1.2 Perikaryon

The part of the cytoplasm surrounding the nucleus is referred to as 'perikaryon'. It is filled with numerous filamentous, membranous and granular organelles. *Mitochondria* are oval-shaped structures lined by a double layered lipid membrane, the inner one folding to form shelf-like extensions known as cristae. They generate energy in the form of Adenosine triphosphate (ATP) by aerobic metabolism of nutrients. *Endoplasmic Reticulum (ER)* (predominantly agranular), a system of parallel and folded membranes, is the site for synthesis of lipid and protein molecules required for the maintenance of membranous structures including neuronal processes. The *Golgi complex / Golgi apparatus* is a network

of stack of membranes that wraps the protein molecules in sacs or vesicles for storage, and eventual transport to the plasma membrane. *Neurofibrils* (microtubules and neurofilaments) are slender interlacing threads coursing the perikaryon from one cell process to another. Other cytoplasmic structures include multivesicular bodies, lysosomes, peroxisomes, chromophilic Nissl bodies composed of granular ER and clusters of free ribosomes, lipofuscin granules, and inclusion bodies.[51]

2.3.2 Dendrites

Dendrites possess characteristically irregular shapes and are rich in microtubules. At the origin, their cytoplasm contains similar organelles as the neuronal perikaryon, such as the microtubules, mitochondria, agranular ER, Nissl bodies, golgi apparatus and neurofilaments. Most of structural elements orient themselves longitudinally and gradually disappear as they run along the dendrite. Fine microtubule-associated proteins (MAP) connects microtubules, the most prominent dendritic structures, to each other as well as other organelles.[52]

2.3.3 The Axon

The vertebrate neurons are classified as Golgi type I and type II, according to the length and projection of their axons.[53] In the former, the axons run for long distances to connect different parts of the nervous system and are myelinated, except for some length from their origin, the regions called the axon hillock and the initial segment.[54] In contrast, axons of Golgi type II neurons project locally and are unmyelinated. Based on this classification and anatomical details of the optic nerve, optic neurons are a classic form of Golgi type I neurons.

2.3.3.1 The Axon Hillock and the Initial Segment

In myelinated neurons, the funnel-shaped projection of the perikaryon from which the axon originates is called the axon hillock. Much thinner part of the axon between the hillock and the myelin acquisition is the initial segment. Unmyelinated RGC axons in the inner nerve fibre layer, pre-laminar and laminar regions represent the initial segment of the optic neurons until they acquire the sheath of myelin in the postlaminar region to become a typical axon.

The hillock can be identified by the cone-shaped orientation of the microtubules and neurofilaments and lack of Nissl bodies. The initial segment is characterized by the presence of a dense granular layer under the axolemma, longitudinal arrangement of filamentous structures, dense appearance of microtubules as they run in fascicles, and gradually diminishing free ribosomes, granular endoplasmic reticulum, and golgi apparatus.[55] Remaining structures including the neurofilaments, agranular ER, mitochondria and multivesicular bodies pass into the axon unchanged.[53, 55]

2.3.3.2 The Axon Proper

An axon contains a gel-like cytoplasm (axoplasm) surrounded by the plasma membrane called axolemma. Although, the morphology of the axolemma is similar to the cell membrane of the cell body, it is studded with multiple ion channels, which maintain the membrane potential and determine the passage of self-propagating depolarization waves.[53] The axoplasm contains cytoskeletal components (neurofilaments, microtubules and microfilaments) and longitudinally disposed membranous organelles, which include agranular ER, mitochondria, and multivesicular bodies.[56, 57] However, it lacks

ribosomes, granular ER and Golgi apparatus and thus, depends on a specialized transport system for the protein supply.[53, 55]

Neurofilaments are intermediate filaments forming the most important structural component of mature neurons. They are 10nm thick tubular structures with an empty core and a dense wall made up of heteromers composed of light (NF-L, 68k Da) and medium (NF-M, 150kDa) or heavy (NF-H, 200 kDa) polypeptide subunits.[58] They form important space-occupying cytoskeletal elements, which determine not only the shape and structure of axon,[59, 60] but also play a major role in their growth and maintenance.[61] *Microtubules* are fewer, 20-26nm diameter tubular structures with a clear lumen (except a central dot) surrounded by a 6nm thick wall made of helically arranged globular subunits, α and β-tubulins.[62] Microfilaments are 5-9nm diameter solid rods composed largely of a protein called actin.[62] In addition to the formation of cytoskeleton, all the above-mentioned tubulo-filamentous structures play an important role in transport of proteins and organelles to and from the axon, details of which are described later.

2.3.4 The Myelin

In a myelinated nerve, axons are surrounded by an interrupted electrically insulating lipid-laden compact sheath called the myelin. Discovered in 1854 by Rudolf Virchow,[63] myelin is a multi-spiral sail-like extension of the plasma membrane of specialized glial cells (Oligodendrocytes in CNS and Schwann cells in PNS). Most CNS axons of more than 0.2μm are myelinated,[64, 65] including the axons in the optic nerve of an adult rat.[66]

A maturing axon acquires its full length of myelin by a process called myelination. Myelin synthesis is initiated by an unidentified signal, which stimulates mature and differentiated

oligodendrocytes to send multiple, narrow, tortuous, finger-like protoplasmic projections to tightly wrap around segments of numerous axons in the form of concentric lamellae.[54, 67, 68] This brings the intracellular and extracellular surfaces of the cytoplasmic membrane in apposition, which appear as alternate layers of protein-rich electron-dense 'major dense lines' and lipid-rich lighter 'intraperiod lines' of myelin on electron microscopy and X-ray diffraction studies.[69, 70]

A.

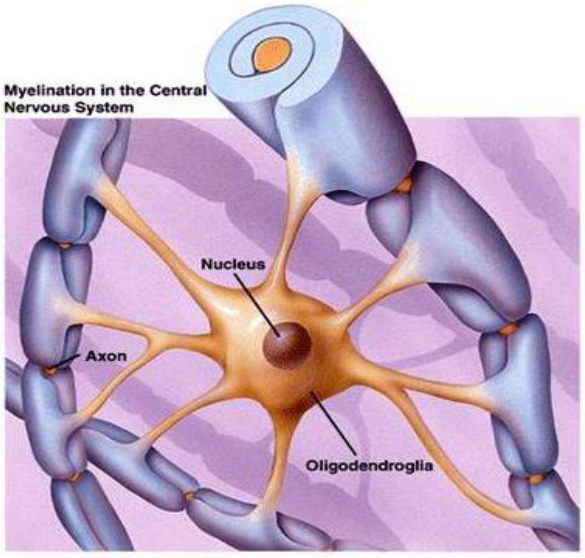

B.

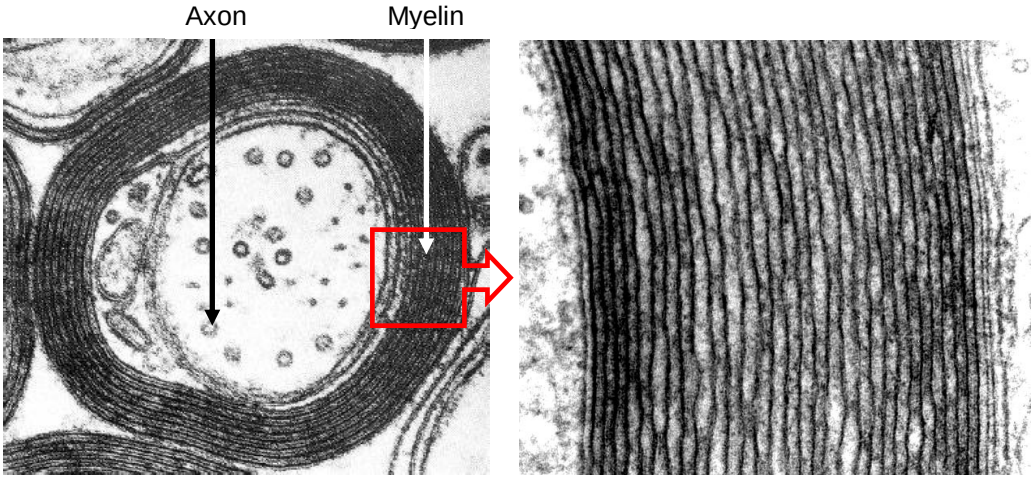

Figure 7. A). Schematic diagram showing the process of myelination in the CNS. B) Electron microscopic appearance of myelin showing alternate major-dense and intraperiod lines

The myelin, unlike other biological membranes, has a high proportion of lipid (75-80%) and low proportion of proteins (15-30%).[71] Its characteristic composition makes the depolarization wave skip from one node to another node (saltatory conduction) without travelling through the whole length of the axolemma.[72]

Myelin sheath is important for the maintenance of structure and function of the axon. The process of myelination determines the axonal growth and maturation [73] and defective myelin formation results in decrease in the density and phosphorylation of neurofilaments with a reduction in axon calibre and slow axonal transport.[74, 75] In addition, the myelin establishes specific relationship to axolemma in different domains of axons, which is essential for the development and maintenance of mature neurons.[76, 77]

2.3.5 Axo-glial relationships and domains of a myelinated axon

Based on the relationship between the axon and the myelin, the axon is divided morphologically into four domains. The part of the axon which remains uncovered by the myelin is called the node of Ranvier, in honour of Ranvier who in 1878 described these nodes as periodic annular constrictions (*etranglements annulaires*). Between the adjacent nodes lies the region called the internode, in which the myelin surrounds the axon as compact concentric lamellae of alternate light and dark bands. Near the margin, the myelin lamellae separate to enclose the cytoplasm filled loops called myelin terminal loops (MTLs). The part of axon that lies in relation to the MTLs is called the paranode. Here, MTLs form septate-like junctions in close apposition to the axolemma and wind spiraly around it. They gradually recede in a step-like fashion giving this domain a characteristic 'herring-bone configuration'. The most peripheral part of the internode, which lies just adjacent to the paranode, is called the juxtaparanode.[78]

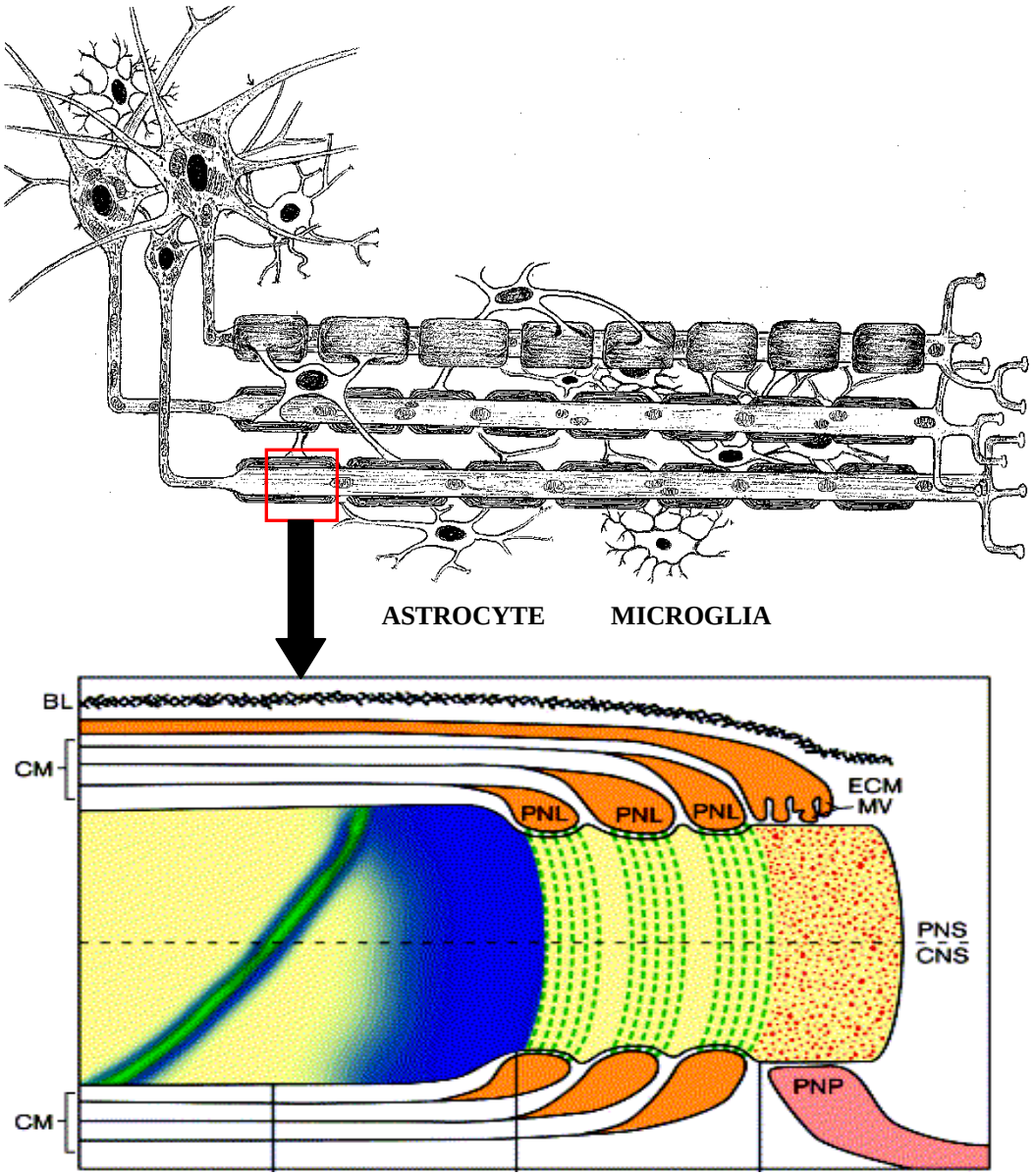

Figure 8. Longitudinal domains of myelinated axons.Longitudinal section through the nodal region showing the relationship of myelin in various domains of axons in the PNS (top half) and CNS (bottom half). In the PNS, the axon is myelinated by a Schwann cell that is surrounded by a basal lamina (BL); in the CNS, myelin is formed by oligodendrocytes. (Modified from source- Peles E, Salzer JL. Molecular domains of myelinated axons. Current Opinion in Neurobiology 2000;10(5):558-565)

Multiple protein molecules present in different domains impart specialized function to each domain.[78-81] The nodal axolemma contains a high density of voltage-gated Na^+

channels, isoform Nav1.6, which together with Na^+-K^+ ATPase cause inward current flow during normal action potential.[82-84] In the paranodal region tight axoglial junctions formed between the axonal (Caspr-1/paranodin, contactin) and glial adhesion (neurofascin-155) molecules [85-90] demarcate axonal domains by limiting the lateral diffusion of membrane components.[91, 92] This prevents ectopic impulse propagation and the leakage of action currents into the internodal periaxonal space by retaining Nav1.6 in the node.[93] Disruption of this barrier, as occurs in the absence of myelin components (galactolipids and glycoproteins), disturbs the nerve function.[94-97] The juxta-paranode region can be considered a specialized part of internode, which is rich in large sized delayed rectifier K^+ channels promoting repolarization, maintaining internodal resting potential and preventing ectopic impulse propagation.[98, 99] Therefore, normal axo-glial relationships and organization of multi-protein/molecular complexes in various axonal domains are important to maintain the structural and functional integrity of the neuron. Defective synthesis, transport and organization of these molecules may result in anomalous morphologic organization of axo-glial region [97] and more diffuse distribution of Na^+ and K^+ channels, manifesting clinically as significant conduction disturbances and pathologically as nerve degeneration.[97, 100]

2.4 Glial cells in the CNS

Nonneuronal cells related intimately to neurons are called glial cells. First described by Virchow in 1846 as “nerve-glue”, they are the supporting cells that form connective tissue of the nervous system, including the retina and the optic nerve. Based on the light microscopic examination of tissue stained by various metallic impregnation methods, Ramon y Cajal & Rio Hortega (1913-1921) classified glial cells as oligodendroglia,

astroglia and microglia. While the optic nerve contains all three types, glial cells of the retina include Müller cells, astrocytes and microglia.[101]

2.4.1 Oligodendrocytes

Oligodendrocytes (also known as Oligodendroglia) are small spherical cells with few long, thin and delicate microtubule-rich cell processes. Their cytoplasm is rich in mitochondria, granular ER, golgi apparatus, polyribosomes and lacks in intermediate filaments and glycogen. Their nuclei are small, regular and contain dense chromatin. The development, growth and survival of oligodendrocytes is regulated by axonal signals in the forms of growth factors called neuregulins.[102, 103] These axonal factors, bind to the epidermal growth factor (EGF) receptors of progenitor cells,[104] which pass through the stages of late progenitor to immature cell stage to finally become mature differentiated oligodendrocytes.[105, 106]

Based on their location in relation to neurons, oligodendroglia are classified as 'satellite oligodendrocytes' and 'interfascicular oligodendrocytes'.[37] The former lie in close association with the cell bodies of the neurons and the later as their name suggest, lie aligned in rows between the nerve fascicles. While satellite cells provide nutritional support to neurons,[107, 108] interfascicular cells express genes encoding myelin proteins, fatty acid and cholesterol biosynthesis so as to form myelin sheaths around the axons (refer section 2.3.4). Specific association of lipid rafts of myelin with axolemma [109] help in the establishment of proper axoglial contacts and control of axon growth. Besides the above mentioned functions, oligodendrocytes express genes required for maintaining cell cytoskeleton/structure and genes regulating cell adhesion [110, 111]. Thus,

oligodendrocytes not only maintain their own cell structure,[112] but also regulate the structure and function of neurons.

2.4.2 Astrocytes

Astrocytes (also known as Astroglia) are medium-sized star-shaped oval or spherical cells which form a supporting framework for neurons. Their cytoplasm is rich in mitochondria (gliosomes), glycogen granules and glial fibrillary acidic protein (GFAP) rich fine gliofilaments, which extend into their multiple long protoplasmic processes. The expanded terminations of astrocytic processes, called as 'end-feet', encircle the endothelial cells to form part of the blood-brain barrier (BBB).[37] This barrier prevents influx of toxins into the CNS. Besides providing physical support to the neurons, astrocytes also provide metabolic support, regulate local concentration of neurotoxins, modulate extracellular concentration of ions (K^+) and play a pivotal role in neuroimmunology.[101, 113-115]

Based on their location, astrocytes are classified into two main types.[See Figure 9] Present in relation to the nerve fibres such as in optic nerve, 'fibrous astrocytes' possess long processes with thick bundles of gliofilaments. 'Protoplasmic astrocytes' showing extreme branching, are found in relation to the axon terminals, dendrites and synapses. Retinal astrocytes are mainly of protoplasmic variety. While both elongated and star-shaped astrocytes are found throughout the retina,[116] a special variety of protoplasmic astrocytes called 'Müller cells' span radially across the retina, their endfeet forming the inner and outer limiting membranes.[101]

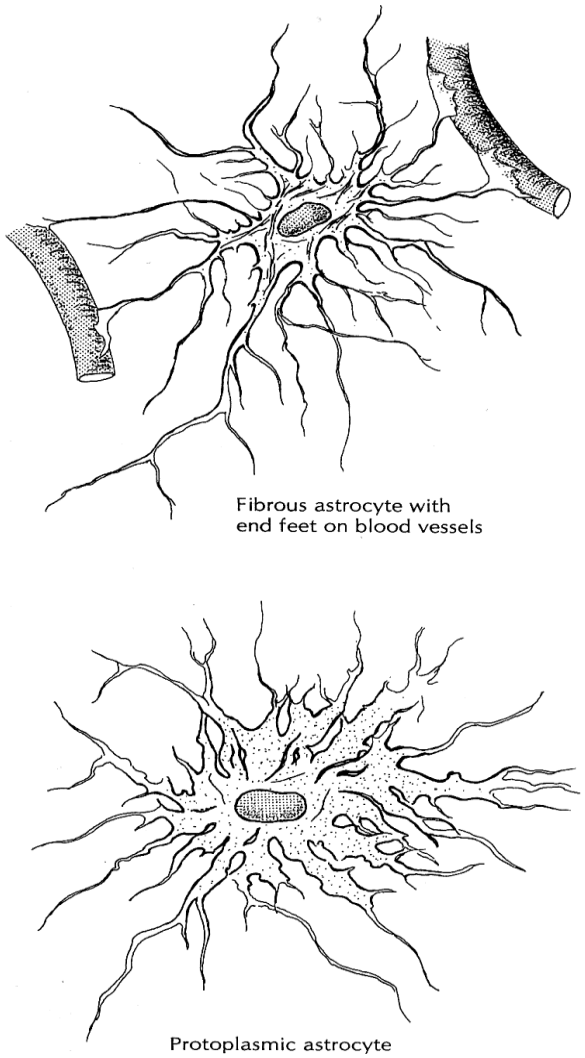

Figure 9. Types of astrocytes in the Central Nervous System

2.4.3 Microglia

Microglia are the smallest glial cells constituting 10-20% of the total glial cells of CNS. They represent the innate immune system in the brain. They act as phagocytes and protect the brain from the invading micro-organisms. They form a first line of defence in response to neuronal death.[117] These are derived from myeloid progenitor cells (as are macrophages and dendritic cells) which come from the bone marrow. During embryonic development, they migrate to the CNS to differentiate into microglia.

There are mainly three types of microglial cells- amoeboid, ramified and reactive. The round 'amoeboid' variety, possessing pseudopodia and thin filopodia–like processes [118, 119] is phagocytic in nature and their main function is to remove inappropriately growing axons during CNS development.[120] Postnatally, amoeboid cells change into small round non-phagocytic 'ramified' or 'resting' microglia possessing numerous branching processes, which maintain the microenvironment of the tissue by removing the metabolites and toxic factors released from the surrounding cells.[121, 122] Under pathological conditions, such as trauma, stroke or any inflammation-mediated degeneration of the central nervous system, the resting microglia proliferate and change their shape to become rod-shaped 'activated microglia', which possess numerous lysosomes and phagosomes and release pro-inflammatory and neurotoxic factors such as cytokines, eicosanoids, reactive oxygen species (ROS), and nitric oxide.[123] The process of activation of these glial cells is termed as 'reactive gliosis'.[124]

2.5 Axonal transport

Neuron is an asymmetrical cell with the soma sending out and sustaining nerve cell processes. This is especially important for axons because they lack the ability to synthesize proteins, lipids, organelles or synaptic neurotransmitters required for maintaining their structural integrity and functional viability. These molecules and organelles are synthesized in the soma and conveyed to axon terminals by an active axonal transport system. Therefore, axons depend not only on soma for the synthesis of its' material, but also on specialized axonal transport system for transfer of this material in very lengthy axons. Two types of transport systems in axons are: 'Fast' and 'Slow'.

2.5.1 Fast Axonal Transport

Fast axonal transport is a two way system- anterograde and retrograde. Anterograde transport occurs towards the axon terminal or plus-end of the axon, with the speed of several μm/sec to up to 400mm/day. It is crucial for neuronal survival because it transports vesicles containing lipids and proteins for constitutive renewal of axonal membrane, synaptic vesicles containing neurotransmitters and enzymes required for their activation, mitochondria, lysosomes and other tubulovesicular membranous organelles.[125, 126]

Retrograde transport conveys material from the axon terminal towards the cell body or minus-end of axon, with 30-60% slower velocity than the anterograde system. Transported material mainly includes used-up material in the nerve terminal for recycling such as degraded vesicular membranes.[127] It also contains signalling molecules secreted by post-synaptic neurons which are taken up by terminal endocytosis to act as messengers or regulatory substances of pre-synaptic neurons. Moreover, activated receptors, natural toxins and viruses as well as experimental horseradish peroxidise (HRP) tracers reach somata by this system.

Fast axonal transport is a microtubule-dependent movement performed by the motor proteins kinesin and dynein.[128] Kinesin family proteins form an anterograde motor system transporting synaptic vesicles, mitochondria, and coated vesicles towards the plus-end of the microtubules (axon terminal), whereas, dynein transfers material retrogradely towards the minus-end.[126, 129-131] Motor transport carry cargo material over microtubule for long distances in axons except in areas where microtubules are lacking,

such as in axonal tips, where myosin-driven actin filaments take over the transport function.[132, 133]

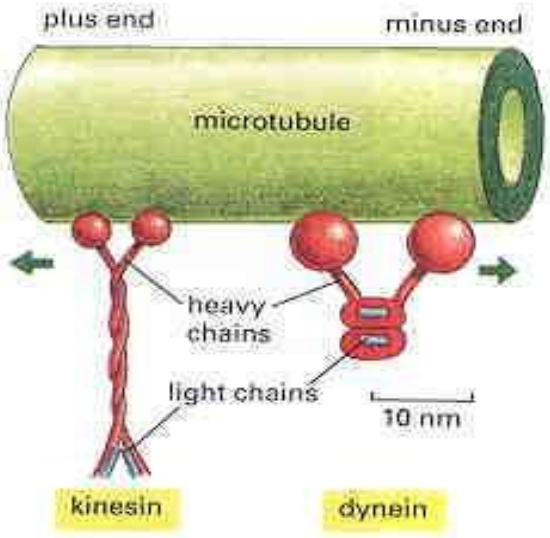

Figure 10. Motor proteins involved in fast axonal transport.

2.5.1.1 Mechanism for anterograde transport

Kinesin is a highly elongated molecule, about 80nm in length, with a heterotetrameric structure comprising of two globular heavy (124 kDa) and two fan-shaped light (64kDa) subunits [See Figure 10].[134-138] Electron microscopy and DNA-sequence analysis reveals the heavy subunit to be comprised of three parts:

a. Head, which is a 10 X 9 nm globular N-terminal domain of 50kDa, carrying 340 amino acids including an ATP-binding and a microtubule-binding domain.
b. Neck, a 50-60kDa rod-like domain, which has the ability to form a stable α-helical coil.
c. C-terminal domain, which binds to the light subunit and other proteins.[135, 136, 138-142]

During transport, receptor (kinectin) on the membrane-bound organelles attaches to the light subunit of kinesin, with the head of the kinesin heavy subunit attaching to the microtubules.[143, 144] One head from each heavy subunit dimer interacts with tubulin forming the microtubule protofilament, with the other unattached head pointing towards the plus-end of the microtubule.[145] All attached heads of kinesin molecules are similar, unlike free heads which have variable compositions, confirmations and orientations.[146] Difference in orientation of attached and free heads is because of dissimilarities in neck and head-neck junctions of both dimers.[147] On binding to the microtubule, ATPase activity in the heavy head region is enhanced and adenosine diphosphate (ADP), so formed, is rapidly removed by microtubules.[148-151] Rapid dissociation of ADP-kinesin from the microtubules and confirmational changes in the kinesin motor domains and microtubule protofilaments produced by the released energy translocate kinesin molecule quickly over microtubules.[152-154]

Other non-kinesin mechanisms also operate in the axon to maintain fast retrograde transport. An ATP-dependent, myosin-driven, actin-based motor system is one such transport mechanism.[155, 156] Also, there is indirect evidence available to show that a few other low molecular weight, GTP-binding proteins might be involved in fast axonal transport of organelles.[157, 158]

2.5.1.2 Mechanism for retrograde transport

The motor protein assigned the task of fast retrograde axonal transport is a microtubule-associated ATPase, dynein, previously called microtubule-associated protein (MAP)-1C.[130, 131, 159, 160] It is a 1000 kDa double-headed molecule, about 40nm in length.[161, 162] Its structure is composed of:

a. Two heavy (400 kDa) chains forming globular heads, each having four binding sites for ATP molecules.
b. Intermediate regions or stalks connecting the heavy chains to a basal domain.
c. A basal domain composed of multiple light chains of 53 to 74 kDa.[162-165]

Newly synthesized inactive dynein molecules, released from the cell body, are translocated to axon terminals in membrane-bound vesicles by the kinesin-based fast transport.[166] Following an unclear step of activation at axon tips, functional dynein molecules translocate the used-up membrane-bound organelles retrogradely by an ATP-driven microtubule-based fast motor mechanism similar to kinesin.[130, 159, 167] During this transport, it works in conjunction with another protein moiety, dynactin.[167] After delivering the loaded material, these functionally active dynein molecules join the pool of slow anterograde transport system to deliver more cytoskeletal proteins.[160, 165, 166]

In conclusion, fast anterograde transport mediated by motor proteins, kinesin and dynein, supply proteins, enzymes and organelles necessary to maintain the structure and function of axonal membrane as well as synapse. Kinesin forms microtubule-based fast unidirectional motor transport system transporting organelles towards the axon; whereas, dynein is a bidirectional motor carrying used up material towards the cell body by microtubule-based fast retrograde transport and cytoskeletal elements towards the axon by actin/microtubule dependent slow transport system, which is discussed below.

2.5.2 Slow Axonal Transport

The slow axonal transport system is different from the fast axonal transport in terms of mechanism and composition.[163] It moves different material at different rates towards the

axon terminal. The slowest subcomponent, SCa, transports protein constituents of microtubule and neurofilament cytoskeleton with the speed of 0.25mm/day;[168, 169] whereas, the faster subcomponent, SCb, conveys microfilament network, enzymes of intermediary metabolism, and synaptic proteins at the transport speed of 2-3mm/day.[168, 170-174] Although both subcomponents represent different compartments of the axon, they play very important role in maintaining the axon structure and function.

2.5.2.1 Mechanism for slow transport

It is still unclear about what constitutes the anterograde slow transport. Research has suggested that the slow transport of different molecules occurs by different mechanisms and that specific motor molecules play a role in it.[163, 175] Most of the studies have so far focused on the slow transportation of the cargo including protein constituents of neurofilaments and microtubules. This section focuses on the theories of transport proposed for each of them.

Neurofilaments

There are three different NF subunits- NF-L, NF-M and NF-H. Transport of these subunits is a complex phenomenon. Initially, NF-L is self-assembled in the soma from NF-L monomers,[176] with each monomer composed of three domains- N-terminal head, α-helix rod and C-terminal tail region.[See Figure 11][177-179] Assembled NF-L act like a framework to which NF-M or NF-H copolymerize and form heteromers.[180]

NOTE:
This figure is included on page 30 of the print copy of the thesis held in the University of Adelaide Library.

Figure 11. Steps in the assembly of NF-L and basic structure of NF-L monomer. (Source- Kim SK et al. Journal of Neuroscience;2007)[176]

After release from the cell body, NF hetero-oligomers are largely transported in the polymerized form by slow transport system at a variable speed ranging from SCa to SCb and even slow.[181-183] The rate of transport is controlled by the phosphorylation of C-terminal of neurofilament proteins, which changes the characteristics and movement of NFs. The addition of phosphate group is done by mitogen activated protein kinase (MAPK).[184-186] Phosphorylation of NF-M enhances microtubule-dependent NF transport by increasing direct and indirect association of NF oligomers with fast motor proteins, dynein/kinesin ('cargo model').[175, 187-191] In contrast, addition of phosphate group to NF-H slows the rate of transport by multiple ways.[192] Firstly, it directly inhibits the association of NFs with motor proteins.[189] Secondly, it increases NF-NF interactions to form compact longitudinal bundles of NFs in axon and thus, indirectly slows their transport.[189, 193, 194] Finally, by producing a conformational change in neurofilament structure, it increases formation of cross-linkages with surrounding proteins.[195] Phosphorylation of NF-L has no effects on the rate of transport.[189] Therefore, opposite

effects of phosphorylation of different subunits results in slow axonal transport of NF oligomers.[182, 189, 196, 197]

Phosphorylation of NF proteins is reversible and because NFs undergo phosphorylation-dephosphorylation cycle during transport,[198-200] researchers believe that slow transport might actually be not slow, but the result of fast movements of NFs with intermittent prolonged stationary phases.[190, 201, 202] The hypothesis is supported by some direct observational studies, which show that movement of NFs is rapid, intermittent, asynchronous and bidirectional.[202-205] Moreover, dynein-based movements of molecules in opposite (anterograde and retrograde) directions, further slows down the rate of translocation.[175] Thus, slow transport is the net result of not only alternate phosphorylated and dephosphorylated states of NF proteins, which determine the rapid movement and stationary phases of transport, respectively, but also, of the opposing forces generated by the dynein motor protein.

There are some predictions about the role of NFs in the maintenance of growth and structure of axon. In a growing neuron, most of phosphorylated NF oligomers reach the growing end of axon terminal (growth cone) through kinesin-based rapid but intermittent transport to form new cytoskeleton.[191, 206] The unused oligomers turn around to enter the active dynein-based retrograde transport system.[207, 208] It is also considered that when axons cease to grow, all the anterogradely transported NFs reaching the axon tip, pause and reverse their direction, and finally move back into the axon to integrate into the axon cytoskeleton so as to increase the axon diameter.[208] In this manner, fast but intermittent anterograde and dynein-dependent retrograde transport of NFs maintain the growth and calibre of the axons.

Microtubules

Microtubule synthesis and transport down the axon are important for the normal neuronal development.[209] However, unlike neurofilaments, microtubule transport, is quite unclear. There is a controversy about the form in which they are transported in axon. According to the *'subunit transport'* model, the basic structural subunits, α-β tubulin heterodimers or oligomers, are carried down the axon and assembled into microtubule arrays in the axon.[210-212] Tubulin dimers form in the cell body by spontaneous binding of the GTP-loaded subunits, α and β tubulins, with minus-end of α-tubulin of one heterodimer joining with the plus-end of β tubulin of the other to form oligomers.[213] Once assembled and released from the cell body short segments of the microtubule oligomers are transported down the axon by the microtubule and actin-dependent dynein/dynactin motor protein complexes.[214-217] Current studies support the *'polymer transport model'*, which states that the microtubules are formed (nucleated) in the cell body and are transported in the axon actively as short polymers.[216-219]

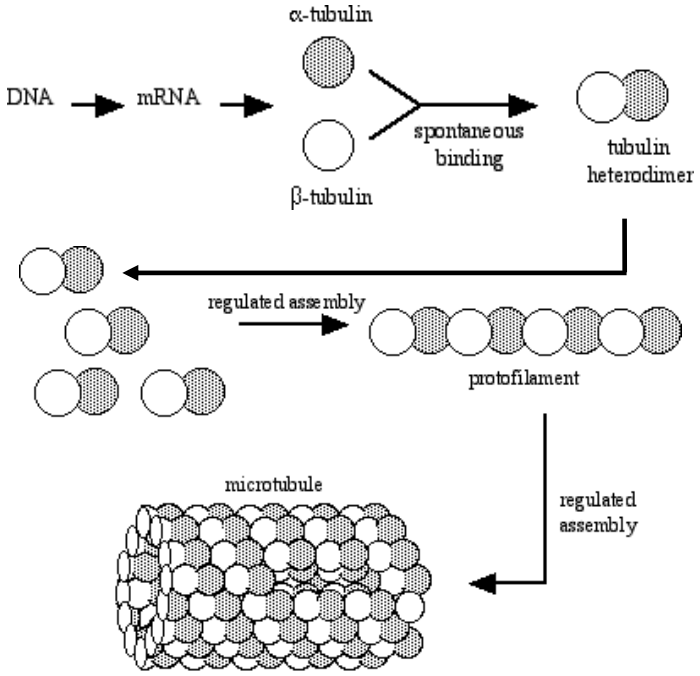

Figure 12. Structure and synthesis of microtubules.

The microtubule transport is explained by the 'sliding filament' theory.[See Figure 12] Cargo-binding domain of dynein molecule is linked via dynactin protein to highly resistant actin filaments or surrounding microtubules and it generates force against them to translocate/slide microtubule segments attached to motor domains.[166, 188, 216, 220-222] All axonal microtubules have uniform orientation with their plus-end directed distally.[213, 223, 224] Although, transport of microtubules is slow, like neurofilaments, it is due to rapid, infrequent bidirectional and asynchronous nature of the movement.[225] Reaching axons, minus end of new labile microtubule polymers join the plus end of stationary ones and thus, the microtubules elongate.[212, 226]

In conclusion, growth and maintenance of the structure of axon requires the synthesis of cytoskeletal proteins (NFs and microtubules) in the cell body and an energy-dependent slow transport system to carry them to the axon terminal.[70, 227] NF oligomers and short segments of microtubules are transported anterogradely in a slow but characteristic fashion by the kinesin/dynein-based microtubule-dependent fast motors to join the stable pool at the growing end of axon. If unused at the distal end, they are translocated retrogradely for incorporation into the axonal cytoskeleton to increase the axon calibre. Because distal end of the axon is the first site of utilization of the cytoskeletal constituents, any defect in their synthesis/transport or depletion of energy source makes the axon vulnerable to degeneration, especially at the distal end.

2.6 Excitotoxicity

First described by Olney in 1972, excitotoxicity is defined as the pathological process of neuronal death due to prolonged or excessive stimulation of glutamate receptors by glutamate or other structurally related excitatory amines such as NMDA, α-amino-3-

hydroxy-5-methyl-4-isoxazolepropionic acid (AMPA) and kainate.[228-230] Glutamate, an endogenous physiologic excitatory amine of CNS, helps in the conductance of visual impulses through the glutaminergic receptors present across the retina.[231-233] Once released, excessive stimulation of post-synaptic glutamate receptors is prevented by rapid uptake of glutamate by retinal astrocytes and Müller cells.[234, 235] Pathological accumulation of glutamate either due to excessive discharge from the dying cells or a reduced clearance result in excitotoxic neuronal death.

Excitatory amino acids, which are widely distributed in the CNS, not only play an essential role in normal synaptic transmission and synaptic plasticity, but also in many neurodegenerative diseases. Brain pathologies associated with it include acute seizure, ischemia/ stroke, hypoglycaemia, Huntington's disease, HIV encephalopathy, Parkinson's disease, Alzheimer's disease and many other metabolic conditions.[8, 236-238] Also, the toxic effects of glutamate on inner retinal layers is known for years.[239] This process has been found underlying eye conditions such as glaucomatous [13, 240, 241] or ischaemic retinopathy.[242]

Glutaminergic receptors are classified into two groups: ion-channel forming (ionotropic) and G-protein coupled (metabotropic) receptors.[243] The former group is subdivided into NMDA, AMPA and kainite receptors, and the later group contains mainly two variety of receptos- phospholipase C coupled receptors that stimulate phophoinositide hydrolysis and adenylyl cyclase coupled receptors that inhibit cyclic AMP production.[244] Endogenous glutamate can activate all of the receptor classes, with the highest affinity for the NMDA receptor. NMDA and kainite, the exogenous amino acids which do not exist in the CNS, are selective agonists for particular receptor types. In comparison to the

metabotropic receptors,[245] overactivation of the ionotropic NMDA receptors play a major role in excitotoxicity.[236, 238, 246]

2.6.1 NMDA-receptor system

NMDA receptors are a subgroup of post-synaptic ligand-gated ionotropic glutamate receptors, which bind to excitotoxin L-glutamate.[247] These receptors require the presence of glutamate as well as coagonist glycine.[248] The basic structure of NMDA receptor consists of four heteromeric complexes each having a central water-filled pore.[249, 250] Each heteromeric complex is composed of obligatory NR1 and modulatory NR2 subunits.[248, 251] NR1 subunits possess four trans-membrane hydrophobic amino acid sequences (TRI-IV) with an intracellular C-terminus and an extracellular N-terminus.[252] NR2 has a variable composition with subunits of type NR2A-NR2D.[253] Presence of both NR1 and NR2 subunits is essential for the formation of functional receptors because NR1 subunit carries the high affinity binding site for the co-agonist glycine and NR2 is loaded with glutamate binding site.[247, 254]

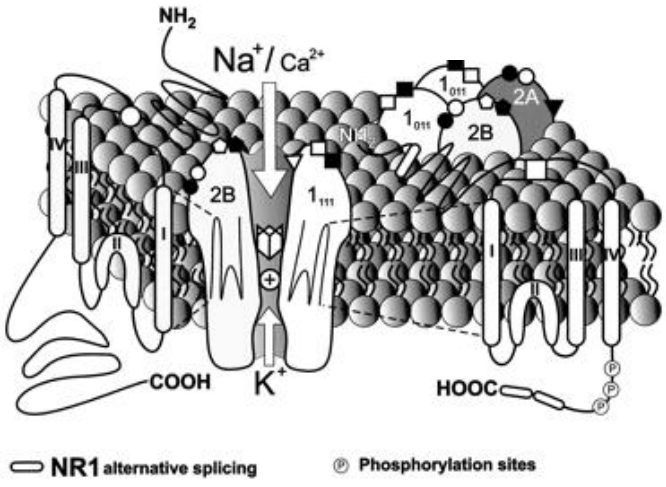

Figure 13. NMDA receptor

Both subunits provide different biophysical and pharmacological properties to the NMDA receptors.[255] Another subunit, NR-3, is identified only during the early development phase.[256]

2.6.2 Mechanism of excitotoxicity

Prolonged or excessive stimulation of NMDA receptors causes influx of large amounts Ca^{2+} into the cell to activate Ca^{2+}-dependent lytic enzymes which disrupt the cell structure and cause cell death.[257, 258] Series of intracellular changes which follow NMDA receptor activation are as follows.

2.6.2.1 NMDA receptor activation

NMDA receptors are associated with high conductance Ca^{2+} channels.[259] In normal resting non-depolarizing conditions, they are blocked by Mg^{2+} in a voltage-dependent manner.[260] Activation of NMDA receptor by either NMDA or glutamate causes loss of Mg^{2+} block with opening up of Ca^{2+} channels and influx of Ca^{2+} into the cells.[257-259, 261, 262] Inward Ca^{2+} current mediated depolarization release glutamate extracellularly, which activates other ionotropic glutamate receptors producing an influx of Na^{+} and Cl^{-} ions accompanied by osmotically–driven influx of H_2O and further membrane depolarization.[263] The deleterious actions of the ionotropic glutamate receptor stimulation are thus self-reinforcing and result in chronic or delayed excitotoxicity.[264, 265]

2.6.2.2 Ca^{2+} overload: cytoplasmic events

Following NMDA receptor activation, the entry of Ca^{2+} initiates intracellular cascade of reactions such as sustained activation of cytoplasmic Ca^{2+}/calmodulin dependent enzymes such as proteases (calpains),[266-268] protein phosphatase (calcineurin),[269] and nitric oxide synthase (NOS).[270-273] Calpains lyse all major proteins in the cell including those forming the cytoskeleton.[274-277] Calcineurin activates Na^{+}-K^{+}-ATPase (by removing phosphate group), which increases the consumption of ATP, thus, depleting the energy source.[278, 279] NOS causes S-nitrosylation and subsequently oxidation of other endopeptidases (Xanthine oxidase, and Phospholipase A2) involved in cell death.[275, 280] NOS also results in the generation of superoxide anion, peroxynitrite and other reactive oxygen species (ROS).[246, 281, 282] Although, calpain, NOS and generation of free radicals are the major pathways involved in excitotoxicity, [283-288] mitochondrial dysfunction is the main event in excitotoxic cell death.[289-291]

2.6.2.3 Mitochondrial cascade

Mitochondria play a protective role by uptaking excessive calcium from cytoplasm.[289, 290, 292, 293] During excitotoxic insult, potential generated by the cytosolic Ca^{2+} triggers a quick entry of the Ca^{2+} into the mitochondria by a potential-driven Ca^{2+} uniporter.[291, 294-296] Like cytoplasmic pathway, production of nitric oxide, peroxynitrate (ONOO-) and other ROS is enhanced.[297, 298] Increased mitochondrial Ca^{2}+ alongwith ROS causes uncoupling of electro transport chain.[297] by inhibiting mitochondrial respiratory complexes, with a drop in ATP/ADP, making mitochondria incapable of maintaining membrane potential and resulting in opening up of mitochondrial transition pores (MTP).[270, 299-307] This causes mitochondria to swell and release cytochrome c into the

cytoplasm followed by the sequential activation of caspase 9 and caspase 3, resulting in programmed neuronal cell death.[299, 306, 308, 309]

2.6.2.4 Mitochondrial-nuclear interplay

Studies have also shown the release of another caspase-independent mitochondrial death factor, called apoptosis inducing factor (AIF).[309-313] Synthesis of ROS, particularly peroxynitrate, causes breakdown of mitochondrial DNA and activation of Poly (ADP-ribose) polymerase 1 (PARP-1), which in turn translocates flavoprotein, AIF to the nucleus to cause chromatin condensation and DNA fragmentation.[310, 312, 314-316] Therefore, mitochondrial dysfunction is the main process involved in caspase-dependent and independent pathways resulting to excitotoxic cell death.[317, 318]

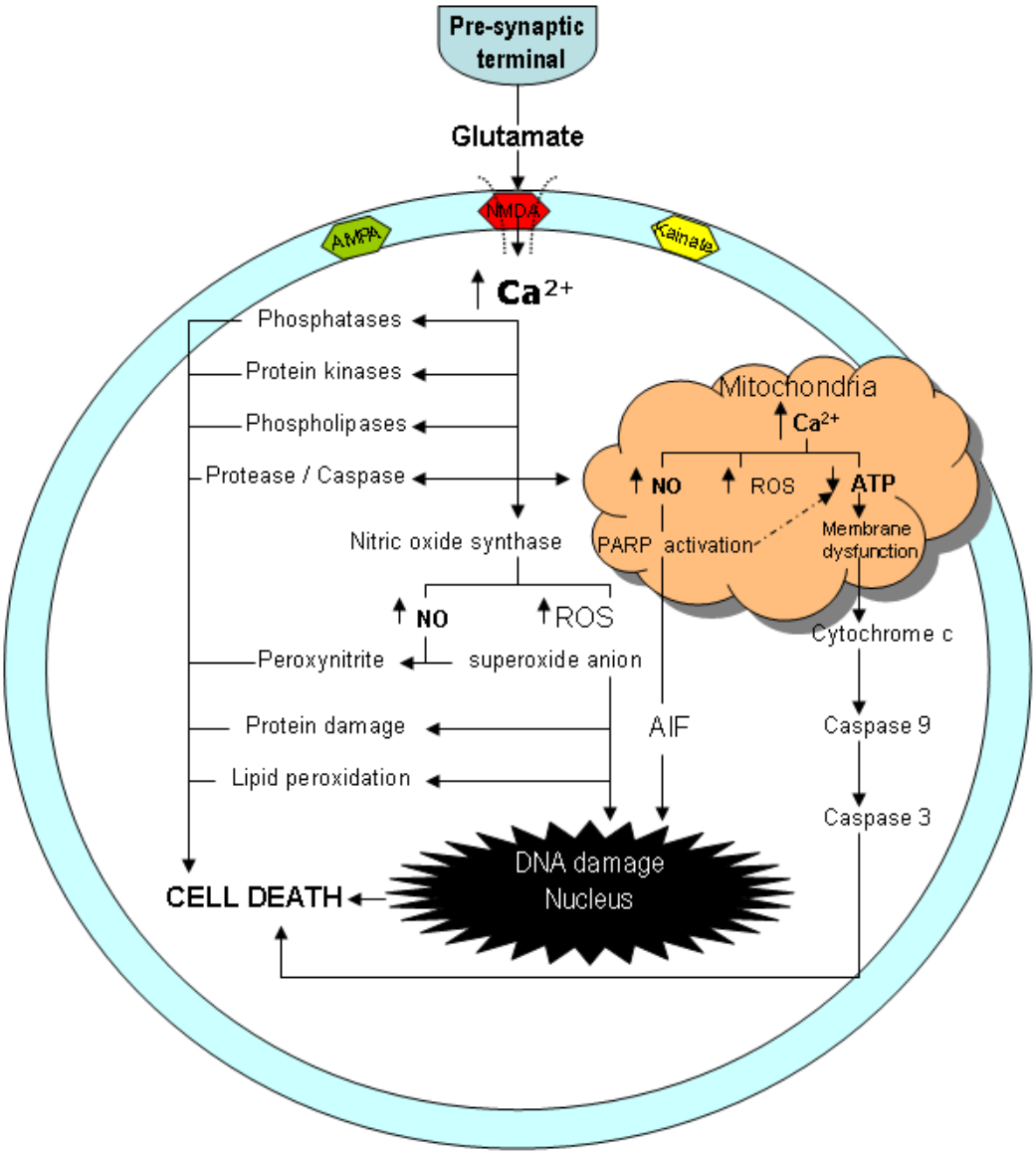

Figure 14. Mechanism of excitotoxicity. Activation of NMDA receptor by glutamate causes influx of calcium which activates various proteases, phosphatases, phospholipases, protein kinases and metric oxide synthse in the cytoplasm. Nitric oxide synthase increases production of nitoric oxide (NO) and reactive oxygen species (ROS), both combine together to generate peroxynitrite. ROS further lead to lipid peroxidation and protein damage. Similar events occur in the mitochondria when it uptakes calcium from the cytoplasm. In addition, NO formation results in activation of Poly (ADP-ribose) polymerase 1 (PARP-1) generates apoptosis inducing factor (AIF) which translocates to the nucleus and causes DNA damage. Reduced adenosine tri-phosphate (ATP) production leads to mitochondrial membrane dysfunction, which results in release of cytochrome c into the cytoplasm. Cytochrome c activates capase 9 which increases caspase 3 activity. All cytoplasmic, mitochondrial and nuclear changes if go uncontrolled results in cell death.

Chronic NMDA receptor stimulation, like acute excitotoxicity, leads to activation of Ca^{2+}-dependent cytoplasmic enzymes, impaired mitochondrial function and generation of free radicals.[319-322] Besides metabolic defect due to mitochondrial dysfunction, so called slow 'excitotoxic' process, stimulation of several intracellular transduction pathways cause apoptotic cell death in chronic excitotoxicity.[275, 323-325] This includes increased expression of pro-apoptotic tumor suppressor gene p53 [242, 326] as well as pro-apoptotic mitogen-activated protein kinases such as signal-regulated protein kinases, c-Jun N-terminal kinases (JNK) bound protein 1 & 2 and p38 kinase.[275, 327-334] Chronic activation of NMDA receptors upregulates Cysteinyl Leukotriene Receptor 1 (CysLT1), a mediator of neuronal cell death and degeneration.[335, 336]

2.7 Cell death

Events following any insult exceeding the limits of physiological adaptation of cell result in cell injury. The injury remains reversible up to certain extent, however, if it becomes uncontrolled and severe, it may result in cell death.[337] The cell, therefore, passes through the stages of adaptation, reversible injury and irreversible injury to finally result in cell death. Various classifications of cell deaths have been described in the literature. However, the most common modes of cell death are:

2.7.1 Necrosis

Necrosis is a mode of cell death where severe exogenous insult results in the disruption of membrane structural and functional integrity causing influx of ions and water into the cell. Rapid degradative action of the enzymes results in different cytoplasmic and nuclear changes. The mitochondria swell and undergo cristaeolysis. They also show formation of amorphous dense deposistes in the matrix. Disruption of the swollen granular endolpamic

reticulum and disintegration of polyribosomes releases 'free' ribosomes into the cytoplasm. The cytoplasm shows formation of 'myelin figures' and deposition of amorphous deposits. The nuclear changes which may follow include fading away of the chromatin (karyolysis), nuclear shrinkage and chromatin condensation (pyknosis) or nuclear fragmentation (karyorrhexis). The disruption of the cytoplasmic organelle and cell rupture release intracellular debris into the extracellular space initiating an inflammatory response.[228, 338]

2.7.2 Apoptosis

Apoptisis is an active and subtle form of cell death designed to remove unwanted body cells (physiologic cell death) and cells injured as a result of cytotoxicity (pathologic cell death). In contrast to the necrosis, the earliest changes begin in the nucleus, where the chromatin condenses peripherally under the nuclear membrane into dense round masses (pyknosis). The cell shrinks but the organelles remain relatively normal. Intact mitochondria are required to maintain this energy-driven process. The cell membrane remains intact but shows formation of surface blebs. The cell then undergoes fragmentation to form membrane-bound apoptotic bodies containing fragmented cytoplasm and/or nucleus, which are removed by the adjacent phagocytic cells including macrophages, epithelial cells and fibroblasts.[228, 339] Major morphological differences of Apoptosis and Necrosis are given below.[See Table 1]

2.7.3 Autophagy

Autophagy is a process of cell death in which the cytoplasmic contents sequestered into double-membrnae lined autophagosomes fuse with the lysosomes to form autophagolysosomes. The lysosomal enzymes digest most proteins and carbohydrates.

The digested autophagolysosome either persists in the cell as residual body or is exocytosed.

Table 1. Morphological differences between apoptotic and necrotic cell death

Characteristics	*Necrosis*	*Apoptosis*
Cell size	Increased	Decreased
Cell membrane permeability	Increased	Normal
Cell membrane budding	Absent	Present
Mitochondria	Swollen with flattened cristae	Normal
Nuclear chromatin	No or slight condensation/ fragmentation	Condensed and fragmented
Apoptotic bodies	Absent	Characteristic
Myelin figures	Present	Absent
Inflammatory response	Present	Absent
Fate of the cell	Lysis	Phagocytosis
Appearance in tissue sections	Necrotic cells with surrounding tissue oedema and inflammatory cells	Inconspicuous, apoptotic bodies, phagocytosed by the natural phagocytic cells

2.8 Nerve Degeneration

Nerve degeneration is defined as the loss of structure or function of axons following injury to their cells of origin (somagenic degeneration) or interruption of their continuity with the cell bodies (axogenic degeneration).[28] Clinically, neurodegenerative disorders seen by a neurologist include conditions such as CNS ischaemia/ stroke, AD, Huntington's disease,

Parkinson's disease, HIV encephalopathy and MND. Ophthalmologists see this process in the form of glaucomatous, ischaemic and other degenerative retinopathies. For years, experiments have been conducted to explain the pathological aspects of degeneration in most of the neurodegenerative brain disorders.

2.8.1 Wallerian degeneration

Augustus Waller proposed the most well known theory of 'Wallerian degeneration' [340] in 1849. According to this theory, if a nerve is physically transected any-where along its length, the distal stump degenerates but the proximal portion survives. The sequence of changes occurring in the distal stump of severed axons is termed 'Wallerian degeneration'.[56, 341, 342] The degeneration progresses sequentially through various stages.

During the initial stage after severance (*Stage I*), interference with the fast anterograde and retrograde transport system [343] results in the pellet-shaped dense accumulations of tubules, vesicular organelles, mitochondria and dense bodies in the distal end of the proximal and the proximal end of the distal stump, respectively.[344] Nodal regions of the distal stump show accumulation of organelles beneath the axolemma, with the neurofilaments occupying the central portion of the axoplasm.[344, 345] In the paranodal region, MTLs become widened, separated and detached from the axolemma resulting in elongation of the paranode.[346]

Stage II begins with the disintegration of axoplasm in the distal stump. During this stage, breakdown of both axonal cytoskeleton and organelles occurs, which gives the axoplasm a granular appearance.[56] Studies have found a difference in the sequence of breakdown

of cytoskeletal elements and organelles in the CNS and PNS. Disintegration of both the elements begins simultaneously in PNS whereas cytoskeletal disruption occurs prior to the axolemmal and organellar changes in the CNS neurons.[56, 347]

Next stage (S*tage III*) includes events resulting from axoplamic disintegration. Disruption of the blood-nerve barrier leads to extravasation of fluid and development of endoneurial edema along the whole length of the degenerating axon.[348] Activated mitogen protein kinases in neurons induce further degeneration.[349-351] Damage to axons triggers a stereotypical response in the surrounding glia. Activation of neuregulin/erbB2 system in the enwrapping oligodendrocytes/Schwann cells induces mitotic activity and leads to their proliferation.[349, 350, 352] Neuronal factors called toll-like receptor (TLR) agonists stimulate these cells to release pro-inflammatory cytokines.[353, 354] Release of TNF-α induces pain and demyelination [354-356] and chemoattractant factors, LIF and MCP-1, provoke recruitment of macrophages at the site of nerve injury.[357] Lastly, axonal disintegration activates resident and recruits circulating macrophage-lineage cells at the site of injury.[358-360]

Events in the *Stage IV* include responses generated from the activation and proliferation of mature glial cells and macrophage-lineage cells. Proliferation of Schwann cells in the PNS lead to formation of Bungner bands (Bungner bands are tubes formed by the interdigitating Schwann cells lined on outside by the basal lamina).[56, 361] Downregulation of genes in these cells responsible for the formation of myelin induced demyelination.[349, 350, 362] Macrophage-lineage cells, astrocytes and possibly fibroblasts begin to clear the axonal and myelin debris.[358, 360, 361, 363] The stage of Bungner bands and the process of debris clearance continue for many weeks after injury till the contact with the remaining

axon stump is maintained.[56, 360, 361, 364] Final outcome depends on whether the nerve regenerates or not.

In the final stage (S*tage V*), glial cells in the bungner bands express NGF receptors which helps in the process of nerve regeneration.[365-367] If the axons regrow and establish contact with the Schwann cells tubes, nerve regenerates.[361] However, failure to do so results in nerve atrophy [56] characterized by the disappearance of Schwann cells and bungner bands as well as fragmentation and loss of the basal laminas.[361] The total cross sectional area of the atrophic nerve reduces and the nerve tissue gets replaced by the collagenous scar tissue.[347, 368]

The fundamental features of Wallerian degeneration are similar in the CNS and PNS except that unlike PNS, the molecular and cellular events after axonal disruption such as increase in the permeability of blood-nerve barrier, activation of the glial cell, and clearing of the debris, are much slower in the CNS.[348, 349] It is doubted that this may limit the chances of regeneration of neurons in the CNS.[369]

Studies have been conducted to confirm the direction of spread of Wallerian degeneration in the distal stump and a few have demonstrated that the degenerative changes progress from the site of transaction down to the terminal end.[370] However, there is no firm evidence whether this wave spreads anterogradely or retrogradely.[371]

NOTE:
This figure is included on page 46 of the print copy of the thesis held in the University of Adelaide Library.

Figure 15. Axonal self-destruction and neurodegeneration. (A) Healthy neuron; (B) Wallerian degeneration; (C) Dying back. (Source- Raff M, Whitmore AV, Finn JT. Science. 2002 May 3; 296(5569):868-71. Review)

2.8.2 Dying-back degeneration

'Dying-back' degeneration is a slowly evolving process, where the axon and myelin degeneration begin at the nerve terminal and progresses proximally towards the cell body.[372, 373] Because the degenerative changes are similar to those seen following axotomy and because the final pathways of axonal breakdown in dying back degeneration are similar to WD, they are also called 'Wallerian-like degeneration'.[56, 372] First described by John Prineas in 1969, dying back phenomenon is now found to underlie many chronic neurological conditions including degenerative, metabolic, nutritional, inherited, toxin-induced, inflammatory and ischaemic nerve disorders.[56] The major ones include inherited neurodegenerative disorders such as Hereditary Spastic Paraplegia (HSP), Amyotrophic Lateral Sclerosis (ALS), Friedreich's ataxia [374-376] as well as metabolic neuropathies seen in diabetes, porphyria, thiamine and vitamin E deficiency states.[377-379] Some malignancy-associated and drug-induced neurotoxicities are also considered to show dying back pathologies.[380, 381]

The pathologic process of dying back degeneration has been studied in a wide variety of natural and experimental conditions. Experiments are done on various toxin-induced, metabolic and genetic models.[22, 382-385] In the most commonly used model of toxin-induced neuropathy, a wide range of toxins such as, acrylamide, hexacarbons, ethanol, trimethyltin and many others, are used to produce nerve damage.[22-27] Streptozotocin induced experimental diabetes is also a popular model to study diabetic neuropathy.[386, 387] Because each toxin has its own biophysical and pharmacokinetic characteristics, in spite of similar morphological changes, investigators have proposed different mechanisms of dying-back degeneration for different toxic and metabolic conditions.

The pathological changes in dying-back degeneration are somewhat similar to those described with WD. A model using neurotoxic hydrocarbons demonstrated the initial changes of axonal swellings in the nodal-paranodal regions, paranodal myelin retraction and nodal elongation in the distal regions of axons.[388] Morphologically, the axons appear intermittently swollen.[389, 390] Ultrastructural studies reveal that the focal axonal swellings contain NFs, dense granules and protein-rich tubulo-vesicular membranous organelles such as granular mitochondria and agranular endoplasmic reticulum.[391-393]

As the insult continues, swellings spread to the internodes and the myelin sheath thins out, absent or may show vacuole formation.[388, 394] Slowly, demyelinated paranode undergoes either shrinkage or remyelination.[388, 395] Prolonged injury results in the granular disintegration of axoplasm and changes in surrounding glial cells and the degenerative process progresses gradually from the distal to the proximal end.[388]

The pathologic process of centripetal dying back degeneration has always been ill-understood. On one hand, interference in the perikaryal processing of proteins and membrane-bound vesicles required for axon terminal maintenance is considered as the possible mechanism.[396, 397] Conversely, defective axonal transport of this material is believed to be the underlying cause.[397] Based on various suggested mechanisms, 'dying-back' neuropathies are classified into three major types:

1) Neuropathies where axonal transport is defective.

2) Neuropathies due to defective production of energy in the cell body and

3) Neuropthies which are due to defective pyridoxal-phosphate pathway.

Table 2. Classification of dying-back neuropathies based on their mechanisms.

	Transport dependent	*Energy dependent*	*Pyridoxal-phosphate dependent*
Toxin-induced	N-hexane	Arsenic	
	Methyl n-butyl ketone 2,5- hexane dione Carbon disulphide Acrylamide Organophosphorous	Thallium	
Drug induced	Dapsone	Nitrofuran drugs	Isoniazid
	Clioquinol and others		Hydralazine Ethionamide
Nutritional		Thiamine deficiency Riboflavin deficiency	
Metobolic		Alcohol induced Tropical neuropathy Friedrich's ataxia	Porphyria

In conclusion, defective axonal transport, energy deprivation and pyridoxine deficiency are considered to be the mechanisms underlying dying-back degeneration in various polyneuropathies. However, no firm evidence is available to establish whether the primary site of injury is axon or the cell body. In these models systemic toxins simultaneously damages axons and cell bodies and therefore have limited value in investigating primary site of insult. This limitation demands for a study that can produce isolated somogenic or axogenic damage.

2.8.3 Segmental Demyelination

Neuropathies which show a widespread loss of myelin with preservation of axon structure are said to undergo a different type of degeneration called as segmental demyelination. Segmental demyelination refers to focal degeneration of the myelin sheath sparing the axon. This reaction can be seen in focal mononeuropathies but also in generalized sensorimotor or predominantly motor neuropathies. Acquired segmental demyelinating polyneuropathies are often immune-mediated or inflammatory in origin. However, segmental demyelination can also occur in some hereditary polyneuropathies.

2.9 Optic Atrophy/ Neuropathy

Clinically presenting as loss of vision, optic nerve atrophy is classified into two major groups- inherited and acquired. Inherited optic atrophy, as the name suggests, is congenital. Its causes are 1) Leber's hereditary optic neuropathy (LHON), 2) Kjer's dominant optic atrophy, 3) Leigh's syndrome, 4) Fredreich's Ataxia and 5) other inherited mitochondrial disorders.[398] Acquired damage to the optic nerve results from glaucoma, trauma, ischaemia (anterior and posterior ischaemic optic neuropathy), inflammation (optic neuritis), pressure (retro-orbital tumour), toxins, and metabolic diseases like diabetes.

2.9.1 Inherited optic neuropathy

Various mechanisms are proposed to explain the pathogenesis of optic neuropathies. Most inherited conditions are known to be due to mitochondrial genetic defects.[398-400] The most common autosomal dominant LHON and Kjer's optic atrophy are due to the pathogenic point mutations in subunit genes (OPA1) of mitochondrial DNA, encoding complex1 of the oxidative phosphorylation pathway.[401-405] Impaired ATP production in the cell body and resulting failure of active transport deprives the axons of the mitochondria especially at the sites where high energy is required which include the nodal regions and axon terminal.[406, 407] In optic nerve, such high energy sites include unmyelinated pre-laminar and laminar parts as well as nodes in the retrolaminar myelinated regions, where the voltage gated Na^+ channels are clustered.[408-410] Although it is known that the mitochondrial DNA mutations disrupt energy production in RGCs and distribution of mitochondria in the optic nerve axons, pathological changes of optic nerve degeneration are still unclear.[411, 412]

2.9.2 Acquired optic neuropathy

Unlike inherited variety, acquired optic neuropathies are explained by various mechanisms. Most acquired causes of optic nerve degeneration (toxic and metabolic conditions such as, tobacco-alcohol amblyopia, Cuban optic neuropathy, vitamin B or folic acid deficiencies and drug-induced neuropathies) are the result of mitochondrial dysfunction.[38, 398, 413, 414] Glaucoma, one of the major blinding diseases, which causes optic nerve damage by mechanical compression and/or decreased blood flow of the optic nerve, is shown to be to be multifactorial in origin.[415]

Glaucomatous optic neuropathy

The cause of the damage to the RGCs and the optic nerve head in glaucoma remains unclear. A major conventional theory is the 'mechanical theory'. According to this theory, elevated intraocular pressure compresses axons at the level of the optic nerve head causing direct mechanical injury or results in the blockage of retrograde axonal transport of trophic factors from the axon terminal and subsequent RGC loss.[415, 416] According to another major theory called as 'vascular theory', the raised IOP interferes with the blood supply to the retina as well as the optic nerve head producing ischemic damage to these structures.[415] Mitochondrial genetic mutation is considered to be the cause of optic nerve degeneration in a few glaucoma patients.[417] The concept of excitotoxicity has also gained credence as a potential mechanism.[418]

Optic nerve damage in glaucoma results from the changes in neuronal, glial, and extracellular matrix components.[419] Studies have shown that astrocytes in the optic nerve head region are believed to play a major role in glaucoma. Increased IOP activates astrocytes in the laminar region to increase the synthesis and release of abnormal elastin by reactive astrocytes, which results in fibrous thickening of the nerve head.[420, 421] Moreover, pressure-induced increased expression of neurotoxic cytokine, TNF-α, as well as epidermal growth factor receptors (EGFR) in the activated laminar astrocytes causes activation of the nitric oxide synthase.[422-428] Increased synthesis of NO and the resulting oxidative stress causes degeneration of RGC axons.[426]

Like other neurodegenerative conditions, excitotoxicity may play an important role in the pathogenesis of glaucoma.[2, 13, 241] Overstimulation of NMDA receptors produce

oxidative stress in RGCs, which results in mitochondrial DNA damage and subsequent cell death.[417, 429]

Other acquired optic neuropathies

Many experimental studies have indicated the role of glutamate excitotoxicity in ischemic optic neuropathy.[13, 430] During the optic nerve crush, delayed (secondary) loss of RGCs is also the result of release of excitatory neurotransmitters by injured RGCs.[431, 432] Therefore, excitotoxicity plays an important role in all major acquired eye conditions, such as glaucoma, ischaemia and trauma.

In all acquired eye conditions where RGCs suffer insult due to excitotoxicity, mitochondrial cascade of events result in cell death. Respiratory dysfunction after mitochondrial damage in RGCs causes oxidation of proteins required for the active transport and maintenance of axons meanwhile preventing migration of neurotrophic factors and antioxidants to RGCs.[433-437] One of the studies has identified that glaucoma causes dephosphorylation of NF-H in RGCs.[438] Significance of this removal of phosphate group has not been discussed in relation to the optic nerve; however, studies have shown that dephosphorylation of NF-H causes rapid movement of NFs in the axons, resulting in abnormal accumulations of these cytoskeletal elements in axons.[192, 390]

In conclusion, eye diseases damage the retina by various mechanisms. Excitotoxicity induced mitochondrial damage plays an important role in most commonly seen acquired eye conditions. Although RGCs and optic nerve head are the prime focus of interest in most eye researches, not many studies have focused on the spatiotemporal changes and the mode of axonal degeneration in the retro-orbital optic nerve.

2.10 Experimental methods of retinal injury

Various models of ischaemic, glaucomatous and traumatic etiology are available to study different types of retinal injuries. To study ischaemic retinopathies, a model of transient retinal ischaemia can be created by ligating both the common carotid arteries,[439] selectively ligating the ophthalmic vessels [440] or occluding the ophthalmic vessels with a thrombus formed by using Rose-Bengal dye and argon laser treatment.[441]

To investigate acute angle-closure and chronic open-angle glaucoma, pressure is raised in the eye of the experimental animal temporarily or permanently by different methods. A widely used method for acute glaucoma is to increase the intra ocular pressure acutely and transiently by increasing pressure in anterior chamber with isotonic saline.[442] For chronic ocular hypertension, outflow of aqueous humour is blocked by argon or diode laser trabeculoplasty,[443-445] injection of hypertonic saline into the episcleral veins [446] or cauterizing them with argon laser photocoagulation.[447, 448] Less popular and traumatic model involves retinal crush injury where the posterior globe of the eyeball is incised to coagulate intraretinal arterioles.[449]

Trauma to the retina can be produced directly or indirectly. Damage to RGCs is indirectly produced by intraorbital optic nerve transection [431] and optic nerve crush.[450] They are not only popular models to examine RGC injury, but also are widely-employed methods to study Wallerian degeneration.[32, 451, 452] The experimental method used in the present research study involved direct retinal injury produced by intravitreal injection of NMDA, a model which can explain both ischaemic and glaucomatous eye conditions.[13, 242, 453, 454]

2.11 Justification for the use of NMDA model

Studies have indicated axonopathy as an early feature in neurodegenerative diseases associated with excitotoxicity.[455-458] Despite numerous researches, it is still unclear whether the nerve degeneration associated with excitotoxicity is due to primary insult at the perikaryal level in the grey matter (somagenic) or a primary excitotoxic injury in the white matter (axogenic). Studies using excitotoxins on cell cultures or other in-vivo models result in simultaneous damage to the axons and cell bodies and therefore have limited value in investigating primary site of insult. This limitation demands for a study that can produce isolated somogenic or axogenic damage, hence the current study.

NMDA model of retinal injury is a perfect model to study excitotoxic somagenic nerve degeneration. Usually, an excitotoxin delivered to the CNS, could trigger injury not only in the somatodendritic region, but simultaneously, in the axonal region. As RGC axons have a relatively long projection within the eye before reaching the optic nerve, intravitreal excitotoxic injury, which is physically isolated from the retro-orbital axons, may be the result of toxic insult to RGCs and/or intraocular axonal compartment. Studies have confirmed perisynaptic localisation of NMDA receptors in RGCs {Zhang, 2006 #6} Although there is evidence for the presence of non-NMDA glutaminergic receptors for AMPA and kainite in the postsynaptic myelinated axons in the central neurons [459] and the expression of NMDA receptors on oligodendrocyte processes in white matter,[460] there is no direct evidence of presence of functional NMDA receptors on axons.[461] Therefore, retro-orbital optic nerve axonal degeneration observed in NMDA-induced retinal insult is logically a consequence of primary damage to RGCs; however, damage to

intraorbital axons can also be considered a primary site of insult, if future studies provide direct evidence for the presence of functional NMDA receptors over axons.

Evidence is available that that both necrotic and apoptotic pathways are involved in the process of excitotoxicity,[1] with acute excitotoxicity inducing rapid necrotic cell death and chronic excitotoxicity causing apoptosis,[242, 337] Some studies have reported the presence of hybrids forms of cell death existing on a continuum between the classically defined apoptosis and necrosis.[462-464] It is also identified that the axons remain viable and metabolically active for some duration after somal death and that there may be independent factors controlling the somal response and neurite degeneration.[465] Although research focused on the changes in cell bodies, cellular and molecular events causing axonal degeneration post excitotoxic somagenic insult still remains unclear.

Although NMDA model has been used extensively to evaluate the mechanism of excitotoxic injury to RGCs,[20, 21] it has been used meagerly to study optic nerve degeneration.[466] As excitotoxicity is believed to be the underlying mechanism of RGC death in glaucomatous and ischaemic retinopathies, this study will help in better understanding of acquired optic neuropathies in these clinical conditions.

Chapter 3: AIM & OBJECTIVES

The underlying rationale for studying pathological changes in the optic nerve after excitotoxic injury to the retina is that a better understanding of the neuropathology may lead to the development of novel diagnostic and treatment strategies for chronic neurodegenerative conditions including glaucoma, many of which still have poor clinical outcomes. Although the pathological changes distal to the optic tract remain uncovered in this thesis, the scope of the study is broad. Akin to other areas of research, it does not intend to represent an exhaustive description of the field, but rather to explore some aspects of optic nerve pathology, with a view to provide original contribution to the field of ophthalmology-based neuropathological research. Because all research contributing to this thesis was performed on the living rat, *the main aim of this thesis was to study aspects of optic nerve pathology after NMDA-induced excitotoxic injury to the rat retina.* The major objectives of the research were,

- To study the temporal pattern of changes in the retinal and optic nerve morphology in the experimental and control animals by LM.
- To evaluate the morphological changes in the retina and the optic nerve quantitatively using different parameters.
- To reveal the mode of RGC death and morphological aspects of optic nerve axon degeneration by electron microscopy in NMDA- injected eyes.
- To quantify apoptotic cell death using terminal transferase-dUTP nick-end labeling (TUNEL) stain.
- To explore changes in the axon transport system after intravitreal NMDA injection by studying immunohistochemical expression of NF-L and β-APP in the retina and the optic nerve.

- To investigate the astrocytic and microglial cell response to axon degeneration secondary to excitotoxic perikaryal injury by comparing the changes in the immunological expression of ED-1 and GFAP proteins in the retina and optic nerve of the experimental and control eyes.

Chapter 4: MATERIALS & METHODS

4.1 Introduction

The current study is based on an *in-vivo* animal model where the retinal and optic nerve pathology can be studied after exclusive excitotoxic damage to the cell body. The study is aimed to establish the spatiotemporal pattern of somagenic degeneration in comparison to the previously old neuropathy models, which were mostly devised to study axogenic degeneration produced by either direct injury to the neuronal axons or simultaneous damage to the cell body as well as axons.

To achieve the research aim and objectives, various components of the study design were established and selected judiciously based on literature review, logical thought processing and piloting. These components mainly consisted of (i) selection of an agent, which produced selective damage to the cell body of a neuron, (ii) selection of an *in-vivo* system, where exclusive damage to the cell body could be produced, (iii) to deduce an intravitreal injection and tissue dissection technique, which caused no or minimal damage to the optic nerve while operating on the eye, (iv) to establish various aspects of nerve injury which could be studied using available resources, (v) to set up parameters to ascertain retinal and optic nerve damage by LM, EM and immunohistochemistry and finally, (vi) to deduce simple ways to correlate the retinal injury with optic nerve damage.

The initial stage of this study was the selection of an agent and an *in-vivo* model to where selective perikaryal injury could be produced. A well recognised experimental glaucoma model of NMDA-induced retinal injury in rat was selected. This is because studies have confirmed perisynaptic localisation of NMDA receptors in RGCs.[405] Although there is evidence for the

presence of non-NMDA glutaminergic receptors for AMPA and kainite in the postsynaptic myelinated axons in the central neurons [459] and the expression of NMDA receptors on oligodendrocyte processes in white matter,[460, 467] there is no direct evidence of presence of functional NMDA receptors on axons.[461] Also, because RGCs somata are physically isolated from the optic nerve and an intravitreal injection of NMDA produces dose-dependent damage to retina,[468], retro-orbital optic nerve axonal degeneration observed in NMDA-induced retinal insult is logically a consequence of primary damage to RGCs; however, damage to intraorbital axons can also be considered a primary site of insult, if future studies provide direct evidence for the presence of functional NMDA receptors over axons.

After approval from the animal ethics committee from the Institute of Medical and Veterinary Science (IMVS), Adelaide, a sham experiment was conducted on rats to firmly establish the intravitreal injection technique and to determine the suitability of sterile isotonic saline as an inert vehicle for the preparation of NMDA solution. A dissection technique was developed, where the eyeball and the optic nerve pathway (including the optic nerves, optic chiasm and optic tract) could be dissected without producing significant injury to these structures. After appropriate tissue fixation, processing, sectioning and staining, spatiotemporal pattern of light microscopic and morphometric changes following NMDA was followed by the ultrastructure study of the retina and optic nerve. Immunological changes in the axon transport system and glial cell response were studied using immunohistochemistry. Due to certain limitations, study of genetic changes is not included in this research, which could have helped in understanding produced a complete and reliable picture of optic nerve degeneration after excitotoxic perikaryal injury. Following sections describe the materials used in the study with the source of their supply followed by detailed description on various techniques used for injection, animal perfusion and killing, tissue fixation, processing, sectioning, staining and data analysis.

4.2 Materials

4.2.1 Experimental animals

Male Sprague-Dawley rats weighing 300-350g (source- Animal House, IMVS, Adelaide, South Australia) were kept at room temperature, with food and water *ad libitum* and housed at room temperature in a 12hrs light/dark cycle (lights on at 0700, lights off at 1900). Experiments were conducted in accordance with international standards on animal welfare and conformed to the Australian Code of Practice for the Care and Use of Animals for Scientific Purposes (7th edition 2004). All experiments were approved and monitored by the Institute for Medical and Veterinary Science Animal Ethics Committee. (Ethics Approval No. 53/06, see Appendix I)

4.2.2 General Reagents & Equipments

The following chemicals and materials used in this research were obtained from the companies or individuals listed in Table 3.

Table 3. Chemical/ Reagents and their sources.

Chemical/ Reagent	*Source*
N-Methyl-D-Aspartate (Mol. Wt. 147)	Sigma-Aldrich, USA
Sodium Chloride injection 0.9%	Astra International, U.K.
Paraformaldehyde powder	Sigma-Aldrich, USA
Sodium dihydrogen orthophosphate (NaH_2PO_4)	BDH Chemicals, Victoria, Australia
Disodium hydrogen orthophosphate (Na_2HPO_4)	Merck Pty. Limited, Victoria, Australia
Sodium Hydroxide (NaOH)	Ajax Finechem, NSW, Australia
Glutaraldehyde 25% solution	PST ProSciTech, Queensland, Australia

Distilled water	Neuropathology division, IMVS, Adelaide
Isoflurane	Veterinary Companies of Australia Pty Ltd., NSW
Ketamine	Lyppard, Australia
Xylazine	Lyppard, Australia
Minims benoxinate (oxybuprocaine) hydrochloride 0.4%	Chauvin Pharmaceuticals Ltd, UK
Oxygen	Animal House, IMVS, Adelaide
Xylene	Ajax Finechem, NSW, Australia
Absolute Alcohol	Ajax Finechem, NSW, Australia
Haematoxylin stain	HDS Scientific, VIC, Australia
Eosin stain	HDS Scientific, VIC, Australia
Histolene	Ajax Finechem, NSW, Australia
DePeX	BDH, England, UK
Glutaraldehyde 25% solution	PST ProSciTech, QLD, Australia
Sodium Cacodylate-trihydrate (Cacodylic acid)): MW-214.02	PST ProSciTech, QLD, Australia
Sucrose	Merck Pty. Limited, VIC, Australia
Osmium Tetroxide	PST ProSciTech, QLD, Australia
Ethylene alcohol	Ajax Finechem, NSW, Australia
Propylene oxide	BDH Chemicals, Victoria, Australia
MNA, MW-178.19	TAAB Lab, England, UK
DSA, MW-266.38	TAAB Lab, England, UK
TAAB Embedding Resin	TAAB Lab, England, UK
DMP-30 [2,4,6-tri (dimethylaminomethyl) phenol], MW- 265.40	TAAB Lab, England, UK
Toluidine blue	PST ProSciTech, QLD, Australia
Acetone	Merck Pty. Ltd, VIC, Australia
Uranyl Acetate	Electron Microscopy Unit, IMVS, Adelaide
Lead Citrate	Electron Microscopy Unit, IMVS, Adelaide
ApopTag Plus Peroxidase In Situ Apoptosis Detection kit S7101	Chemicon International, Temecula, CA, USA

Xylene	Ajax Finechem, NSW, Australia
Absolute alcohol	Ajax Finechem, NSW, Australia
Hydrogen Peroxide 30%	Ajax Finechem, NSW, Australia
Methanol (100%)	Ajax Finechem, NSW, Australia
Citric acid (for Citrate buffer pH 6.0)	May & Baker Ltd, England, UK
EDTA	Merck Pty. Limited, VIC, Australia
Normal Horse Serum	SAFC Biosciences, Kansas, USA
NF-L mouse anti-rat primary antibody (Monoclonal)	Sigma-Aldrich, USA
Beta-APP mouse anti-rat primary antibody (Monoclonal)	Sigma-Aldrich, USA
ED-1 mouse anti-rat primary antibody (Monoclonal)	Serotec, UK
GFAP rabbit anti-horse antibody (Polyclonal)	DAKO, Denmark
Biotinylated anti-mouse secondary antibody	Vector laboratories, Burlingame, CA, USA
Biotinylated anti-rabbit secondary antibody	Vector laboratories, Burlingame, CA, USA
Streptavidin peroxidase conjugate	Pierce, California, USA
3,3'-diaminobenzidine tetrahydrochloride	DAKO, Denmark

The following equipments and instruments used in this research were obtained from the companies or departments listed in Table 4.

Table 4. Sources of scientific instruments.

Instrument	*Source*
Hamilton Syringe	Hamilton, USA
30G needles	Becton Dickinson & Co., New Zealand
Digital pH meter	TPS Pty. Ltd., QLD, Australia
Non-critical electronic balance (K0040)	A&D Company Ltd.
Stirrer with hot plate	FSE scientific
Glassware	Neuropathology Division, IMVS, Adelaide
500ml IV saline infusion bags	Animal House, IMVS, Adelaide

IV infusion stand	Animal House, IMVS, Adelaide
Dissection instruments- forceps, scalpels, bone cutters	Animal House, IMVS, Adelaide
Paraffin processing & sectioning	
Automatic tissue processor (Tissue-Tek VIP5)	Sakura, Australia
Embedding platform (Tissue-Tek Cryo Console)	Miles Scientific, Australia
Microtome (Leica RM 2235)	Leica, Germany
Tissue flotation bath (TFB35)	Medite, Germany
Polysine slides	Menzel GmbH & Co., Braunschwerg
Oven	SEM, Australia
Coverslips	HDS, Victoria, Australia
Resin processing & sectioning	
Analytical balance	IMVS, Adelaide
Suspension Mixer/ Rotator	Ratek, Australia
Embedding capsules	TAAB Lab, England, UK
Flat moulds	TAAB Lab, England, UK
Hot oven for polymerisation	SEM, Australia
Glass knife machine (Leica EMKMRZ)	Leica, Germany
Ultramicrotome (Leica EMUC6)	Leica, Germany
Diamond knife	Electron Microscopy Unit, IMVS, Adelaide
Copper/Rhodium Grids 150 mesh square	ProSciTech, QLD, Australia
Grid storage box (numbered)	ProSciTech, QLD, Australia
Immunohistochemistry	
Microwave-1 (Panasonic NE-1037)	Panasonic company
Microwave-2 (NEC)	NEC Electonics
Wax Pen	DAKO, Denmark
Light microscopy	
Light microscope equipped with camera (Olympus BX 41 & BX-UCB)	Olympus, Japan
Image analysis software system-AnalySIS	Analysis, Germany

Transmission Electron Microscopy	
Transmission electron microscope (Philips CM100 TEM) with automated stage, including relocation software, multiple specimen and tilt rotate holder; SIS Megaview II CCD camera and AnalySIS software.	Adelaide Microscopy, The University of Adelaide, Adelaide

4.3 Methods

4.3.1 Experimental Plan

Eight rats were used for the sham experiment. Sixty rats were used for the NMDA experiment, which were divided into experimental groups (0hrs, 24hrs, 72hrs and 7days). [See Table 5]

Table 5. Experimental plan of the research showing experimental groups and number of rats used in each group.

	Number of animals		
Experimental Group	*For paraffin processing*	*For resin processing (optic nerves)*	*For resin processing (optic tracts)*
0 hrs	5	5	5
24 hrs	5	5	5
72 hrs	5	5	5
7 days	5	5	5
Total	**20**	**20**	**20**

4.3.2 Making NMDA Solution from powder

NMDA solution was prepared as a 4 mM stock solution in 0.9% isotonic normal saline. 0.000588grams powder was measured on analytical balance and then mixed thoroughly with 1ml of normal saline on vibrator. 5µl of 4mM NMDA (20nmol) caused temporal retinal and optic nerve damage during the pilot study, this dose was used for intravitreal injection to cause retinal excitotoxicity.

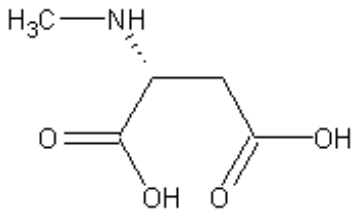

Figure 16. Chemical Structure of N-Methyl-D-Aspartate.

4.3.3 Intravitreal Injection technique

The excitotoxic RGC injury model was prepared in a manner similar to that described in the literature.[469, 470] To ensure comfort to the animal, general as well as local anaesthesia was used. General anaesthesia was induced by placing the rat in a transparent, plastic induction chamber and delivering 4L/min isoflurane in 4L/min oxygen via a calibrated vaporizer. Depth of anaesthesia was checked by pinching the toe of the rat and assesing the withdrawal reflex. Absence of response to painful stimuli indicated appropriate level of anaesthesia. Maintenance of anaesthesia was achieved with 2.5L/min isoflurane in 2.5L/min oxygen delivered through a rodent nose cone covering the mouth and nose of the animal. For topical anasesthesia, 0.4% benoxinate eye drops were instilled in both eyes.

Placing the rat in an appropriate position, a sterile loop made form silk 1-0 was placed around the globe of each eye without any traction. For NMDA experiment, a single dose of 5μl of 4mM NMDA (20nmol) was injected into the vitreous space of the left eye using a microsyringe fitted with a 30-gauge needle. This is because the pilot study indicated that this concentration of NMDA caused temporal changes in the retina and optic nerve over 7 days post injection. In order to minimise the possibility of retinal injury from intravitreal injection, the needle was inserted 2mm behind the limbus from pars plana in the superotemporal quadrant and directed towards the optic nerve. When the tip of the needle reached the mid-vitreous, which could be

seen clearly through the pupil, the injection was administered slowly over 30 seconds. The needle was withdrawn gradually and the eyeball checked for any leakage or bleeding. Right eyes received 5µl of the NMDA vehicle or sham solution (sterile 0.9% saline) to serve as positive controls. Negative controls were performed by injecting needle introduced into the posterior chamber of the left eye but nothing was injected into the vitreous, right received saline for positive control. Throughout the injection procedure, care was taken to maintain appropriate tension in the loop (neither too loose nor too tight) so as to avoid injury to the eyeball as well as the optic nerve.

Animals used to study the morphological changes in the optic tract received 20nmol NMDA into both eyes in order to avoid the bias in the result due to crossing over of the nasal half of optic nerve axons in the optic tract. For the sham experiment, left eyes were injected with 5µl of sterile 0.9% saline and the right eyes remained untouched.

After successful intravitreal injections, anaesthesia supply was turned off and animals were allowed to recover which took no more than 5 minutes. During this recovery period, they were weighed, labelled and transferred back into the cages for variable durations as per the time frame. Clinical examination was conducted and their level of activity checked intermittently after the procedure to ensure an uncomplicated recovery. Rats recovered very quickly without any post-operative infection, signs of distress or weight loss.

4.3.4 Perfusion fixative preparation

For paraffin processing, rats were perfused with 4% paraformaldehyde fixative for better antigen expression, and for resin processing, 5% glutaraldehyde fixative was used.

4.3.4.1 Paraformaldehyde fixative (4%)

Because 4% paraformaldehyde fixative is an unstable solution with a short shelf life, the solution was always prepared fresh and used within 24 hrs of preparation. To prepare 500ml 4% paraformaldehyde fixative:

Step 1. 8% Paraformaldehyde

20 grams of paraformaldehyde powder dissolved in 250ml distilled water in a glass flask was heated at 55-60^{O}C for one hour while continuously stirring it. The flask mouth was covered with a parafilm to prevent inhalation of toxic fumes. After an hour of heating, the solution is left to cool down to room temperature. The milky solution was then cleared with 1M (or 5M) NaOH and filtered using a filter paper.

Step 2. 0.2M Phosphate buffer stock

Appropriate amount of NaH_2PO_4 and Na_2HPO_4 were dissolved in the distilled water as per the measurements given in Table 6.

Table 6. Table showing different phosphate buffer salts, their molecular weights, and the amount used to prepare different volumes of 0.2M Phosphate buffer stock solution.

0.2M Phosphate buffer salt		*Mol. Wt.*	*g for 250ml fixative*	*g for 500 ml fixative*	*g for 1L fixative*
NaH_2PO_4	$.H_2O$	137.9	0.655	1.31	2.62
	$.2H_2O$	156.01	0.741	1.482	2.964
Na_2HPO_4	.anhydrous	141.96	2.864	5.728	11.456
	$.2H_2O$	178	3.591	7.183	14.365
	$.12H_2O$	358.14	7.226	14.451	28.902
Distilled Water			125ml	250ml	500ml

NaH_2PO_4= Sodium dihydrogen orthophosphate; *Na_2HPO_4*= Disodium hydrogen orthophosphate; *Mol. Wt.*= Molecular Weight; *H_2O*= Water; *M*= Molar; *g*= Gram; *L*=Litre

Step 3. 4% Paraformaldehyde in 0.1M PBS, pH 7.4

Freshly prepared and cleared 8% Paraformaldehyde solution was added to 0.2M phosphate buffer solution and the level brought up to 500ml with distilled water. After adjusting the pH to 7.4 (7.38-7.42) with 1M NaOH at room temperature, the solution was stored at 4^{o}C to be used within 24 hrs.

4.3.4.2 Glutaraldehyde fixative (2.5%)

To prepare 500ml 2.5% glutaraldehyde fixative, 50ml of 25% glutaraldehyde was added to the freshly prepared 4% paraformaldehyde in 0.1M PBS mixture at step 3. The steps followed for 4% paraformaldehyde were same as described above.

4.3.5 Animal perfusion

Animals were killed humanely by cardiac perfusion at various time intervals (immediately, 24hrs, 72hrs and 7days after injection); 20 NMDA injected rats were perfused with 500ml of 4% parafomaldehyde in 0.1M phosphate buffer fixative and the tissue taken for paraffin processing after dissection. Although the paraffin sections provided excellent retinal morphological detail and an opportunity for immunohistochemical analysis, resin sections were necessary for ultrastructural details of RGCs, optic nerve and optic tract; hence, two sets of animals (n=40) were killed by intracardiac perfusion with a solution of 2.5% glutaraldehyde with 4% paraformaldehyde in 0.1M Phosphate buffer pH 7.4. All eight rats for the sham experiment were also perfused with 2.5% glutaraldehyde fixative.

For the procedure, the rats were anaesthetised with freshly prepared ketamine/xylazine solution (each 10 ml mixture contained 1.0 ml ketamine and 0.5 ml xylazine in 8.5 ml normal saline) administered via intraperitoneal injection using a 25 gauge 12.5mm needle at a dose of 0.1 ml/10 grams body weight. Animals were restrained by grasping the loose skin of the back and neck and the needle inserted into the left caudal area of the abdominal cavity, thus avoiding injury to any vital organs.

Under deep anaesthesia, animals were fixed with a tape (with ventral surface facing forwards and the limbs stretched). A vertical midline incision was made extending from the upper end of the sternum to the lower abdomen. Separating the skin and cutting the abdominal muscles along the subcostal margins, the chest was opened through lateral thoracotomy and the anterior thoracic wall lifted after cutting through the diaphragm. Care was taken not to damage the underlying heart, lungs and major vessels. Further procedure was done rapidly to

minimise ischaemic damage to the tissues. The pericardium was incised to expose the heart. Placing an incision in the right atrium, the animal was perfused with 50-60 ml saline followed by approximately 1ml/gm of fixative (minimum 300ml) infused through a butterfly needle inserted into the left ventricle. The perfusion has completed when the fluid escaping from the right atrium was clear (~10 minutes). To achieve adequate fixation, the perfused animal was left for 45min to 1hr before decapitation and the head left in the fixative for a further 1hr before dissection.

4.3.6 Tissue Dissection

To minimise stretch injury to the optic nerve caused by direct enucleation of the globe, the eye, optic nerves and tracts were dissected through the cranial route. After separating the scalp and temporalis muscle from the skull, craniotomy was performed and the brain was raised slightly to visualize the optic nerves entering the middle cranial fossa through the superior orbital fissure on its undersurface. Intracranial parts of the optic nerves were separated from the optic chiasm with fine scissors and the brain lifted out of the cranium after incising the remaining cranial nerves also.

Table 7. Tissue specimens obtained from individual animal.

No.	*Left side (NMDA injection)*	*Right side (Saline injection)*
1.	Eye	Eye
2.	Intraorbital ON, PS for TS (segment 1)	Intraorbital ON, PS for TS (segment 1)
3.	Intraorbital ON, DS for LS (segment 2)	Intraorbital ON, DS for LS (segment 2)
4.	Intracranial ON, PS for TS (segment 3)	Intracranial ON, PS for TS (segment 3)
5.	Intracranial ON, DS for LS (segment 4)	Intracranial ON, DS for LS (segment 4)

NMDA= N-Methyl-D-Aspartate; ON= Optic nerve; PS= proximal segment; TS= transverse section; DS= distal segment; LS=- longitudinal section.

In the base of the skull, the eye and optic nerves were approached by carefully opening each orbit. The walls of the orbit were cut with fine bone cutting scissors. Utmost care was taken at this stage so as not to damage or stretch the optic nerves as they entered the cranium through the optic canal. Retro-orbital tissues including the lacrimal gland, fat and extraocular muscles surrounding the intraorbital part of the optic nerve were removed, leaving behind the eye and the optic nerve. Eyes were separated by cutting the optic nerve 1mm behind the globe. The optic nerve was divided into four equal segments from proximal (nearer to the eye) to the distal end (away from the eye i.e. nearer to the brain) with each segment measuring approximately 2mm.[See Table 7]

Optic tracts were dissected from the base of the brain from a set of animals, which received NMDA injection into both eyes. Throughout the dissection, the dissecting field was irrigated intermittently with the fixative to prevent drying up of the tissues. Dissected eyes, optic nerve segments and optic tracts were postfixed in the perfusion fixative for 24hrs to be processed later.

4.3.7 Paraffin processing and sectioning

4.3.7.1 Cassette Preparation

The eyes and optic nerves for light microscopy and immunochemistry were embedded in paraffin. After leaving in 4% paraformaldehyde fixative for overnight (~24hrs) in refrigerator, the dissected tissues were shifted into the cassettes for automatic processing in the Tissue-Tek VIP processor. The eyes were directly placed in the cassettes after creating a window on one side. However, each optic nerve segment was laid between two rectangular foam pads in

the cassette to prevent their escape from the cassette slits. All the cassettes were labelled properly and left in 10% neutral bufferred formalin before processing.

4.3.7.2 Processing and embedding

Fixed tissues were processed for overnight under vacuum in the automatic processor.The processing schedule was 20 minutes in each graded ethanol bath (50%, 70%, 80%, 95% and 2 X 100%), followed by two xylene baths of 1.5hrs each, and finally four paraffin baths of increasing time of 30 minutes, 60 minutes, 60 minutes and finally 90 minutes each. The processed tissue was embedded in paraffin blocks using embedding equipment (Tissue Tek VIP; Sakura Finetek, Torrance, CA). For the longitudinal sections of the optic nerves, segments 2 and 4 were laid parallel to the surface of the mould and for the transverse sections, segments 1 and 3 were made to stand perpendicular. Prepared moulds were left to set on the cold plate at temperature -0.5^{o} C for 25-30 minutes, following which paraffin blocks were taken out and stored at the room temperature before sectioning.

4.3.7.3 Sectioning

Each block was cut using a rotary microtome to obtain seven micron thick sections. Paraffin blocks were set on ice for 5-10 minutes to harden the cutting surface. Prolonged cooling was avoided which could crack the surface of the block. A sharp trimming knife was installed in the microtome. The paraffin block was trimmed using a knife to leave some wax around the tissue and to obtain parallel sides. The trimmed block was fitted on the block holder and oriented. The block was advanced until it touched the knife edge. The full face of the block was trimmed by taking thicker (20 μm) sections, following which a series (or ribbon) of sections of 7μm thickness were cut and spread on a hot water bath (at 45^{o}C). Separating sections whilst

floating on the water with gentle pressure from the tip of forceps, two sections were collected on each clean polysine glass slide. Poly-L-lysine provides excellent adhesiveness to the slides without any background staining. The slides were held vertical and the sections rolled to draw any water under the sections. Eight slides were prepared from each block and each slide carried two sections. After labelling the slides with the animal and tissue specimen number, slides were dried on a heater for about 15-20 minutes to ensure the section was firmly attached and then left in the oven set at 45^{o}C for overnight for maximum section adhesion.

4.3.8 Haematoxylin & Eosin (H & E) staining

Three (out of eight) slides with the paraffin sections of eyeballs and optic nerves were randomly selected for H & E staining. Slides were placed in a metal slide holder and,

- Sections were deparaffinised and rehydrated using

  Xylene 2 X 2 minutes (blot excess xylene before going into ethanol)

  100% alcohol 1 minute

  90% alcohol 1 minute

  Tap water 1 X 5 minutes

- After rinsing the slides in water, excess water from the slide holder was drained before going into haematoxylin. Also, the surface of haematoxylin was skimmed using a Kimwipe to remove oxidized particles.
- Sections were placed in Lillie Mayers alum Haematoxylin for 5 minutes. They were then rinsed in tap water for the second time followed by dipping (5-6 quick dips) in a differentiator bath of acid alcohol to clear the cytoplasmic staining. After a further rinse in running tap water, sections were then placed in saturated aqueous lithium carbaonate for

10-15 seconds or until the sections turn blue. They were then rinsed in running tap water for 5 minutes.

- After draining the excess water from slide holder,
- Slides were counterstained with eosin (Eosin {yellowish} 15g, Erythrosin 5mg, Calcium Chloride 5g, Water 2L) for 2 minutes. The slides were then dehydrated with

95% alcohol	5dips
100% alcohol	15 seconds
100% alcohol	15 seconds
Histolene	2 minutes
Histolene	slides left until mounted

- Slides were coverslipped using Gurr's Depex mountant. A drop of mounting medium was placed on the slide. Holding the coverslip at an angle, it was allowed to fall gently onto the slide. After the depex spreads evenly underneath the coverslip covering all the tissue, a gently pressure was applied on the coverslip with a forceps to remove any air bubbles.
- Slides were left overnight in the fumehood to dry at room temperature.

4.3.9 TAAB-resin processing and sectioning

4.3.9.1 Processing and embedding

To obtain greater cytological and nuclear details, semi-thin (less than 1μm) and ultrathin (60-80nm) sections of the eyes, optic nerves and optic tracts were obtained from the manually processed and resin-embedded tissue. Because the eye specimens were too big for resin sectioning, they were trimmed to preserve only a small part from the posterior globe adjacent to the optic disc. A standard method for resin processing of nerve specimen used in the division of Neuropathology, IMVS, Adelaide was followed. All the steps were performed in

fume hood to avoid inhalation of toxic chemicals. Infiltration of resin was improved with agitation (using a rotator). To begin with, tissues obtained form the rats perfused with 2.5%glutaraldehyde fixative were transferred into polypropylene vials and post-fixed in the same fixative for overnight at room temperature.

After overnight fixation in glutaraldehyde, the tissue vials were shifted onto the rotator, where the tissues were rinsed several (minimum three) times in sodium cacodylate buffer (with sucrose, pH 7.4), keeping the tissue for at least 30 min in the buffer each time. Taking the vials off the rotator, the tissue was post-fixed in 1% osmium tetroxide (OsO_4) for overnight at room temperature. Shifting the vials back onto the rotator next day, the tissues were thoroughly rinsed in sodium cacodylate buffer (with sucrose, pH 7.4) three times for 30 minutes each, following which they were dehydrated in a graded alcohol series.

70% alcohol	1 X 30 minutes
95% alcohol	1 X 30 minutes
100% alcohol	3 X 30 minutes

Dehydrated tissue was then infiltrated in fresh TAAB-Epoxy resin, method of preparation of which is described below (see Table 6). Because alcohol is immiscible with resin, propylene oxide (2-epoxypropane) was used as a linking agent (clearing agent) after dehydration. Tissue was shifted straight from 100% alcohol into

Propylene oxide: resin (1:1)	1 X 30 minutes
Propylene oxide: resin (1:3)	1 X 30 minutes

Taking the vials off the rotator, the tissue was left in pure resin for one hour under vacuum to hasten the infiltration of viscous TAAB resin into the tissue. Care was taken to cover the

tissues well with the resin. Because the tissues were very small, 0.5-1 ml of resin was sufficient for each specimen. After giving two more changes of resin, each for 1hr, the tissues were left under vacuum in pure resin for overnight.

The following day, the tissues were shifted into freshly prepared resin several times. (under vacuum)

TAAB resin	1 X 1hr
TAAB resin	1 X 2hrs
TAAB resin	1 X 3hrs

After preparing labels indicating the animal number and tissue specimen number, the tissues were embedded in resin and left in oven at 60^{o}C for overnight to polymerise. Flat-bottomed capsules were found most suitable for the eyeballs, optic nerves segments for longitudinal sections and optic tracts. Flat cuboidal moulds were used to embed the optic nerve segments for transverse sections.

4.3.9.2 TAAB EPON Resin mixture preparation

Epoxy resin is a chemical substance which contains three-membered ring formed by an oxygen atom bonded to two carbon atoms.[471] When heated, cross linkages between the molecules causes its polymerization into an irreversible rigid three dimensional structure. Epoxy resins, therefore, have high mechanical strength and produce little shrinkage.[471]

For the processing, resin was prepared fresh each day. To prepare different amounts of resin, each content was weighed on the analytical balance according to the measurements provided

in the table [See Table 8]. Contents were thoroughly mixed with a glass rod or a stirrer for one hour at room temperature. The unused resin was discarded after polymerization.

Table 8. Amount of ingredients needed to prepare TAAB EPON resin.

Ingredients	*Amount (g)*			
MNA	3.16	6.31	9.47	12.63
DDSA	1.57	3.15	4.72	6.29
	4.73	9.46	14.19	18.92
Resin	5.27	10.54	15.81	21.08
TOTAL	**10**	**20**	**30**	**40**
DMP-30	0.13	0.27	0.4	0.54

MNA= Methyl Nadic Anhydride; DDSA= Dodecenyl Succinic Anhydride; DMP= 2,4,6-tri (dimethylaminomethy)l phenol; g= Grams

4.3.9.3 Semi-thin sections and Toluidine blue staining

Semi-thin sections (less than 1μm) were cut on a mechanical ultramicrotome in which the cutting stroke is motor driven to provide a regular, smooth motion for sections of even thickness and constant reproducibility. Initially, the polymerised resin blocks containing tissue specimens were trimmed with a razor blade to remove excess resin from the sides and surface. The trimmed block and glass knife with a sharp edge were fixed in the block holder and knife stage of the ultratome, respectively. Because glass knives are hard but brittle, care was taken in their handling. Also, because knives deteriorate with storage, they were prepared immediately before use. The block was brought to the knife edge under microscopical control and 0.5μm thick sections were cut. Floating each section onto a water bath adjacent to the knife edge, sections were collected with a brush and floated on a few drops of water taken on labelled polysine slides. Sections were stretched by heating for up to 20 seconds on the hot

plate (heated to 110°C). Tipping-off the water carefully, sections were dried on the hot plate for 1 hour and stained later.

Epoxy-resin embedded semi-thin sections are commonly stained with toluidine blue stain.[472] The technique is useful for determining the general morphology of a specimen before sectioning further. For staining with toluidine blue, sections were flooded, on a hot plate (at 110°C), with filtered toluidine blue solution (prepared by mixing 1g toluidine blue and 1g borax in 100ml distilled water) for up to 30 seconds. Care was taken not to let the sections become dry at this stage. Slides were then washed in running tap water for a few seconds to wash off the excess stain and left to dry at room temperature. The sections were mounted and coverslipped (as described previously).

4.3.9.4 Grid preparation and staining

Thin sections (60-80nm) were cut in the same manner as semithin sections, but using a diamond knife. The diamond knife was kept wet for a minimum of 15 minutes before sectioning. Thickness of the sections floating on the water bath adjacent to the knife edge was checked using standard colour codes. Only silver to gray appearing sections, which varied in thickness from 60-80nm, were picked on the 150 mesh acetone-washed copper grids. Prepared grids were left to dry for overnight at room temperature.

Thin epoxy resin sections were stained with Uranyl acetate and Lead citrate stains. Stored stains were centrifuged at 3,000 rpm for 5 min before use. Precipitates, which developed with standing over time, settled at the bottom and supernatants collected into separate embedding capsules. Grids were stained with uranyl acetate for 1 minute (at 45°C) followed by thorough

rinsing in the water collected from micropore system and warmed on the hot plate. After draining the excess water by touching the grid to a filter paper, the grid was stained with lead citrate for 30 seconds (at 45^{o}C) followed by a quick rinse in the water again. Stained grids were dried at room temperature and stored in appropriately labelled grid storage box.

4.3.10 TUNEL labeling

Gavrieli et al (1992) described a method for staining cells that have undergone DNA fragmentation by internucleosomal endonuclease cleavage.[473] The method is referred as Terminal deoxynucleotidyl transferase-mediated dUTP nick end labeling (TUNEL) method. For the present study, TUNEL methodology was used for the detection and quantification of apoptosis induced by NMDA in inner neural retinal elements. Because negative results do not necessarily mean the absence of DNA cleavage, but may result from loss of TdT activity or degradation of trinucleotides, positive controls (spinal cord ischaemia slides supplied by neuropathology division, IMVS) were always stained with each staining run to confirm that staining had indeed worked and to avoid analysing false negatives.

Paraffin-embedded eyeball sections were deparaffinised in three changes of xylene for 5 minutes each, followed by rehydration with 2 changes of 100% alcohol for 2 minutes each, 95% alcohol for 1 minute and 70% alcohol for 1 minute. Sections were then rinsed in 0.1M PBS (pH 7.4) for 5 minutes followed by incubation in 10μg/ml proteinase K (stock solution 5mg/ml, 40μl pipetted into 10 ml 0.1M PBS) for 15 minutes at room temperature. Washed in distilled water, sections were then incubated in 10%H2O2 for 5 minutes to block endogenous peroxidise activity. After washing in PBS twice for 5 minutes each, and treatment with equilibration buffer (11μl buffer per section) for at least 10 seconds, tissues were incubated in

TdT enzyme reaction mixture (70% reaction buffer and 30% TdT) for 1 hour at 37°C in a humidified atmosphere. Slides were rinsed in stopwash buffer for 10 minutes and in PBS three times for 1 minute each. Sections were covered with conjugate buffer for 30 minutes at room temperature, rinsed in PBS four times for 2 minutes each, incubated in DAB (294μl DAB buffer with 6μl DAB substrate) for 6 minutes, rinsed in distilled water and after counterstaining with haematoxylin, slides were coverslipped.

4.3.11 Immunohistochemical staining

Immunohistochemistry is the process of localization of protein molecules in tissues based on the principle of binding antibodies to their specific antigens. Antigen-antibody interaction is detected by using various markers such as fluorescent dye, radioactive materials, gold and enzymes.[474-477] Major advantage of using immunohistochemistry is that, unlike traditionally used staining methods, it identifies specific protein or enzymes present in the tissue. Availability of numerous antibodies help in locating unlimited number of cellular protenacious structures. Therefore, immunohistochemistry has become an important and widely used technique in clinical and medical research laboratories.

A set of 4 antibodies, namely NF-L, β-APP, GFAP and ED-1, were used to characterize reactive and degenerative changes in the retina and optic nerve after NMDA-induced excitotoxic retinal injury. Immunohistochemistry was performed on paraffin-embedded tissue using the standard and sensitive labelled streptavidin-biotin (LSAB) method.

Paraffin sections of paraformaldehyde fixed tissues were deparaffinized with xylene (two changes of xylene for 2 minutes each) and then rehydrated with absolute alcohol (twice for 2

minutes). To inactivate endogenous peroxidase and to quench the non-specific staining, sections were incubated in 3% H_2O_2 in methanol for 30 minutes (2 ml of 30 % H_2O_2 in 100 ml of 100% pure methanol or 10 ml of 30 % H_2O_2 in 500 ml of 100% pure methanol) and then rinsed with 0.1 M Phosphate Buffer Saline (PBS, pH 7.4) 3 times for 5 minutes each.

To break the protein cross-links formed by the formalin fixation and to uncover the hidden antigenic sites, heat induced epitope retrieval (HIER) technique was used. Batches of slides were placed in 250ml of retrieval solution (see Table 9), and heated in the microwave (Panasonic-1037, at power level 2 or 3), until it reached the boiling point. The slides were further heated in the microwave (NEC company, at power level 2 or 3) for 10 minutes and then allowed to cool for 20 minutes at room temperature. After rinsing with PBS thrice, sections were encircled with a wax pen and blocked with 3% Normal Horse Serum (NHS) for 30 minutes. They were then incubated in primary antibody [See Table 9] for overnight at room temperature.

After 16-18 hrs of incubation in primary antibody, sections were rinsed with PBS and reacted with the matched biotin-conjugated secondary antibody [See Table 9] for 1 hour at room temperature. Rinsing in PBS, slides were then incubated in 'SPC' marked streptavidin peroxidase conjugate (1:1000, prepared with 3% NHS) for 1 hour. Sections were washed with PBS again and then diaminobenzidine (DAB) [221] mixture (prepared by dissolving 300µl DAB and 50µl 30% H_2O_2 with 50 ml of 0.1 M PBS at pH 7.4) was applied to the sections for 6 minutes to make the peroxidase activity visible. Extra and waste DAB mixture was activated using 0.2M sulphuric acid and potassium permanganate. After rinsing in PBS once again, sections were counterstained with haematoxylin, dehydrated in graded alcohols, cleaned in

histolene and coverslipped under DePeX. After drying at room temperature for overnight, slides were observed under light microscope.

Table 9. Details of primary antibodies, antigen retrieval solutions and secondary antibodies used in the immunohistochemical staining.

Primary antibody (in 3%NHS)			***Antigen retrieval solution***	***Secondary antibody, biotinylated***
Antibody for	Host	Dilution	Buffer	(1:250, in 3% NHS)
NF-L	mm	1:3000	citrate buffer (pH 6.0)	anti-mouse IgG
β-APP	mm	1:10,000	citrate buffer (pH 6.0)	anti-mouse IgG
GFAP	rp	1:40,000	citrate buffer (pH 6.0)	anti-rabbit IgG
ED-1	mm	1:500	citrate buffer (pH 6.0)	anti-mouse IgG

NHS= Normal horse serum; NF-L= Neurofilament-light; β-APP= Beta-Amyloid precursor protein; GFAP= Glial fibrillary acidic protein; mm= *Mouse monoclonal;* rp= *Rabbit polyclonal;* IgG= *Immunoglobulin-G*

4.4 Data Analysis

4.4.1 Histological analysis of rat retina

Three randomly selected Haematoxylin and Eosin (H&E) stained paraffin sections of the eyes were examined by light microscopy and retinal damage was evaluated using well described methodology.[478-480] As resin-embedded eye sections contained only a small part of the posterior globe and not the entire retina, they were preserved for electron microscopy. For the paraffin sections, histological and morphometric evaluations were carried out under a light microscope equipped with a digital DP12 Olympus camera. To reduce sampling errors, three adjacent, but, non-overlapping light microscope images (at 200X magnification) were photographed from both posterior (200μm from the optic disc), and peripheral (3mm from the optic disc) retinas. The cell counts in the ganglion cell layer (GCL) and the inner retinal thickness (IRT, from the junction of outer nuclear and outer plexiform layer to the inner limiting membrane along a vertical line) were measured on photographs (268 X 201mm). The number

of cells in the GCL counted over a constant length of 9 inches on the printed image expressed a cell count per 300μm retinal length. All measurements were done in a masked fashion by a single observer, who was prevented from being involved in the animal experiments, tissue processing or staining and photography. Each picture provided for analyses was coded so as not to display any identification of the animal group to the observer. This reduced bias by preserving symmetry in the observers' measurements and assessments.

4.4.2 Morphological assessment of optic nerve pathway

Toluidine blue stained transverse sections of resin-embedded proximal optic nerve, distal optic nerve and optic tract were examined by the light microscope equipped with Olympus DP12 digital camera. Paraffin sections were not used for this purpose as it was difficult to appreciate the axonal and myelin details. Therefore, for morphological analysis of the optic nerve and optic tract, images were generally collected from resin sections using 10X, 20X, 40X and 100X objectives. Images have been rescaled for presentation in this thesis, with appropriately sized scale bars shown.

4.4.3 Quantitative analysis of optic nerve damage

Following an initial survey of the whole sections, optic nerve changes were quantified. A total of ten images representing approximately 25% of total cross-sectional area were obtained using the method of systematic sampling. Every fourth field of optic nerve section was photographed under oil immersion beginning at extreme upper corner at one end, moving towards the other end in the same row. After reaching the extreme other end of the section, the field just below was selected.[See Figure 17] Pictures were taken staying in the same row and the method repeated until the whole nerve section was covered.

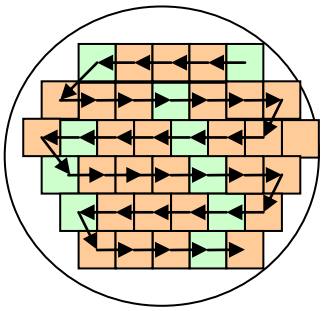

Figure 17. Systematic sampling method for obtaining representative sample photographs from transverse section of the optic nerve.

Optic nerve pathology was analysed in the selected ten fields (field size= 3630 μm^2) using different parameters. Firstly, total number of axons (including normal and abnormal) remaining in each field were counted.[481] Secondly, to assess the axonal pathology, a method modified from Garthwaite et al was used to quantify axonal swelling.[482] Garthwaite et al reported that the density of axons having an average internal diameter above 2.5μm (about average in control rats) was the optimal index of damage. [482] In preliminary analyses with the current model, it was found that more subtle changes could be quantified if the benchmark was increased towards the maximum diameter detected in averaged control sections, about 5μm. Therefore, axons of more than 5μm diameter were counted to express the number of axonal swellings. A third parameter used for assessment of nerve pathology was the myelin damage. All myelin, which appeared thickened, separated, or clumped was counted. All the counts were performed in a masked fashion by a single observer.

4.4.4 Statistical analysis

Retinal and optic nerve images from all 5 animals in each group were analysed. For the retinas, data obtained from three sections (nine images) was averaged for each eye, and thus, two datasets were available for the central and peripheral retina for quantitative analysis of cell

counts in the GCL and IRT. For optic nerves, data obtained from 10 fields for all the three parameters (total number of normal axons, axonal swellings and myelin damage) was averaged for each optic nerve segment and expressed counts per 3630 μm^2.

Analyses were performed using a commercially available statistical software package (SPSS for Windows, version 13.0, SPSS Inc., Chicago, IL). Descriptive analysis provided mean, range, standard deviation and standard error for retinal and optic nerve parameters. Differences in means were analysed using an independent paired sample t-test. This test of significance compared the means of right (saline-injected) versus left (NMDA-injected) retinal and optic nerve data as well as compared the proximal versus distal optic nerve segments at different time points. A p value < 0.05 was considered statistically significant.

Correlation analysis between average number of RGCs (mean of posterior and peripheral retinas) and total number of axons, axonal swellings and myelin damage was examined with the aid of the two-tailed Pearson correlation coefficient. This coefficient reflects the degree of linear relationship between two variables. Expressed as 'R', the Pearson's coefficient value ranges from +1 to -1. A correlation of +1 means a perfect positive linear relationship between the variables. A scatterplot was also prepared to express the degree of relationship graphically. A $p<0.05$ was considered statistically significant.

4.4.5 Ultrastructural study of RGCs and optic nerve

NMDA induced ultrastructural changes in the neuronal cell were analysed by transmission electron microscopy. At lower magnification (X1000), inner retinal layers and various cells in the GCL layer were identified. After identification under low power, RGCs were viewed under

higher magnifications (from X7900 to X92000). In an individual cell, plasma membrane was followed to define the limits of the cell and any structural damage. Distribution and structure of cytoplasmic organelles such as mitochondria, endoplasmic reticulum and Golgi apparatus were studied. Changes in the nucleus were assessed by chromatin distribution and nuclear membrane structure.

For optic nerve, both transverse and longitudinal sections of the optic nerve segments were assessed. Structure of the axon and myelin was examined in detail at each time point. Density and distribution of neurofilaments and microtubules was observed in transverse sections. However, longitudinal sections mainly provided the details of the axoglial relationships in the nodal and paranodal region. Morphology and distribution of the glial cells including oligodendroglia, astrocytes, and microglia were also studied.

4.4.6 Analysis of TUNEL staining

Following TUNEL staining, retinal sections were viewed and photographed using the light microscope equipped with Olympus DP12 digital camera. Images of the inner retina showing ganglion cell layer were collected using the 10X, 20X and 40X objectives. Images were also collected from the positive control slides stained at the same time. Images were opened in Adobe Photoshop 7.0.1 and the normal retina compared with the experimental side at various time points.

4.4.7 Analysis of immunological markers

A qualitative assessment was made under the light microscope at different time points to establish the presence of staining and also to compare the intensity of immunoreactivity between the control and experimental eyes and optic nerves.

CHAPTER 5: PILOT STUDY

Introduction

In order to establish NMDA model and further plan of experiments, two rats from each group of 0hrs, 2hrs, 6hrs, 24 hrs, 72hrs, 7 days and 14 days were taken for preliminary study.

Aims

1. To assess the effects of intravitreal injection of sterile isotonic saline on the retina.

2. To assess whether 5µl of 4mM (20nmol) of intravitreal injection of NMDA causes temporal retinal damage.

3. To assess whether 5µl of 4mM (20nmol) of intravitreal injection of NMDA causes temporal optic nerve damage.

Materials

14 Sprague Dawley rats (Male, 350-400 grams)

Injection Kit: 30G needle, Hamilton syringe, sterile loop, sterile isotonic saline ampoules, freshly prepared 4mM NMDA, blunt foreceps

Perfusion Kit: Perfusion set, Isotonic saline, Small scissors, Artery forceps, Scalpel knife and handle, freshly prepared 4% paraformaldehyde solution

Method

Intravitreal injection and animal killing

To find out answer to aim1, 7 rats were injected with 5µl of sterile isotonic saline into the left eye. Needle was introduced into the posterior chamber of the right eye but nothing was

injected into the vitreous. Animals were perfused with 4% paraformaldehyde in 0.1M PBS fixative solution immediately, 2 hrs, 6 hrs, 24hrs, 72hrs, 7days and 14days after the injection.

To answer aims 2 and 3, 7 rats were injected with 5µl of 4mmol NMDA into the left eye and 5µl of.sterile isotonic saline into the right eye. This dose was used in previous research experiments and resulted in retinal excitotoxicity 1 week post intravitreal injection.[483] Animals were perfused with 4% paraformaldehyde in 0.1M PBS fixative solution immediately, 2 hrs, 6 hrs, 24hrs, 72hrs, 7days and 14days after the injection.

Tissue processing

Eyeballs and optic nerves were dissected as described previously in section. Eyeballs were taken for paraffin sectioning and optic nerves were taken for resin processing. Seven μm thick paraffin sections of eyeballs were taken and stained with Haematoxylin and Eosin stain and a half μm thick longitudinal and transverse sections of intraorbital optic nerve were taken and stained with toluidine blue stain.

Observation and Analysis

Paraffin sections of eyeballs and transverse sections of resin-embedded optic nerves were observed with light microscope under 20X, 40X and 10X (oil immersion) magnifications. Number of cells in GCL per unit length and thickness of inner retinal layer were chosen as parameters to compare injected and control eyeballs. For optic nerve sections, density, shape and structure of axons as well as thickness of myelin were the criteria for comparison. This was designed as an observational study, so data was not quantified.

Results

To answer aim 1, a comparison was made between saline-injected left eye and control right eye. There was no apparent difference in the number of ganglion cells and in inner retinal thickness of the posterior or peripheral retina between two eyes at any time points. Moreover, no change was observed in the structure of axons and myelin in transverse sections of the optic nerve of saline-injected eyes in comparison to the control eyes.

For aims 2 and 3, NMDA injected left side was compared to control right side. No apparent changes were seen in the retina and the optic nerve between two sides at 0 hrs, 2hrs, 6hrs and 24 hrs. Number of RGCs and inner retinal thickness of the posterior and peripheral NMDA-injected retinas appeared to have reduced at 72 hrs. Further decline was seen at 7days and 14 days, with only a few RGCs remaining after 2 weeks.

Resin sections of the left optic nerve showed no apparent changes upto 24 hrs compared to control eye, with evidence of axonal damage appearing at 72 hrs after NMDA injection. Few axons had become swollen with minor differences in myelin thickening. Changes of nerve degeneration increased further at 7 days and 14 days, with almost no normal axon visible at 14 days.

Conclusion

The preliminary study showed no changes in the retina or the optic nerve between saline injected and control eye even after 2 weeks post-injection. Therefore, saline has no observable deleterious effects on the retina and can be used as a safe control injection as well as vehicle for the preparation of NMDA solution from NMDA powder.

Previous reports have shown that the degree of retinal damage depends on the dose of intravitreal excitotoxin.[484-486] Lower doses such as 2nM and10nM NMDA does not affect retina;[453, 485] whereas, 200nM NMDA causes severe retinal damage (85% cell loss in GCL) within a week.[485] This pilot study revealed that the injection of 20nM of NMDA produce temporal retinal damage with obvious loss of RGCs at 72hrs. Even the optic nerve suffers structural damage to axons and glia at 72 hrs. Retinal and optic nerve damage increase on 7^{th} day and further on 14^{th} day. Results confirm that 20nM NMDA can be used as the agent to induce retinal damage and optic nerve degeneration after 24 hrs. As this dose of NMDA caused temporal retinal and optic nerve damage during the pilot study, no further dose response experiments needed to be performed.

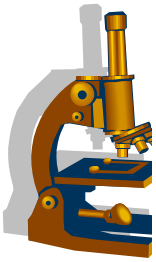

Chapter 6: THE SPATIOTEMPORAL PATTERN OF LIGHT MICROSCOPIC AND MORPHOMETRIC CHANGES

6.1 Introduction

This part of the study involved the use of a compound light microscope for the morphologic examination of the retina and the anterior visual pathway. This is because the advantages of using compound over simple light microscopes are many folds. Besides displaying a much more magnified and coloured view of the tissue, they produce less chromatic and spherical aberrations. Also, they are equipped with lamp units providing stable and controllable illumination. Moreover, they are technically much easier to handle and simple to maintain. Although, limited in their ability to resolve finer details (maximum resolution of 0.2 μm) and to provide three-dimensional details of the focusing object, they provide basic information on which further studies can be based.

The chapter describes the results of histological and morphometric analysis of the retinal, optic nerve and optic tract changes.

6.2 Results

6.2.1 Histological analysis of retinal damage

The first part of the study was focussed on the light microscopic changes in the retina. Negative and positive controls showed no damage at any time point. In comparison to the right sided saline-injected eyes, which showed no changes in the retinal morphology at any time point, histological examination showed progressive degenerative changes in the inner layers of the NMDA-injected retinas beginning after 24 hrs of injection. Although no change

was observed immediately and at 1 day after NMDA injection, thinning of the inner retina and decrease in the number of cells in the GCL were seen at 72 hrs. The damage increased further at 7 days with the inner retina appearing much thinned-out and showing only a few cells in the ganglion cell layer. Although there was a patchy loss of cells in the GCL at some places, the damage was distributed along the entire length of the retina beginning at the optic disc up to the ora serrata. No obvious abnormality was detected in the outer layers of retina at any time point.[See Figure 18] The section below describes the quantitative changes in the cell count in GCL and inner retinal thickness as measured in the posterior and peripheral retinas.

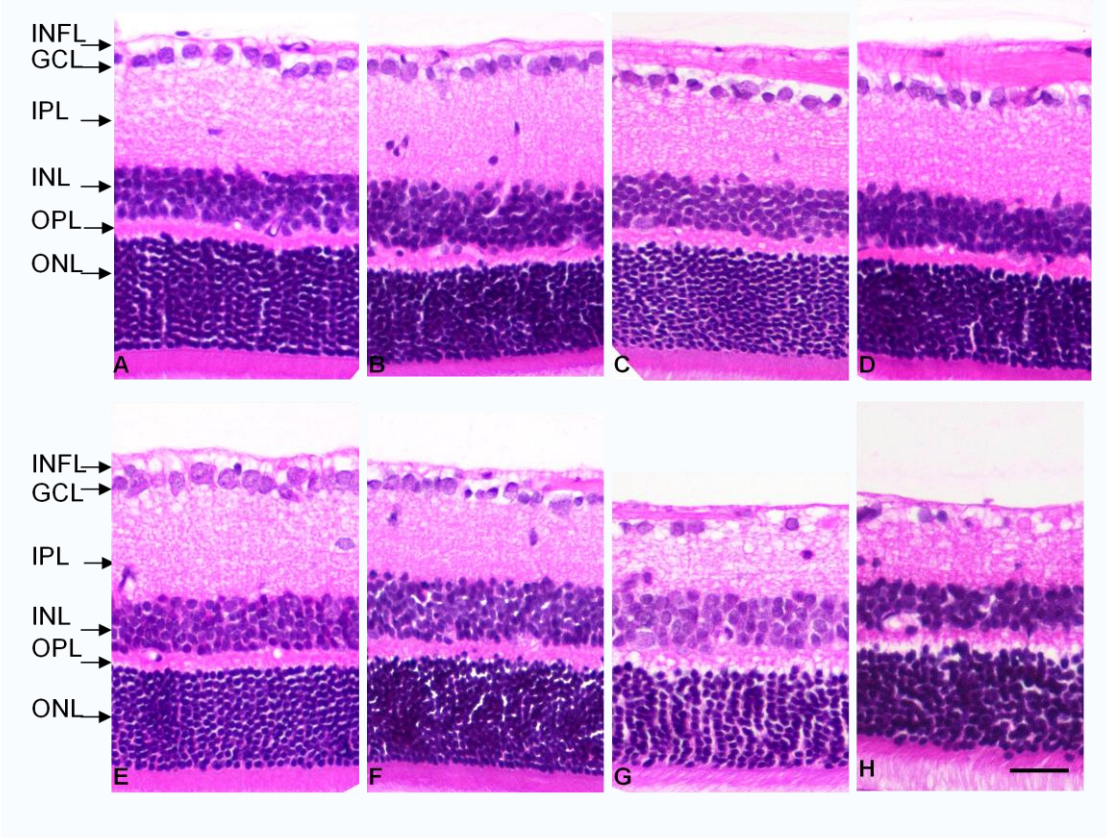

Figure 18. Progressive changes in the retina after NMDA injection in rat as seen in H&E stained paraffin sections.Images are of the posterior retina (200μm from the optic disc). A-D images are from saline injected retinas at 0hrs (A), 24hrs (B), 72hrs (C) and 7days (D). E-F images are from NMDA injected retinas at 0hrs (E), 24hrs (F), 72hrs (G) and 7days (H), X200 magnification. INFL=inner nerve fibre layer; GCL=ganglion cell layer; IPL=inner plexiform layer; INL=inner nuclear layer; OPL=outer plexiform layer; ONL=outer nuclear layer. Bar= 50μm

Cell counts in RGC layer

In saline-injected eyes, the average cell count in the GCL was significantly higher ($p<0.05$) in the posterior retina (16.5 ± 0.3) than the peripheral retina (9.9 ± 0.12). Cell counts in both regions did not change after saline injection at any time point ($p>0.05$). Compared with saline injection, NMDA injection did not produce significant change in cell counts immediately ($p= 0.906$ for posterior and $p= 0.145$ for peripheral retina) and at 24hrs ($p>0.05$ in both regions). However, a significant loss of cells was observed in the GCL in both regions after 72 hrs ($p<0.05$). In comparison to the control eye, 51 % of cells remained in the posterior region and 44% cells remained in peripheral regions in experimental eyes. The cell count decreased further at 7 days in both regions ($p\leq 0.001$), with only 23% and 35% cells remaining in posterior and peripheral retinas. [See Table 10 and Figure 19]

Table 10. Progressive changes in cell count in the GCL. Each value represents mean ± S.E.

Time course of retinal changes				
Time point	RGC count			
	Saline injected (Control) eyes		NMDA-injected fellow (experimental) eyes	
	posterior retina	peripheral retina	posterior retina	peripheral retina
0hrs	16.5 ± 0.3	9.9 ± 0.12	16.4 ± 0.5	10.3 ± 0.2
24hrs	14.5 ± 0.9	9.8 ± 1.16	13.6 ± 0.16	10.3 ± 0.8
72hrs	12.9 ± 0.6	9.6 ± 0.8	6.6 ± 0.7**	4.5 ± 0.3*
7days	14.5 ± 0.4	11.3 ± 0.4	3.4 ± 0.4**	4.0 ± 0.4**

* $p<0.05$ vs. Control fellow eyes (*Student's t-test*)
** $p<0.001$ vs. Control fellow eyes (*Student's t-test*)
NMDA= *N-Methyl-D-Aspartate*

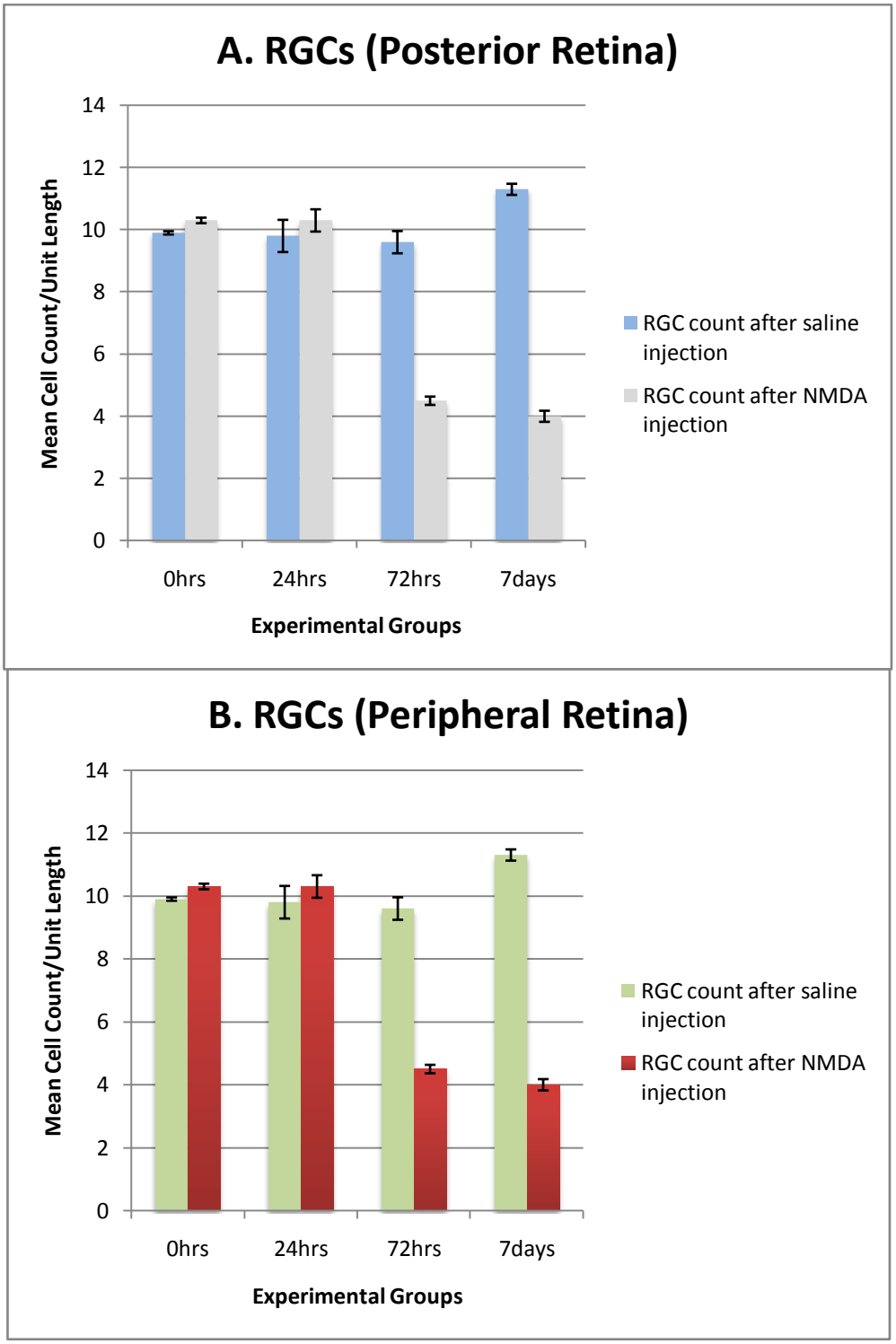

Figure 19. Quantification of RGCs immediately, 24hrs, 72hrs and 7days after saline and NMDA injection from posterior (A) and peripheral retina. (B)

Inner Retinal Thickness

The IRT in posterior and peripheral regions was not significantly different from controls immediately and 24hrs after NMDA injection ($p>0.05$). A significant reduction in IRT occurred in both regions at 72hrs ($p=0.002$ for posterior and 0.012 for peripheral retina). Seven days after NMDA injection, there was a further reduction in IRT in both regions ($p< 0.05$) with the thickness reducing to 68% and 76% in posterior and peripheral regions respectively. [See Table 11 & Figure 20]

Table 11. Progressive changes in inner retinal thickness. Each value represents mean ± S.E.

Inner Retinal Thickness				
Time point	Saline injected (Control) eyes		NMDA-injected (experimental) eyes	
	posterior retina	peripheral retina	posterior retina	peripheral retina
0hrs	93.5 ± 0.5	66 ± 0.7	93.1 ± 0.8	71.7 ± 1.6
24hrs	95.5 ± 6.1	75.5 ± 7.6	94.3 ± 3.4	72.9 ± 4.0
72hrs	95.9 ± 2.5	72.5 ± 4.0	72.2 ± 3.1*	50.5 ± 2.9*
7days	85.7 ± 3.0	70.1 ± 3.6	58.3 ± 5.3**	53.5 ± 3.5*

* *p<0.05* vs. Control fellow eyes (*Student's t-test*)
** *p<0.001* vs. Control fellow eyes (*Student's t-test*)
NMDA= N-Methyl-D-Aspartate

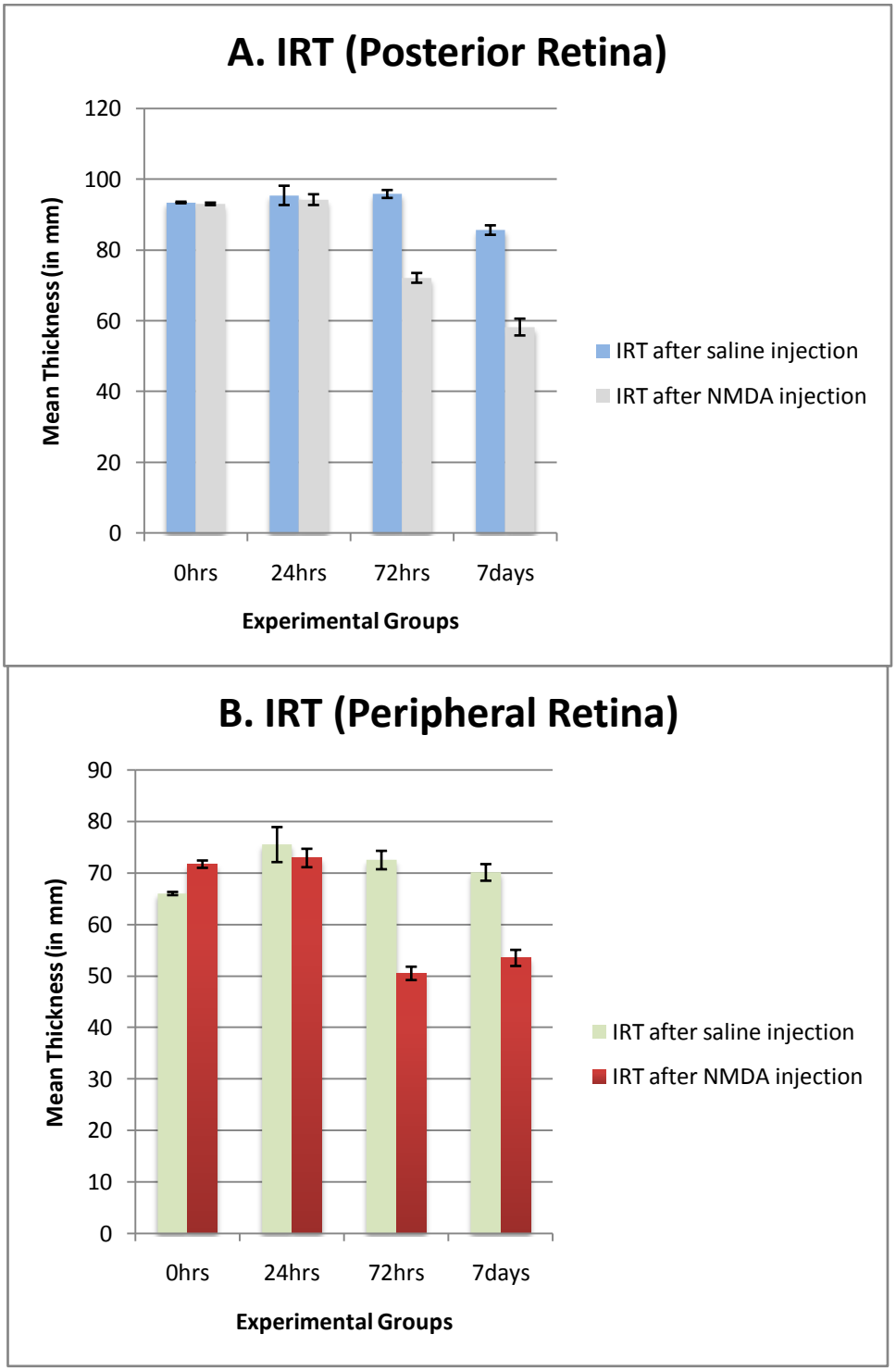

Figure 20. Quantification of IRT immediately, 24hrs, 72hrs and 7days after saline and NMDA injection from posterior (A) and peripheral retina (B).

6.2.2 Morphological examination of the optic nerve and tract

In order to study spatiotemporal light microscopic changes in the optic nerve fibres subsequent to the excitotoxic RGC injury, transverse sections of the proximal segment of the optic nerve, distal segment of the optic nerve and optic tract of the saline-injected right side were compared to the NMDA-injected left side. Negative and positive controls showed no damage at any time point. The following section describes the result of qualitative assessment of the optic nerve and tract changes under the light microscope.

Histology of the normal rat optic nerve

Under low power magnification (X100, X200), a normal optic nerve was surrounded by the epineurium, with septa dividing the nerve into fascicles. Many blood vessels were seen running in the septa. Each fascicle contained nerve fibres of various diameters distributed homogenously across the nerve. Under high power magnification (X400 and X1000), these fibres could be arbitrarily divided into small and large-sized, depending on their diameter. Smaller diameter fibres were numerous and fibres of larger diameter were diffusely scattered between them. Individual nerve fibre contained a centrally lying pale axon surrounded by the thick and compact myelin sheath, which stained intensely with toluidine blue. Under oil immersion (X1000), many glial cells were identified in the inetrfascicular region. Cells in the interfascicular region containing small, regular and dark staining nuclei were identified as oligodendrocytes. [See Figure 21]

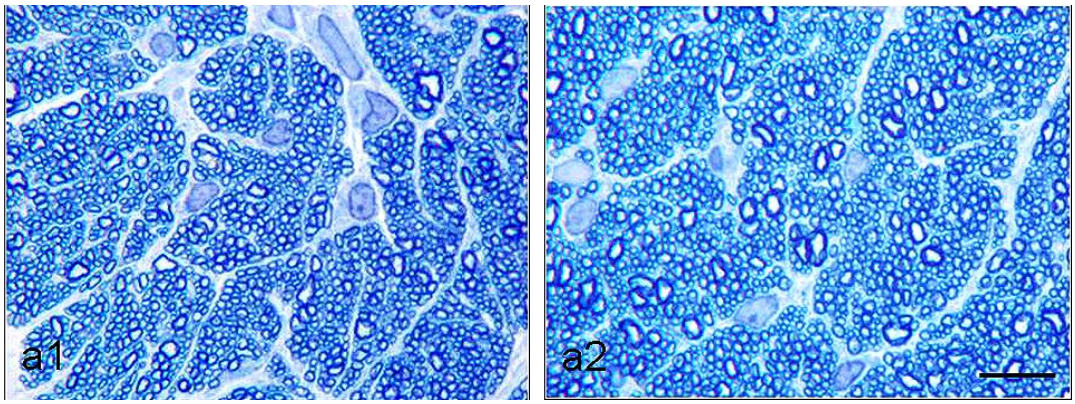

Figure 21. Transverse sections of the normal rat optic nerve. Sections are taken from right optic nerve immediately after saline injection into right eye; toluidine blue stain. (a1-Proximal Segment, a2-Distal Segment). Bar= 10μm

Histology of the normal rat optic tract

Transverse sections of the optic tract appeared as an oval structure sitting over the thalamus containing large neurons. It was easy to identify optic tract as transversely cut and compactly packed fibres in the tract (white matter) with more intense staining than the scattered thalamic nuclei (gray matter). Under oil immersion (X1000), the structure of the optic tract appeared similar to the optic nerve with nerve fibres of various sizes. Each nerve fibre had a pale round central axon surrounded by the thick compact myelin. Unlike optic nerve, the average diameter of axons was slightly greter and the nerve fibres were not packed into fascicles. In the absence of septa, very few blood vessels and glial cells were seen scattered between nerve fibres. [See Figure 22]

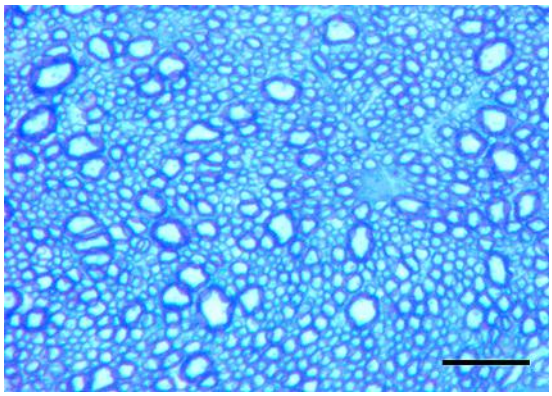

Figure 22. Transverse section of the normal rat optic tract. Section is taken from right side optic tract immediately after saline injection into both eyes; toluidine blue stain. Bar= 10μm

Induction of optic nerve and tract damage by NMDA

24hrs after NMDA injection

No structural changes were observed in the course of optic nerve fibres in any of the animals 24 hrs after NMDA injection and transverse sections from all three segments (proximal optic nerve, distal optic nerve and optic tract) appeared normal. No change was observed in the size of the sections and the axons and myelin retained normal morphology. [See Figure 23 & 24]

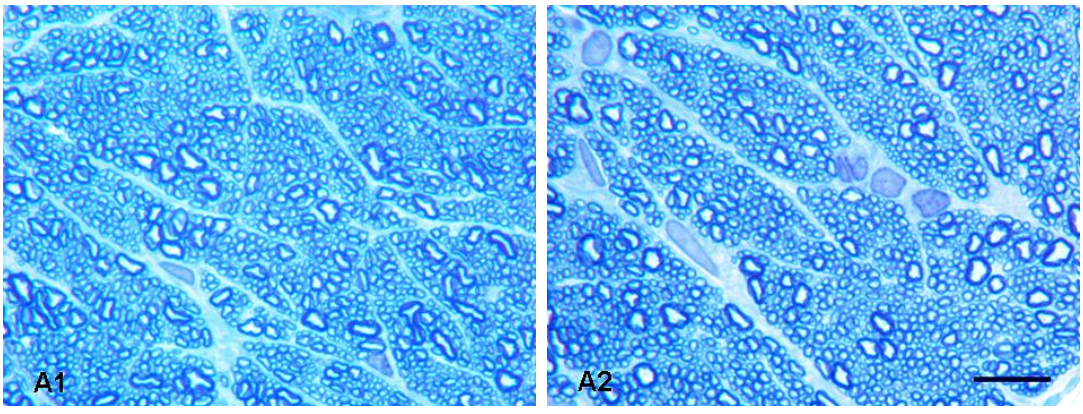

Figure 23. Transverse sections of rat optic nerve 24hrs after NMDA injection, toluidine blue stain. (A1-Proximal Segment, A2-Distal Segment). Bar = 10μm

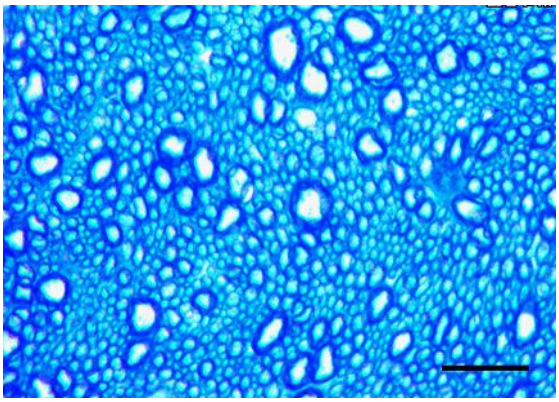

Figure 24. Transverse sections of rat optic tract 24hrs after NMDA injection. Section is taken from right side optic tract 24hrs after NMDA injection into both eyes; toluidine blue stain. Bar = 10μm.

72hrs after NMDA injection

After 72 hrs, all five rats in this group began to show changes in the optic nerve and optic tract. In the proximal optic nerve segment, although most of fibres retained normal morphology, a number of axonal swellings appeared. These axonal swellings appeared to be due to expansion of the myelinated axons with an apparent increase in the axonal diameter. Most of the swollen axons exhibited clearing or clumping/ fragmentation of axoplasm. Many of them remained surrounded by the normal myelin. Only a few swollen fibres developed myelin changes such as thickening or separation of the lamellae which appeared as thicker and darker blue staining under the light microscope. Together with the swollen axons, some nerves showed intense staining with toluidine blue. A few fibres had completely lost their axoplasmic structure and their collapsed myelin (myelin body) was seen as dark blue clumps with no central axon clearing. Also, the axoplasm of some axons became hyperdense with or without associated myelin changes. No changes were observed in the appearance and distribution of glial cells in the interfascicular region.

In comparison to the proximal optic nerve, the distal segment showed more prominent changes. Axonal swelling was more frequent and more marked. Myelin changes were more evident. The number of hyperdense axons also increased. The interfascicular region showed no obvious changes. The glial cell distribution and morphology appeared normal. [See Figure 25]

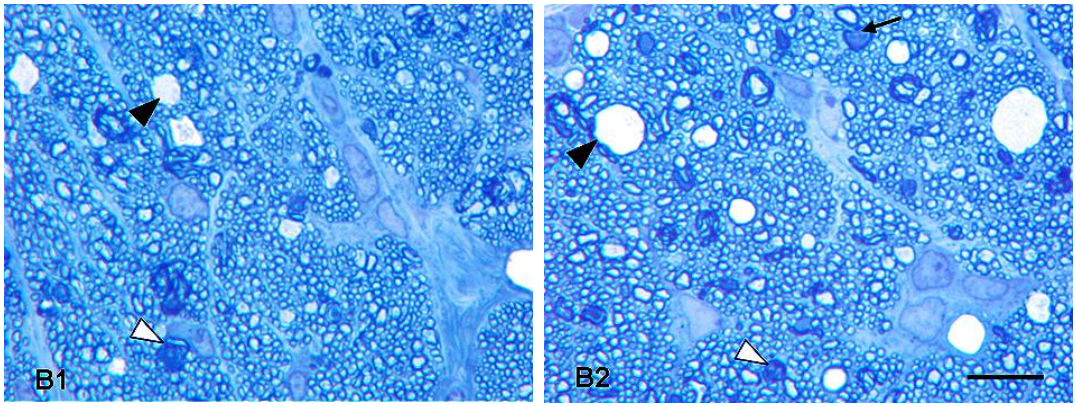

Figure 25. Transverse sections of the optic nerves 72hrs after NMDA injection. toluidine blue stain. (B1-Proximal Segment, B2-Distal Segment). (black arrowheads: swollen axons, white arrowheads: myelin change, black arrows: dense axoplasm). Bar = 10μm

The optic tract showed even greater damage than the distal optic nerve. The number of swollen axons was more and the maximum axonal diameter was increased. These swollen axons showed clearing or fragmentation of the axoplasm. Myelin changes were similar to those seen in the optic nerve, except that they were more numerous. The non-swollen hyperdense fibres picked up uniform dark blue stain. No marked glial cell changes were observed at this stage with light microscopy. [See Figure 26]

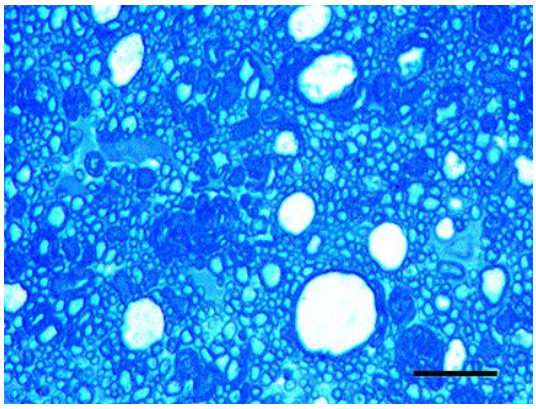

Figure 26. Transverse sections of the rat optic tract after 72 hrs of NMDA injection. Section is taken from the right side optic tract 72 hrs after NMDA injection into both eyes; toluidine blue stain. Bar = 10μm

7days after NMDA injection

Seven days after NMDA injection, both proximal and distal segments of the optic nerve exhibited atrophic changes, with an apparent reduction in the total cross-sectional area seen in both regions. In the proximal segment, the interfascicular septa became more prominent and the fascicle size reduced. The number of axons in each fascicle also decreased. Myelin changes and densely staining axoplasm became more prominent features. The number of swollen axons reduced further in comparison to the 72 hr time point. Although the number of oligodendrocytes remained unaltered, the frequency with which other glial cells were encountered between the remaining axons increased. It was difficult to identify them as microglia or astrocytes under the light microscope. In comparison to the proximal segment, distal optic nerve exhibited similar but more pronounced atrophic changes, axonal swellings and myelin disruption. [See Figure 27]

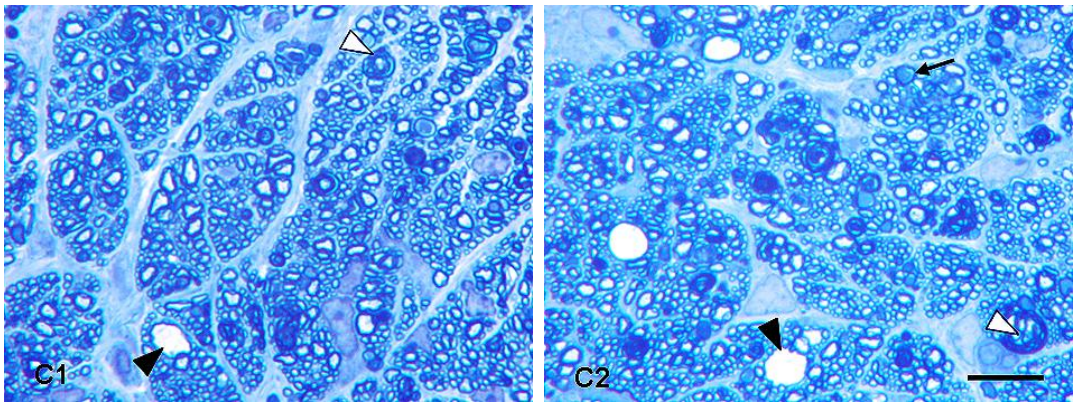

Figure 27. Transverse sections of optic nerve 7days after NMDA injection, toluidine blue stain. (C1-Proximal Segment, C2-Distal Segment) (black arrowheads: swollen axons, white arrowheads: myelin change, black arrows: dense axoplasm). Bar = 10μm

The optic tract at 7 days showed marked changes in comparison to the distal optic nerve. The total number of axons was reduced. Most of the remaining axons showed hyperdense axoplasm or formation of myelin bodies. Only a few swollen axons were seen. More glial cells were seen dispersed between the remaining axons. However, the presence of numerous hyperdense axons made it impossible to identify these glial cells. [See Figure 28]

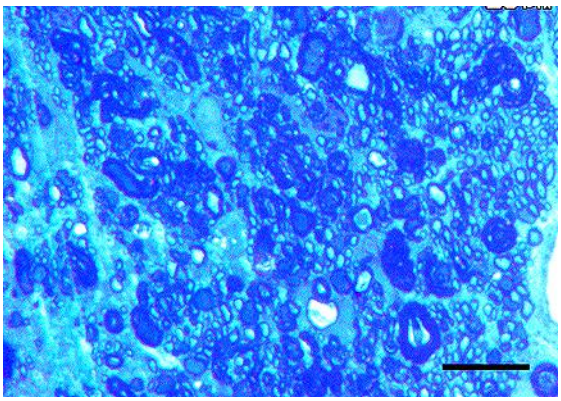

Figure 28. Transverse sections of the rat optic tract after 7days of NMDA injection. Section is taken from the right optic tract 7days after NMDA injection into both eyes; toluidine blue stain. Bar = 10μm

As the degenerative changes in axons and myelin appeared more prominent in the distal region compared to proximal, an attempt was made to quantify the optic nerve pathology by counting the total number of axons, axonal swelling and myelin changes per square field. The next section describes the results of the quantitative anaylsis of the optic nerve data. Optic tract pathology was not used for this purpose because their intense staining made it impossible to count axons.

6.2.3 Quantitative analysis of optic nerve damage

Comparison between the optic nerves of experimental and control eyes revealed that 20 nM NMDA per eye (equivalent to 5μl of 4mM) did not induce optic nerve damage immediately after injection. No difference was observed in total axon count, number of swollen axons or disrupted myelin ($p>0.05$). Prolonged exposure of NMDA (24 hrs) did not produce a significant changes in any of the observed parameters ($p>0.05$). After 72hrs of NMDA injection, a significant loss of axons with increase in the number of axon swellings and myelin damage was observed in both proximal and distal segments of optic nerve in comparison to the control eyes ($p<0.05$). Axon loss and myelin damage in the NMDA-injected optic nerve became more intense at 7 days ($p\leq0.001$); Although the number of swollen axons reduced at day 7 in comparison to 72hrs, they were still significantly higher than the control fellow eye ($p \leq0.001$). [See Table 12]

Table 12. Shows progressive changes in proximal and distal optic nerve segments in control and experimental eyes. Each value represents mean ± S.E.

Optic nerve changes				
Time points	Saline injected (Control) eyes		NMDA-injected fellow (experimental) eyes	
	Proximal optic nerve	Distal optic nerve	Proximal optic nerve	Distal optic nerve
	Total axon count per unit field			
0 hrs	1738.60 ± 36.9	1722.00 ± 12.2	1738.60 ± 22.9	1751.40 ± 18.3
24 hrs	1736.40 ± 20.6	1711.40 ± 24.9	1710.80 ± 16.6	1728.00 ± 10.2
72 hrs	1739.00 ± 40.2	1738.00 ± 19.6	1486.00 ± 30.0*	1315.20 ± 38.6*
7 days	1742.80 ± 27.0	1746.60 ± 15.9	1075.40±31.5**	968.20 ± 21.2**
	Number of swollen axons per unit field			
0 hrs	0.20 ± 0.2	0.20 ± 0.2	1.00 ± 0.5	0.20 ± 0.2
24 hrs	0.60 ± 0.2	0.60 ± 0.4	0.40 ± 0.2	0.80 ± 0.4
72 hrs	1.00 ± 0.3	1.20 ± 0.2	42.60 ± 4.1**	49.80 ± 4.6**
7 days	1.00 ± 0.0	1.80 ± .02	22.80 ± 2.3**	43.80 ± 3.8**
	Number of myelin changes per unit field			
0 hrs	0.60 ± 0.2	0.40 ± 0.2	0.60 ± 0.4	0.20 ± 0.2
24 hrs	1.00 ± 0.3	1.40 ± 0.2	1.80 ± 0.4	1.20 ± 0.6
72 hrs	1.80 ± 0.3	2.60 ± 0.5	137.00 ± 15.0*	226.00 ± 11.7**
7 days	3.60 ± 0.5	3.40 ± 0.5	300.40 ± 43.5*	471.80 ± 21.5**

* $p<0.05$ vs. Control fellow eyes (*Student's t-test*)
** $p<0.001$ vs. Control fellow eyes (*Student's t-test*)
NMDA= *N-Methyl-D-Aspartate*

When a comparison was made between the proximal and distal segments of the optic nerve, no difference was observed in the total number of axons, axon swellings or myelin changes between the two segments of the saline-injected optic nerves at any point of time ($p>0.05$). In contrast, 72 hrs of NMDA exposure produced significantly more damage in the distal optic nerve. A statistically significant difference was observed in the total number of axons remaining, number of swollen axons and the amount of myelin damage between the two segments ($p<0.05$). At day 7, changes in the optic nerve increased, with the distal optic nerve segment of NMDA-injected eye showing more intense changes in all the three parameters ($p\leq0.001$).

6.2.4 Correlation of retinal and optic nerve damage

The number of axons in the distal optic nerve showed a very strong positive correlation with the cell count in GCL in the retina (correlation coefficient R= 0.928, p<0.001). There was a linear relationship between these two parameters. Moreover, a strong correlation was observed between loss of cells in GCL and number of axonal swellings (R= -0.876, p<0.001) as well as myelin changes (R= -0.928, p<0.001). [See Figure 29]

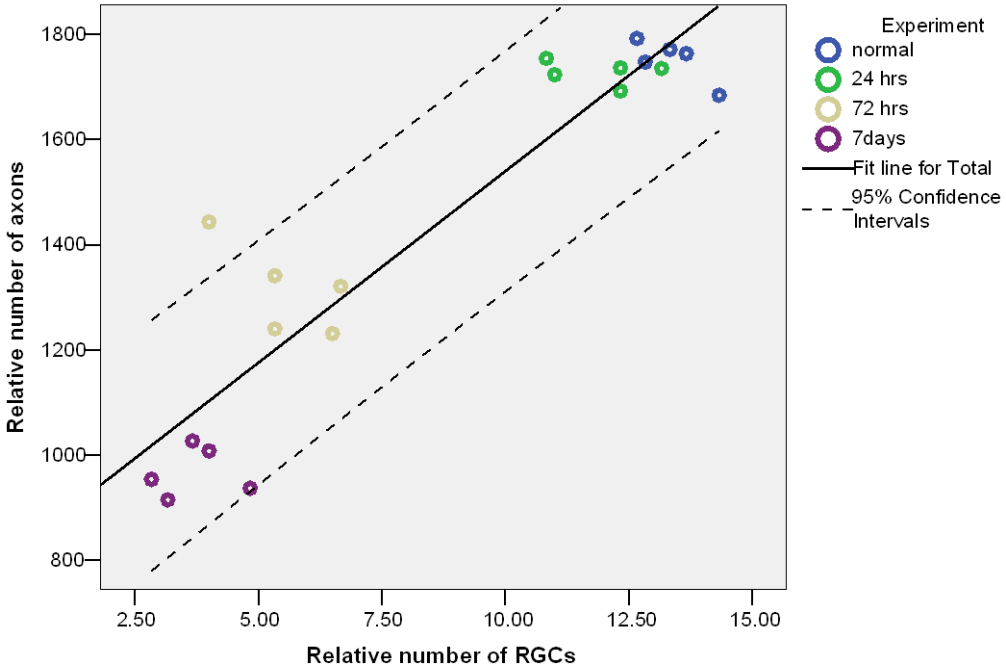

Figure 29. Correlation between the retinal damage and number of axons in the optic nerve of experimental animals. Scatter plot shows correlation between cell count in GCL (mean of posterior and peripheral retinas) and number of optic nerve axons in distal segment (R=0.929. p<0.001). Solid line drawn through data-points shows best-fitting function (along with 95% confidence limits: interrupted line).

6.3 Discussion

Excitotoxicity may be involved in the pathogenesis of glaucoma.[13] The strongest line of evidence relate to the link between the role of excitotoxicity in ischaemia and the role of

ischaemia in glaucoma.[326, 487, 488] In human glaucoma, the optic neuropathy is presumed to start at the level of lamina cribrosa, (a primary axonopathy) as the RGC axons exit the eye, with secondary retrograde degeneration of the RGC somata. Recently, evidence form a mouse model of glaucoma has supported this theory;[489] however, the spatiotemporal pattern of distal axonal degeneration has never been reported.

Despite the importance rat models have attained in ophthalmic research over the last few decades, the mode of optic nerve degeneration secondary to excitotoxic retinal injury is not well characterized. Only a few studies focussed on the nerve pathology after excitotoxic perikaryal insult.[466] In the current study, intravitreal injection of NMDA was used to investigate the effect on the retina and RGC axons outside the eye, both intraorbital and intracranial. In this model, the RGC cell bodies and the toxic insult are physically isolated from the axons; hence, the observed axonal degeneration outside the eye is logically a consequence of the retinal injury, rather than a secondary effect caused by excitotoxic injury to axonal-associated glial tissue.

A study reported time-dependent damage in the reticulogeniculate pathway causing atrophy of the contralateral optic tract and lateral geniculate body at 7 days post intravitreal NMDA injection.[490] The most striking findings from the current study were the synchronous pathological changes in the retina, distal optic nerve and contralateral optic tract beginning within 72 hrs, indicating that the axonal pathology is an early feature of perikaryal excitotoxic injury at a given time point. The observed changes (axon swelling, axon loss and myelin changes) were more prominent in the distal portions of the axon, consistent with a dying-back type axonal degeneration.

In dying-back neuropathies, studies have observed that the distal axon undergoes degeneration and develops characteristic swellings and the proximal axon reduces in calibre to almost 50% of normal.[491, 492] This is due to abnormally rapid transport of NFs to the distal axon, which decreases the availability of these filaments in the proximal region and thus, the proximal axons shrink.[491] As degenerative process progressing from the distal end approaches proximal region, shrunken axons get replaced by the swollen axons.[492, 493] No such shrinkage in the proximal axons was observed in the present study. It is also presumed that in dying-back neuropathies, where the initial site of insult is the cell body,[372, 494, 495] defective perikaryal processing of proteins and organelles needed for terminal region maintenance [396, 397] and reduced synthesis of cytoskeletal elements result in distal axonopathy.[387] Few studies with dying-back neuropathies of toxic and metabolic origin showed that the interference with the metabolic pathways deprive the most vulnerable distal axon of the energy required to maintain its structure and function.[496, 497] The deficiency of pyridoxal phosphate in the cell body, which is later carried down the axon to act as a cofactor for decarboxylation and transamination, is considered as a cause for distal axonal damage.[498] Although, with such models it was unclear whether the inhibition of metabolic process occurred in perikaryon or nerve fibres,[22, 497] this model of exclusive somal injury points to the failure of soma to meet energy requirements of fast transport as one of the possible mechanisms of dying-back degeneration.

Physiologically, glutamate acts as a synaptic neurotransmitter, which is involved in conduction of visual signals across different layers of retina.[499-501] Released sequentially by different retinal elements, it non-specifically activates all ionotropic and metabotropic receptors located on retinal neurons including photoreceptor, horizontal, bipolar, amacrine and ganglion cells.[502, 503] After generating action potential in the post-synaptic neuron, glutamate is

quickly removed by its rapid uptake into neuronal and glial cells through different transporters [235], the majority of which are located in Müller cells.[235] Any pathology which causes excessive activation of these receptors may result in excitotoxic cell death.[504] Because glutamate receptors are distributed throughout the retina, exposure to abnormal levels of this excitotoxin may result in non-selective retinal damage. Therefore, an effort is made to produce selective damage to RGCs by using an excitotoxic agent, NMDA, which is known to produce selective damage to the inner retina.

This study identified that intravitreal injection of NMDA causes severe progressive selective damage to the inner neural retina, evident as decreased cell count in GCL and reduced IRT. Counts in the GCL included RGCs and displaced amacrine cells. No obvious abnormality was detected in the outer layers of retina. In contrast to a few studies which have demonstrated preservation of RGCs with damage to the amacrine cells [505], photoreceptor cells [506] and inner nuclear layer [484] after intravitreal NMDA injection, the results of this study are consistent with the commonly reported loss of cells in GCL and reduced IRT.[453, 483, 486, 507, 508] No obvious abnormality was detected in the outer layers of retina.

Many studies have been conducted to explain the vulnerability of inner retinal neurons to NMDA. Higher susceptibility of the RGCs can be the result of their different NMDA receptor subtype,[509] subunit composition of which display different pharmacokinetic and functional characteristics [405, 510] in comparison to the receptors distributed in glutamatergic excitatory synapses in outer layers of retina, which help in conductance of visual stimuli under physiological conditions.[231-233] Another possible explanation is that RGCs may be possessing higher concentration of NMDA receptors than other cells, which makes them more susceptible to excitotoxic injury. The latter explanation is supported by the results of a study

which demonstrated higher entry (87%) of a channel permeable cation in into the ganglion cells in response to NMDA as compared to the amacrine cells (58%). [468]

Previous reports have shown that the degree of retinal damage depends on the dose of intravitreal excitotoxin.[484-486] Lower doses such as 2nM and10nM NMDA does not affect retina;[453, 485] whereas, 200nM NMDA causes severe retinal damage (85% cell loss in GCL) within a week.[485] With 20nM NMDA used in the current research, loss of 45-55% cells in the GCL loss was seen after 72 hrs and only 25-35% cells remained in the GCL a week after injection. The thinning of the inner retina is believed to be due to the loss of dendritic tree of the RGCs and possibly amacrine cells injured as a result of excitotoxin exposure.

Both the posterior and peripheral retina showed degenerative changes. After 7 days, posterior retina was damaged more (approximately 75% decrease in cell count in GCL and 30% reduction in IRT) than the peripheral retina (65% cell loss in GCL and 24% reduction in IRT). The observed spatial variability in retinal responsiveness may be due to difference in the type and distribution of RGCs in different regions of the retina. No attempt was made to identify regional differences in retinal structure or classify RGCs according to their size, type or distribution. However, there is evidence that, in albino rats, the posterior retina has a comparatively higher concentration of small rather than large-sized RGCs (53% in comparison to 7%).[41, 483, 511] Although, the small RGCs are known to be less vulnerable to excitotoxic injury,[483, 507] their higher cell density in posterior retina (>6000/mm^2) may make this region more susceptible to injury than peripheral retina (1000-1500/mm^2).[41, 511] Using a 20nM intravitreal injection of NMDA in adult male albino Lewis rats, Lam *et al* reported 50% and 25% reduction in GCL cell count in posterior and peripheral retinas, respectively, after seven days.[484] In the present study with adult male Sprague Dawley rats, around 75% and 65%

cell loss was found in these regions after one week. This difference may be due to diverse interspecies differential susceptibility to NMDA.

The degree of optic nerve degeneration correlated strongly with the retinal damage, suggesting that the axon damage and myelin disruption in the optic nerve is related to the somal injury. It is possible that the axonal degeneration simply represents 'withering away' type pathology due to the toxin insult to the soma. However, the synchronous changes observed in the distal portions of the axon suggest the involvement of a positive trigger. The possible involvement of the Wallerian degeneration associated ubiquitin proteosome system and the effect of this injury on axonal transport will be the topic for further research.

In the classical Wallerian degeneration following axotomy, there is a degradation of the axon and its associated myelin distal to the point of transection. Although well-studied, the spatiotemporal pattern of typical Wallerian degeneration following axonal trauma remains controversial, suggesting that in most cases there are early uniform and synchronous changes throughout the severed segment. However, in certain types of neuronal injury, a 'Wallerian-like' degeneration occurs and a 'dying-back' process is seen, in which the distal axon is the first region to be affected and the degeneration spreads in a centrifugal manner (progressing from distal axon towards the cell body).[489] Limited post mortem data from studies in humans have demonstrated cervical spinal cord degeneration within weeks of a cerebral infarct.[512]

As far as the optic nerve damage is concerned, an estimate of axon survival is a key parameter of extent of damage. For many years, automated computer-based programs have been used for axon counting.[513-515]; however, counts generated using such techniques does not always follow strict definitions of parameters and include artefacts also. Therefore,

manual counting was done for the quantifying optic nerve pathology. Also, because sampling a small proportion of the nerve(<8%) yields estimates with significant errors,[516] therefore, although tedious and time consuming, manual counting was performed in a large proportion of the nerve (~25%) to increase the accuracy.

It has been shown that axonal defects in mouse models of Alzheimer's disease precede known disease-related pathology by more than a year.[458] Similar axonal defects in the early stages of Alzheimer's disease in humans have also been reported.[458] These axonal defects consisted of swellings that accumulated abnormal amounts of microtubule-associated and molecular motor proteins, organelles, and vesicles.[458] Impairing axonal transport by reducing the dosage of a kinesin molecular motor protein enhanced the frequency of axonal defects and increased amyloid-β peptide levels and amyloid deposition.[458]

A comprehensive spatiotemporal analysis of disease progression in SOD1G93A mice, a well-described animal model of MND, found that motor neurone pathology clearly commenced at the distal axon and proceeded in a dying back fashion.[517] Human autopsy findings of MND also support this pattern of disease progression.[517]

In human glaucoma, the optic neuropathy is presumed to begin at the level of lamina cribrosa, (a primary axonopathy) as the RGC axons exit the eye, with secondary retrograde degeneration of the RGC somata. Recently, evidence from a mouse model of glaucoma has reported this theory;[489] however, the spatiotemporal pattern of distal axonal degeneration has never been reported.

In conclusion, this part of the study demonstrated that perikaryal excitotoxic injury of the RGC causes synchronous somal and axonal degeneration, with distal portions of the axon showing more prominent pathological changes than proximal portions, consistent with a Wallerian-like dying back-type pathology.

Chapter 7: TUNEL STAINING OF THE RAT RETINA

7.1 Introduction

Retinal neurons may undergo programmed cell death during development or pathological cell death such as in ischaemia, glaucoma, trauma and other retinopathies. In the previous chapter, a significant loss of cells was observed in the GCL following NMDA induced retinal excitotoxicity. The neuronal injury, putatively mediated by the binding of the excitotoxin to ionotropic NMDA receptors, has been not been clearly revealed and different studies demonstrate inconsistencies in the mode of excitotoxic neuronal death.[269, 463, 464, 504, 518-521]

While the identification of apoptosis or necrosis was originally based on the histopathological characteristics, TUNEL staining became the most popular method to identify and quantify apoptotic cell death. It identifies the fragmented DNA produced as a result of endonuclease cleavage. Although researchers argue on the use of this labelling technique for identification of apoptosis,[522, 523] a number of studies using TUNEL in conjunction with electron microscopy have shown that this is a reliable marker to identify apoptosis.[484, 524]

This chapter presents the results of TUNEL staining in order to identify and quantify apoptotic cell death in the rat retina after intravitreal injection of NMDA. It is important to identify the mode of RGC death, which can be necrosis, apoptosis or both, because interfering with the enzymes involved in the progression of apoptosis, an active process, may help salvage the endangered optic neurons.

7.2 Results

TUNEL labelling of paraffin-embedded retinal sections did not reveal any staining in the negative controls eyes. Also no expression was seen in the retinas exposed to 20nmol NMDA. Although the positive controls (spinal cord ischaemia) slides showed TUNEL labelling in the gray matter, no staining was seen at any time point in NMDA-injected retinas. [See Figure 30]

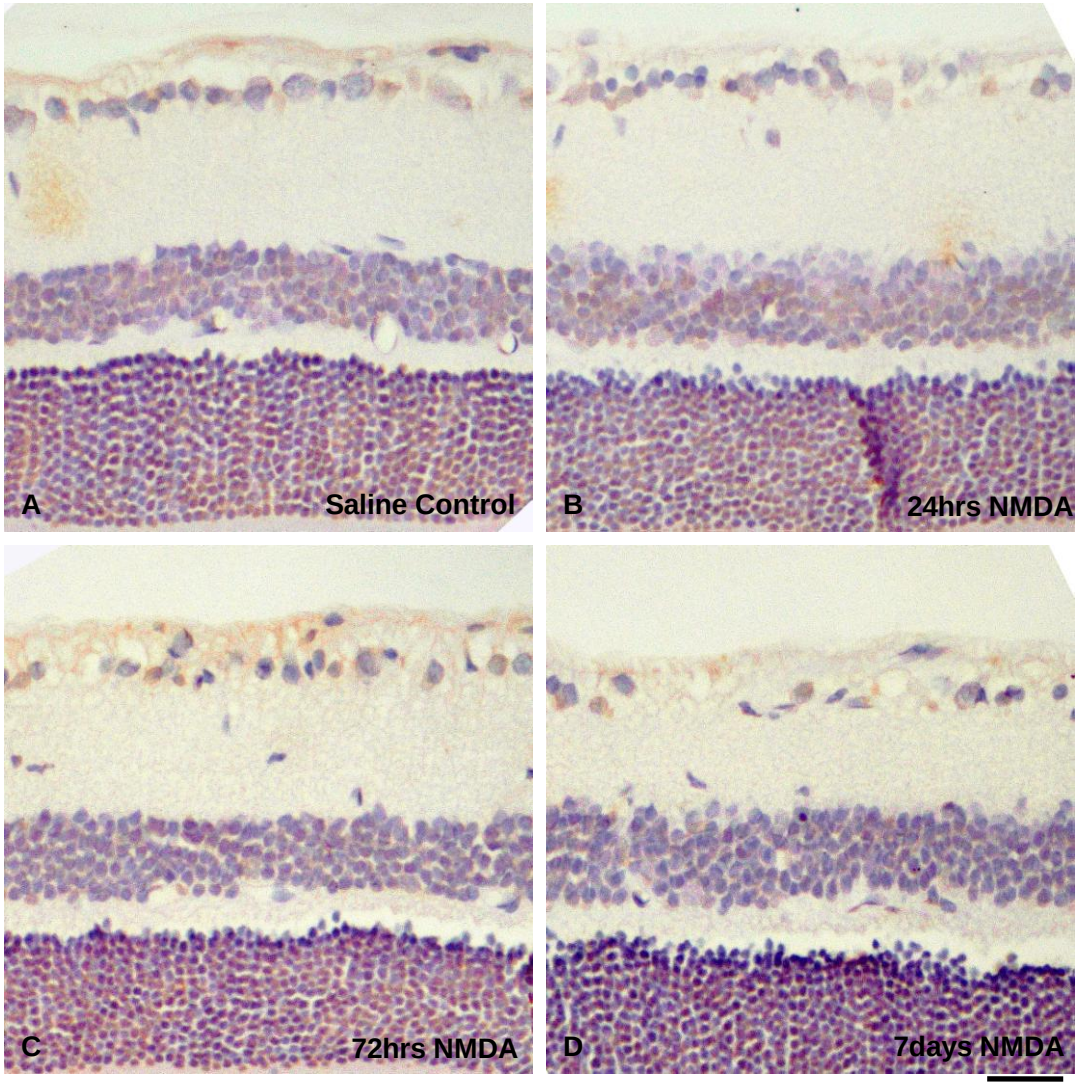

Figure 30. TUNEL staining of the saline-injected retina (A) and NMDA-injected retinas at 24hrs (B), 72hrs (C) and 7days (D) demonstrate no labelling in any retinal layer. Bar=50μm

7.3 Discussion

To demonstrate that 20nM NMDA induces apoptosis in the inner retinal neurons and that TUNEL assay can be used to quantify apoptotic cell death, light microscopy was used to analyse paraffin-embedded retinal sections stained with this method. This method revealed no labelling of fragmented DNA in the neurons seen dying after NMDA exposure in light microscopy photographs in the previous chapter.

A previous study has shown labelling of the nicked DNA in the inner retinal neurons by TUNEL method after intravitreal injection of 80nM NMDA in the adult rat.[484] Kwong et al demonstrated that TUNEL staining can label fragmented DNA much before (~4hrs) the appearance of apoptotic features on electron microscopy (~18hrs).[524] A study by Chidlow et al demonstrated TUNEL positive nuclei in retina at 6hrs which progressively reduced in number over 72 hrs post-excitotoxic insult.[525] In contrast, the current study demonstrated the absence of TUNEL labelling in the retina from day 1 to 7 after NMDA induced retinal injury. This implies the absence of apoptotic cell death in this time frame and suggests the role of other death programmes (necrotic or autophagic) in excitotoxic neuronal cell death after 24hrs of NMDA exposure. The study does not rule out the possibility of the presence of early (before 24hrs) or late (after 7days) apoptotic changes because the retinal sections were examined only between day 1 and 7 of NMDA exposure. Progressive reduction in TUNEL labelling can be supported by a study which showed that the neurons undergoing ischaemic damage show a continuum of changes beginning as apoptosis and later manifesting as necrosis because of incomplete progression of apoptotic cell death events.[526] Another support comes from the study which demonstrated that retinal ischaemia produced by increasing IOP in adult rats produces a reverse phenomenon, where the neurons in the INL and GCL show features early necrosis followed by slowly evolving apoptosis evident on TUNEL staining.[242] Therefore,

further studies may need to be conducted at early (<24hrs) and late time points (>7days) in order to demonstrate any positive TUNEL staining, which might have been missed in this study.

Many studies have questioned the use of TUNEL assay as a specific marker of apoptotsis.[522] Borras D et al showed that DNA fragmentation occurs independent of the chromatin condensation and other apoptotic changes in the neurons,[340, 527] so that even in the presence of cells demonstrating apoptotic features, TUNEL may not show any staining. In contrast, because DNA strand breaks can appear in non-apoptotic cell death, positive TUNEL staining cannot differentiate between apoptotic and non-apoptotic forms of cell death.[523] De Torres et al observed TUNEL staining in the presence necrotic changes in the ischaemic neurons.[528] Light microscopy of the NMDA exposed retina demonstrated a significant number of RGC number yet TUNEL is negative over the same time period. No TUNEL labelling in the current study, therefore, only suggest the absence of DNA fragmentation and not the mode of cell death of RGCs.

It is generally accepted that apoptotic cells can be accurately identified if two methodologies are used in combination, i.e TUNEL and another method example identification of activated caspases, or electron microscopy. Having demonstrated the absence of TUNEL labelling in the NMDA-exposed retina, which just means the lack of endonuclease activation and DNA nicking, no conclusion can be drawn on the type of cell death in the GCL after NMDA injection. The next step will be to study the ultrastructural features of the dying neurons. This will help not only in determining the mode of cell death, but also in correlating the level of somal (RGC) damage with the degenerative changes in the optic nerve axons.

Chapter 8: ULTRASTRUCTURE OF RGCs AND OPTIC NERVE FIBRES AFTER INTRAVITREAL INJECTION OF NMDA

8.1 Introduction

Excitotoxic injury is characterized by a well-ordered sequence of organelle abnormalities resulting in cell death. It is classically considered as a somatodendritic insult due to prolonged or excessive activation of excitatory amino acid receptors. Studies have also indicated axonopathy as an early feature in neurodegenerative diseases associated with excitotoxicity.[455-458] It is unclear whether the nerve degeneration associated with excitotoxicity is due to primary insult at the perikaryal level in the grey matter or a primary excitotoxic injury in the white matter. Despite numerous *in-vitro* and *in-vivo* studies on excitotoxic neuronal death in the retina, it is still unclear whether the perikaryal death process is necrotic or apoptotic. Also, little attention has been focused on the downstream ultrastructural changes in the optic nerve (the RGC myelinated axons), the structure and function of which is critically maintained by the cell body.

The retina and optic nerve, as approachable regions of the CNS, provide a unique substrate to investigate the effect of NMDA induced excitotoxic RGC injury on the optic nerve axons. Light microscopic study revealed that NMDA induced retinal injury produced an axonopathy which was synchronous with the somal degeneration of RGCs and which was most prominent in the more distal portions (closer to the midbrain) of the axon. In the current study, we provide ultrastructural information about the RGC somata and their axons, after NMDA-induced retinal injury.

There are relatively few studies which have studied optic neuropathy at ultrastructural level. Most such studies are based on the genetically modified models of optic nerve axotomy or optic nerve crush injury. To our knowledge, this is the first study to report the pathological changes in the optic nerve at ultrastructural level after excitototxic retinal damage. The first half of this section describes the time-dependent sequential subcellular events and the morphologic phenotype in dying RGCs. In the second half of the section, different morphological aspects of optic nerve degeneration at ultramicroscopic level are described.

To help elucidate ultrastructural changes in the RGCs and the optic nerve axons after intravitreal NMDA injection, this part of the study employed the technique of transmission electron microscopy (TEM).[99] TEM is an imaging technique whereby a beam of high energetic electrons is used instead of light to study the fine details of the objects such as cells, microorganisms, metals and crystalline structures. Although limited in the field of view, transmission electron microscopes magnify the objects up to two million folds in comparison to the light microscopes (which provide a limited magnification of 1000X and a resolution of 0.2 micrometers). Therefore, they provide valuable information which can complement the light microscopic findings. Also because TEM can demonstrate early changes to the different cytoskeletal structures, axonal organelles and myelin changes, this technique is used to provide ultrastructural qualitative analysis of the events resulting in nerve degeneration after excitotoxic perikaryal injury.

8.2 Results

Ultrathin sections of the posterior retina near the optic disc with transverse and longitudinal sections of the proximal and distal optic nerve segments from the resin-embedded normal and NMDA-injected eyeballs were observed under a transmission electron microscope. The

ultrastructure was always interpreted in conjunction with the LM findings for which toluidine blue stained semi-thin sections were observed under a light microscope. LM was used to identify the GCL, which showed neuronal cell bodies of optic nerve axons (RGCs), amacrine cells and various glial cells.[40] RGCs were identified under electron microscope by their profile described in literature and their degenerative changes observed after NMDA exposure. Negative and positive controls showed no damage at any time point.

8.2.1 Ultrastructural changes in RGCs

Ultrastructure of normal retinal ganglion cells

Cells in GCL were differentiated according to their number, size, shape and nuclear staining. Most numerous large-sized cells containing pale nuclei with one or two nucleoli were identified as RGCs, in comparison to amacrine cells, which were smaller and had dark staining nuclei.[529, 530] Microglial cells were identified as occasional small-sized cells with short processes and elongated nuclei, seen distributed in the GCL and INFL. A few blood vessels were also seen in the inner retina. The IPL showed sections of dendritic processes of RGCs. [See Figure 31]

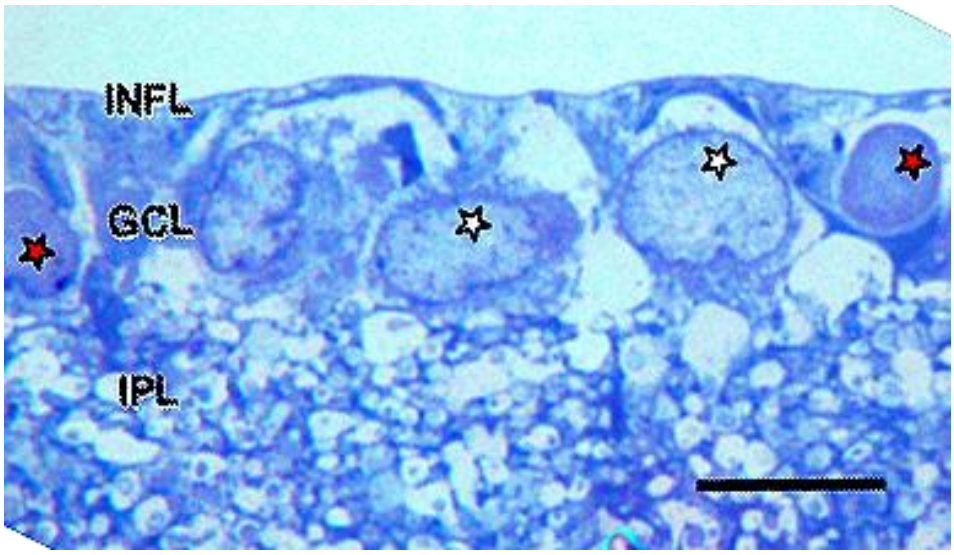

Figure 31. Light microscopic appearance of resin-embedded semi-thin section of saline control normal inner retina stained with Toluidine blue stain. INFL: inner nerve fibre layer, GCL: ganglion cell layer, IPL: inner plexiform layer. GCL shows prominent nuclei of RGCs (white stars) and amacrine cell (red stars). Bar= 10μm

Under TEM at higher magnifications (X7900 to X92000), a normal RGC had a well-defined continuous trace of plasma membrane and a non-uniform distribution of organelles in the cytoplasm, with maximum concentration in the perinuclear region. RGCs contained tubular sacs of rough endoplasmic reticulum (rER) surrounded by large number of ribosomes (Nissl bodies) Various sized mitochondria were identified as round or oval, double-membrane structures with the inner membrane sending off characteristic cristae into the matrix. In addition, the cytoplasm contained elements of the Golgi apparatus (GA), free ribosomes and microtubules sectioned at various angles. A large round nucleus, surrounded by a double layered nuclear membrane, contained homogeneously dispersed karyoplasm (chromatin material) and one or two electron dense nucleoli. RGCs from the control saline-injected eyes at all time points showed a similar profile. [See Figure 32]

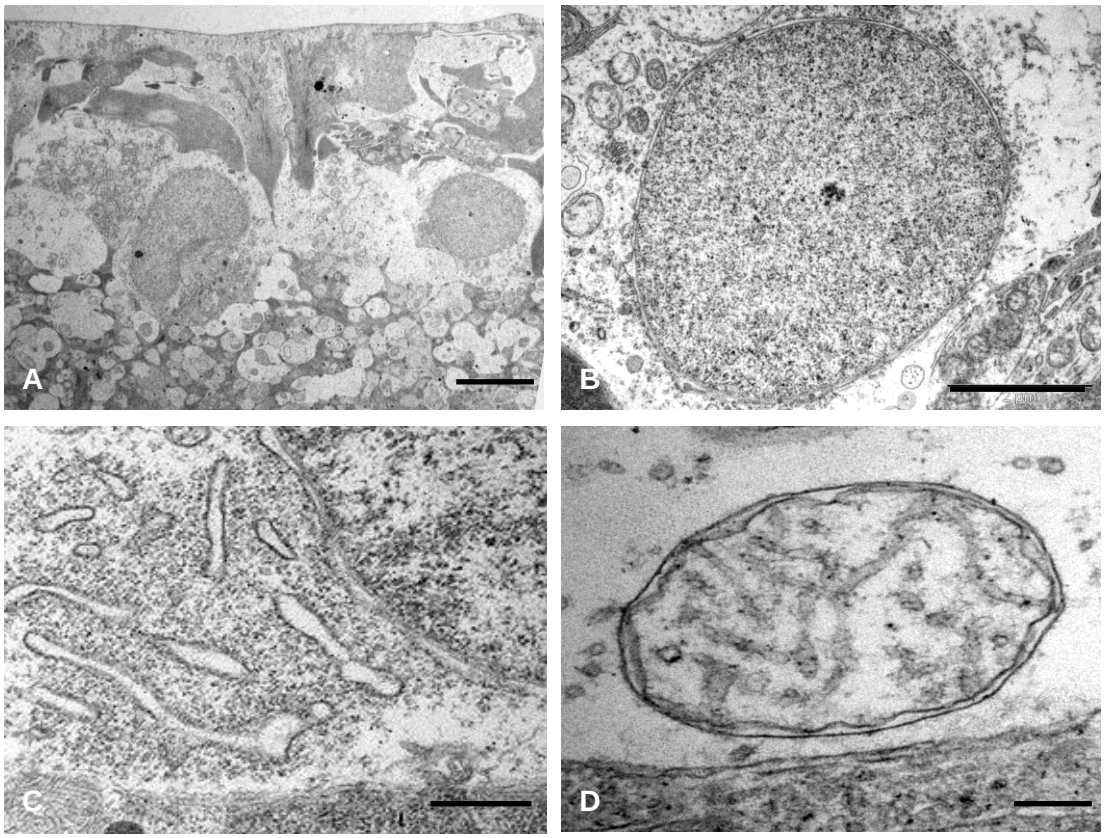

Figure 32. Ultrastructural appearances of normal RGCs from saline injected eye.Typical RGCs are seen (A, Bar=5μm) with normal nuclei (B, Bar=2μm), endoplasmic reticulum (ER) with ribosomes (C, Bar=1.7μm) and mitochondrion (D, Bar= 20nm).

Ultrastructure changes in NMDA treated RGCs

Intravitreal administration of NMDA in adult male Sprague-Dawley rats resulted in excitotoxic damage to RGCs which began as early as 24 hrs. At 24hrs of NMDA treatment, 10-20% RGCs showed cytoplasmic engorgement with vacuous swellings of numerous dendritic processes giving a spongiform appearance to the IPL. Cytoplasm of the swollen RGCs appeared dense and uniformly granular due to the presence of scattered ribosomes which occupied the whole cytoplasm. Some mitochondria appeared swollen and the rER also appeared slightly vacuolated. The cell membrane appeared intact and no nuclear changes were seen at this stage. Axonal processes coursing through the INFL could not be seen due to technical difficulty in processing and mounting sections on the grids. [See Figure 33]

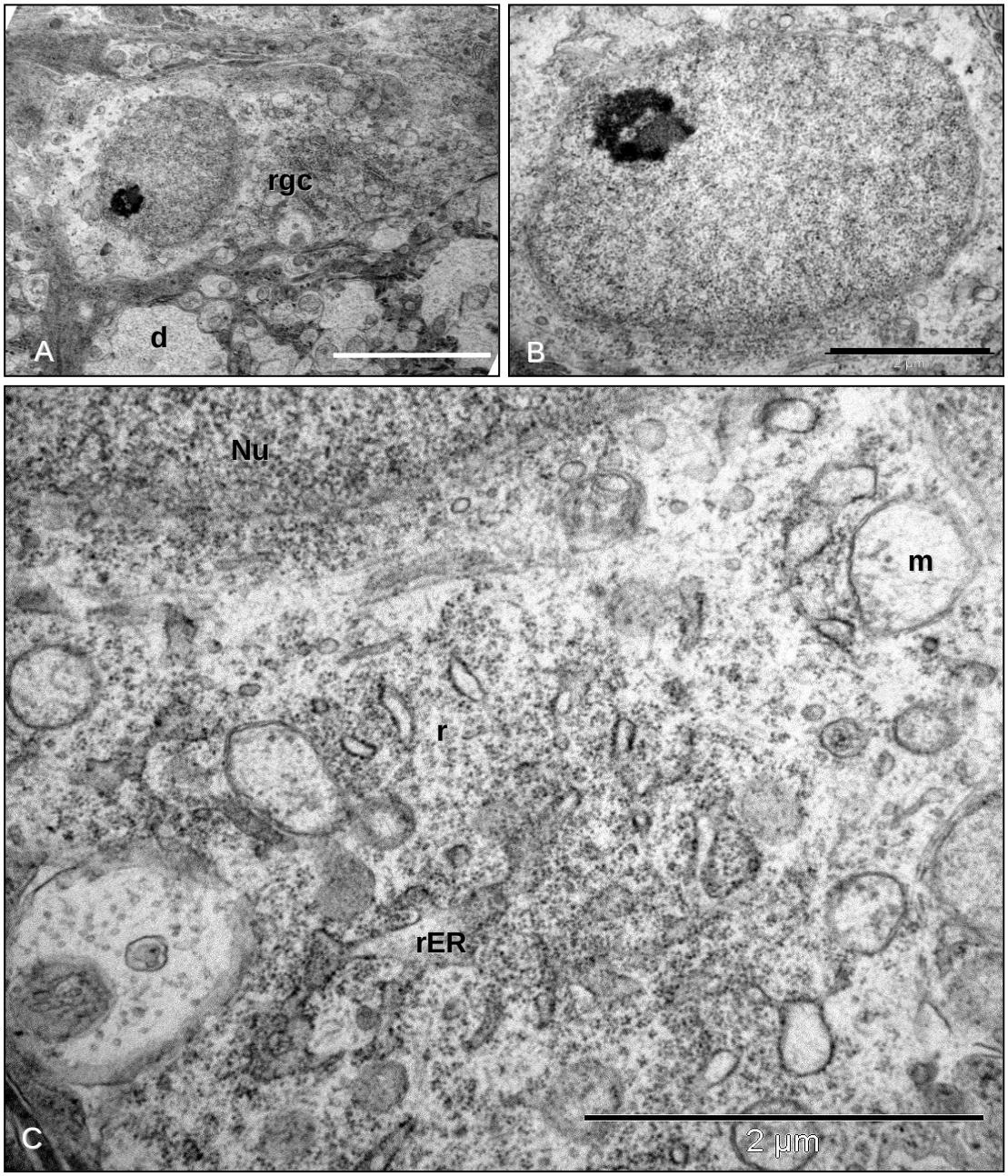

Figure 33. Ultrastructural appearance of RGCs 24hrs after NMDA injection shows (A, Bar=5μm) early dense appearance of the cell (rgc) cytoplasm with dendritic swelling (d),) and normal euchromatic nucleus with a prominent nucleolus (B, Bar=2μm). Notice the dilatation of mitochondrion (m) and endoplasmic reticulum (er) as well as some scattered ribosomes (r) in the cytoplasm (C, Bar=2μm).

At 72hrs after NMDA injection, the dendritic swelling persisted and the ganglion cell density in GCL decreased. RGCs displayed a necrotic form of cell death with features of acute

excitotoxic degeneration seen in a continuum of changes. Most abnormal RGCs had an intact cell membrane with their cytoplasmic matrix containing free monomeric ribosomes, vesicles and dilated cisterns of ER as well as GA. In conjunction with the disaggregation of polyribosomes and disintegration of vacuolated ER, most mitochondria were irregularly oedematous. Some morphologically normal mitochondria were still evident in affected cells. Some cells showed early features of nuclear damage such as, hyperconvoluted nuclei and chromatin condensation into small clumps abutting the nuclear envelope. Nucleoli, however, were morphologically normal.

Some RGCs displayed extreme cytolysis and loss of architecture in the form of disrupted cytoplasmic structures including mitochondria, ER and GA. Their nuclear envelope and membranes surrounding organelles were fragmented and discontinuous. Damage was so severe that demarcation between nucleus and cytoplasm was impossible in some cells. There was a complete loss of nuclear membrane. Highly electron-dense clumped nuclear remnants were dispersed into the cytoplasm, which contained vacuolated and rupturing organelle and onion-like multi-laminated ‘myelin figures’. [See Figure 34]

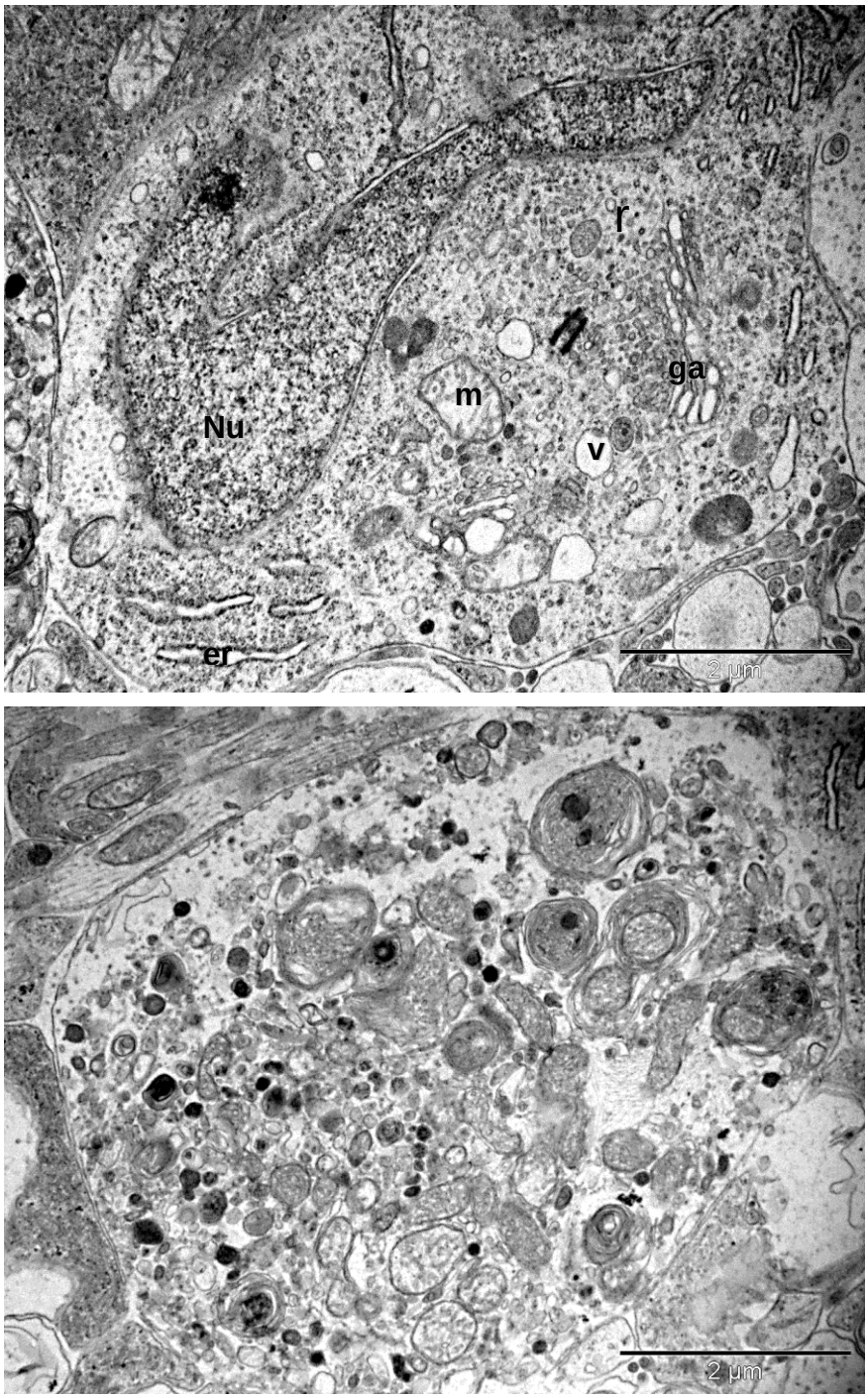

Figure 34. Ultrastructure appearance of RGCs 72hrs after NMDA injection. Neurons are found at different stages of degeneration and the neuronal death is morphologically 'necrotic'. The above figure shows the hyperconvoluted nucleus and cytoplasm filled with multiple vacuoles, ribosomes and swollen organelle. Lower picture shows severe necrotic cell death where the cell has lost its architecture and converted into debris. There is no demarcation between cytoplasm and electron-dense bodies. The cytoplasm is studded with the multi-laminated myelin figures and damaged organelles (Bars=2µm); Nu=nucleus, er=endoplasmic reticulum, ga=golgi apparatus, m=mitochondria, v= vesicles, r=ribosomes

At 7 days, the IPL appeared markedly thinned, with dendrites becoming shrunken and dense. As the purpose of the study was to explore ultrastructural changes, no quantification of IPL thickness was attempted here. However, statistical analysis of retinal thinning done using light microscopy and the results reported in the previous chapter. The GCL showed sparse distribution of RGCs, but preservation of most amacrine cells. At this time point, damaged RGCs showed electron-dense neuronal debris remaining in contact with clusters of reactive microglial cells and astrocytic processes. Very few RGCs showed pyknotic nuclei, but most damaged RGCs underwent necrosis. Numerous dendritic processes, recognised by their higher microtubule composition in comparison the axons, were seen distributed in the GCL. These dendritic sprouts were packed in the form of clusters, which occupied the empty spaces created by necrotic RGCs. Compared to the dendrites in IPL, these processes appeared normal in terms of filamentous and organelle composition, with many displaying mitochondria of normal morphology. Reactive microglia carrying electron dense phagolysosomes were observed at a few places surrounding the neuronal debris. A process arising from one of the dendritic processes ran into the thinned out INFL for a significant distance. This axon-like long process was shrivelled and electron-dense. It had a non-uniform diameter, with many normal mitochondria having intact cristae seen located intermittently. Although, the filamentous composition of the process was identifiable, it was difficult to define its exact composition because of its hyper-dense appearance. [See Figure 35]

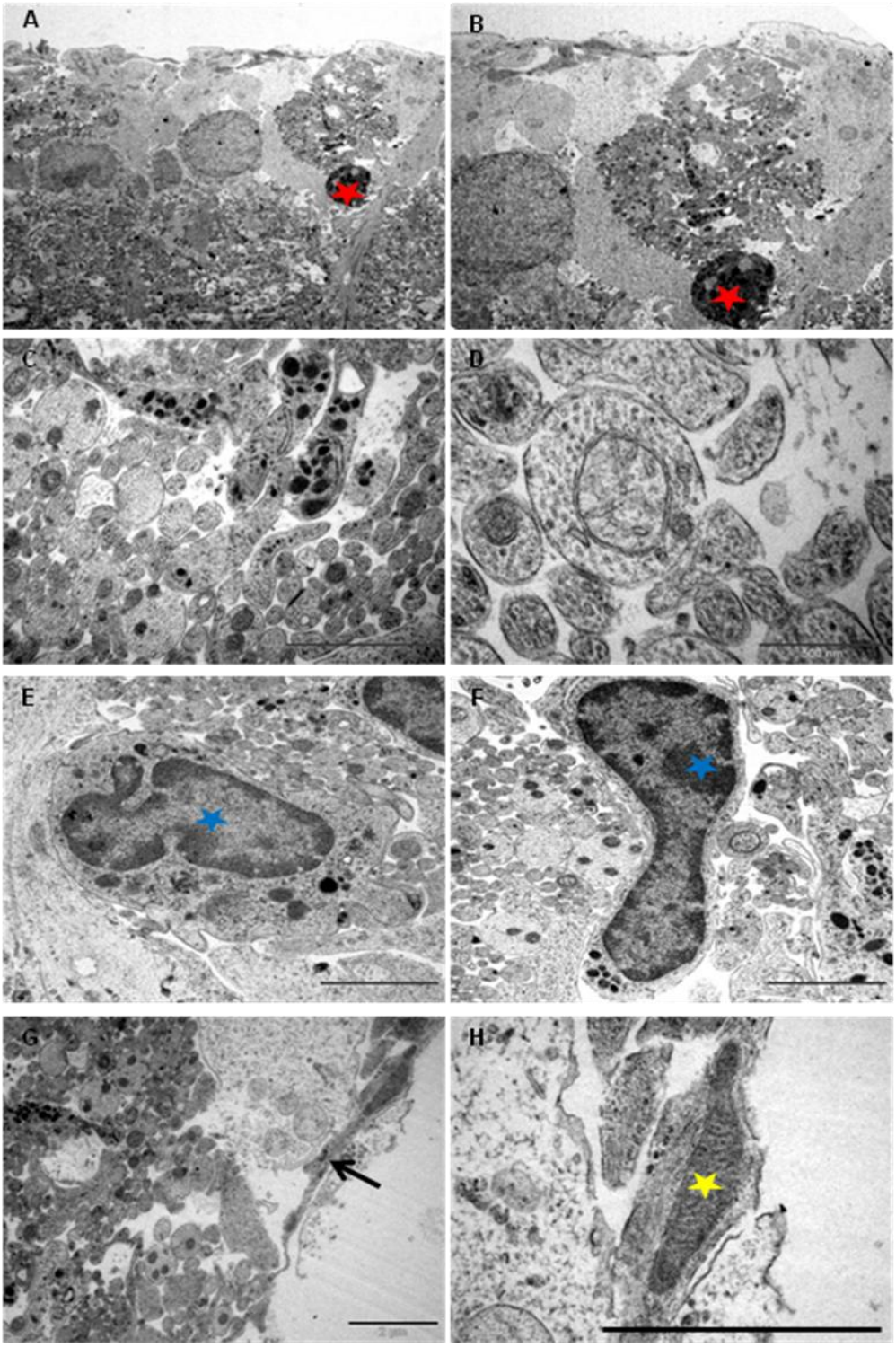

Figure 35. NMDA-induced ultrastructural changes in RGCs at 7 days where necrotic cell in the form of highly electron-dense neuronal debris (B, Red star) is seen lying adjacent to numerous membrane-bound microtubule-rich transverse sections of the neuritic processes (C, Bar=2μm) identified as dendrites under high power (D, Bar=500nm). Figure E and F show reactive microglia (blue stars) surrounding the dendritic sprouts. (Bars=2μm). An axon-like long process (G, Bar=2μm) containing normal mitochondria (H, yellow star, Bar=2μm) is seen in INFL.

8.2.2 Ultrastructural changes in optic nerve axons

Ultrastructure of normal intraocular optic nerve

The parallel-cut intraocular portion of optic nerve axons seen in retinal sections from saline-injected control eyes showed 0.25 to 1 μm thick unmyelinated axons running longitudinally in INFL with axoplasm showing uniformly distributed longitudinal cytoskeletal filaments and organelles. In some axons, where a substantial length of axon was cut along the axis, double-layered mitochondria were located intermittently in segment of axon which appeared dilated. Such mitochondria-rich varicosities were separated by narrowed portion of filament rich axons barely containing any organelle. Optic nerves from the saline-injected eyes (studied immediately, 24hrs, 72hrs and 7days after injection) exhibited similar morphology at all points. [See Figure 36]

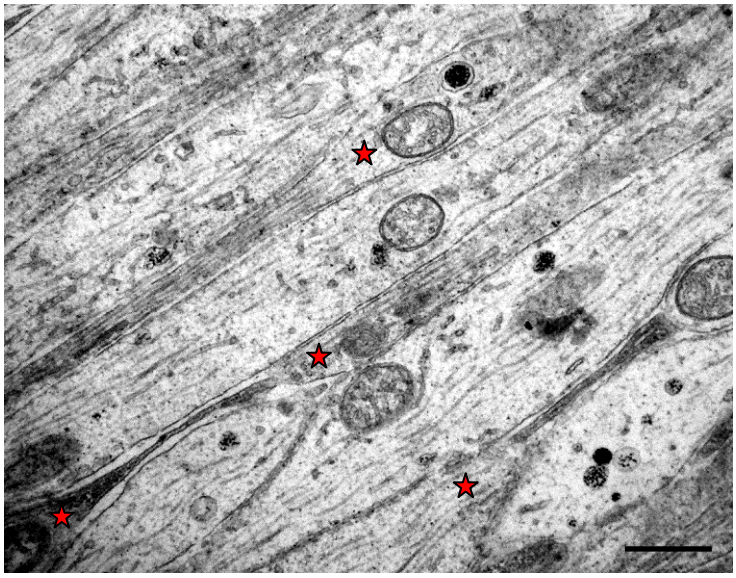

Figure 36. Transmission electron microscopy of the parallel running longitudinal sections of the intraorbital axons.A few fibres cut to a substantial length showed varicosities (red star) and intervaricosity regions simultaneously. (Bar=1μm)

Ultrastructure of normal retro-orbital optic nerve

The retro-orbital optic nerve (both proximal and distal) from saline-injected animals at all time points displayed ultrastructural features similar to those described previously in normal adult rat.[531-534] In transverse sections [See Figure 37, A & B], well-fixed myelinated axons of various diameters maintained round to ovoid sectional profiles with numerous microtubules and neurofilaments dispersed evenly in the axoplasm. Microtubules were seen as hollow round cross-sections and neurofilaments as small electron-dense dots with no central clearing. Also seen in the axoplasm were mitochondria with normal morphology and intact cristae. Surrounding the axons, myelin remained compact with a normal periodicity with no intramyelinic lacuna or vacuoles. Unmyelinated fibres were quite rare.

In longitudinal sections [See Figure 37, C & D], axons ensheathed by darkly stained myelin contained filamentous structures (neurofilaments and microtubules), which showed linear orientation parallel to the length of axons. The nodes of Ranvier displayed a normal morphology with well-preserved paranodal terminal loops contacting axolemma and a non-myelinated nodal gap measuring less than or approximately equal to1μm. Various glial cells surrounded the axons. Oligodendroglial cells had an electron-dense cytoplasm and heterochromatic nuclei. Astrocytes were identified by the electron-lucent cytoplasm and processes which contained bundles of intermediate filaments. Microglia had heterochromatic nuclei similar to oligodendroglia, but their cytoplasm appeared less dense.

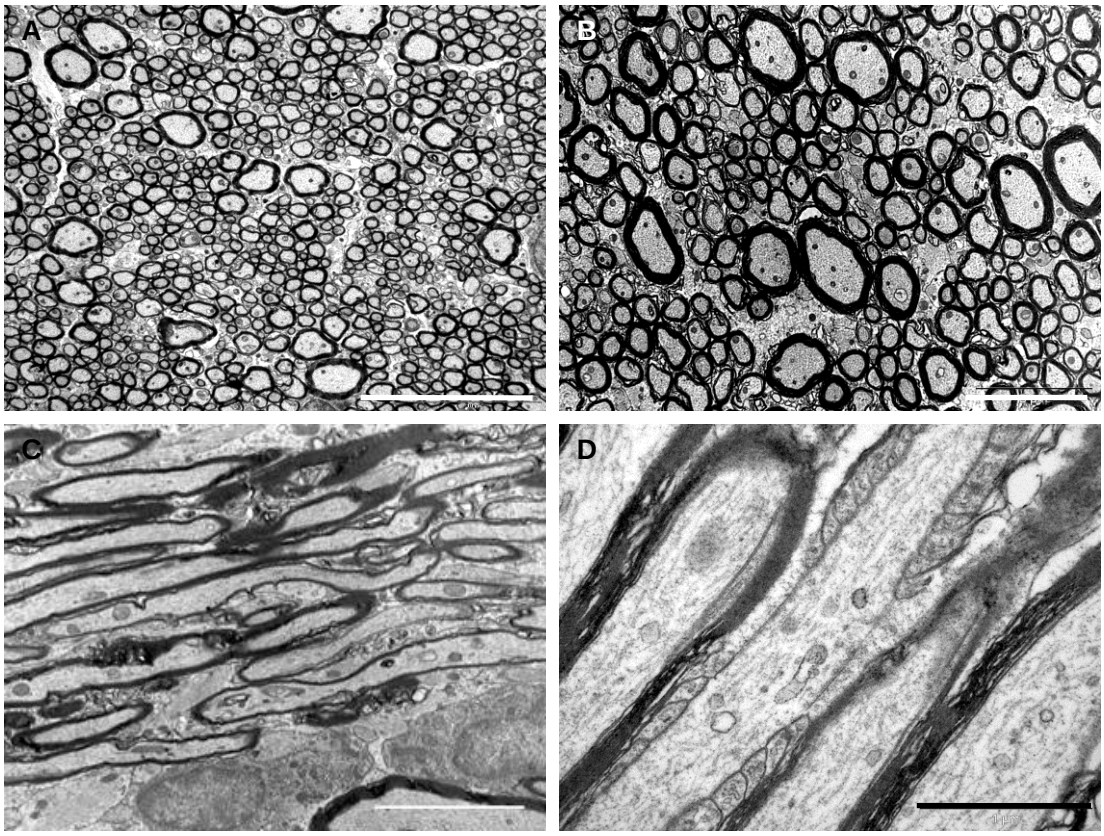

Figure 37. EM of the retro-orbital distal segment of rat optic nerve of the saline-injected control animal immediately after the injection. Axoplasm of the myelinated axons contain numerous neurofilaments, microtubules, mitochondria and various other organelles. The transverse sections (A, Bar=5μm and B, Bar=2μm) show compact arrangement of the myelin lamellae around the axons in the internodal regions. The longitudinal sections show parallel running myelinated axons (C, Bar=5μm). Axon-myelin relationship in the nodal-paranodal region is better appreciated at very high magnification (D, Bar=1μm) Here, myelin terminal loops are seen attached to the paranodal axolemma on either side of the node.

Ultrastructure of optic nerves after NMDA injection

Optic nerves from NMDA-injected eyes, examined immediately and 24 hrs after injection were similar to the optic nerve of saline-injected eyes. Akin to LM findings, the general organization of the optic nerve was maintained and no pathologic changes were observed in the intraocular, intraorbital or intracranial optic nerve morphology.

At 72hrs post-lesion, unmyelinated fibres running in the INFL maintained normal morphology; however, pathology was identified in the retro-orbital optic nerve. After careful observation of

cross sections of proximal and distal segments, three distinct abnormalities were identified with changes appearing more pronounced in the distal as compared to the proximal optic nerve (data not quantified here). These ultrastructural changes had similar spatiotemporal and pathological features to that described in classical Wallerian degeneration.[535, 536]

1) Axonal swellings- Swollen axons appeared pale and enlarged with axolemmal expansion and cytoskeletal disintegration characterizing 'watery degeneration'. The axoplasm was partially or completely devoid of organelles and cytoskeletal elements. Loss of microtubules with relative preservation of neurofilaments was observed in some axons. Many fibres contained dense accumulations of neurofilaments, altered tubulo-vesicular membranous organelles, mitochondria and multilayered whorled masses, which appeared to be arising from the inner layers of myelin. The myelin sheath surrounding these axons remained compact and unaltered at most places. [See Figure 38]

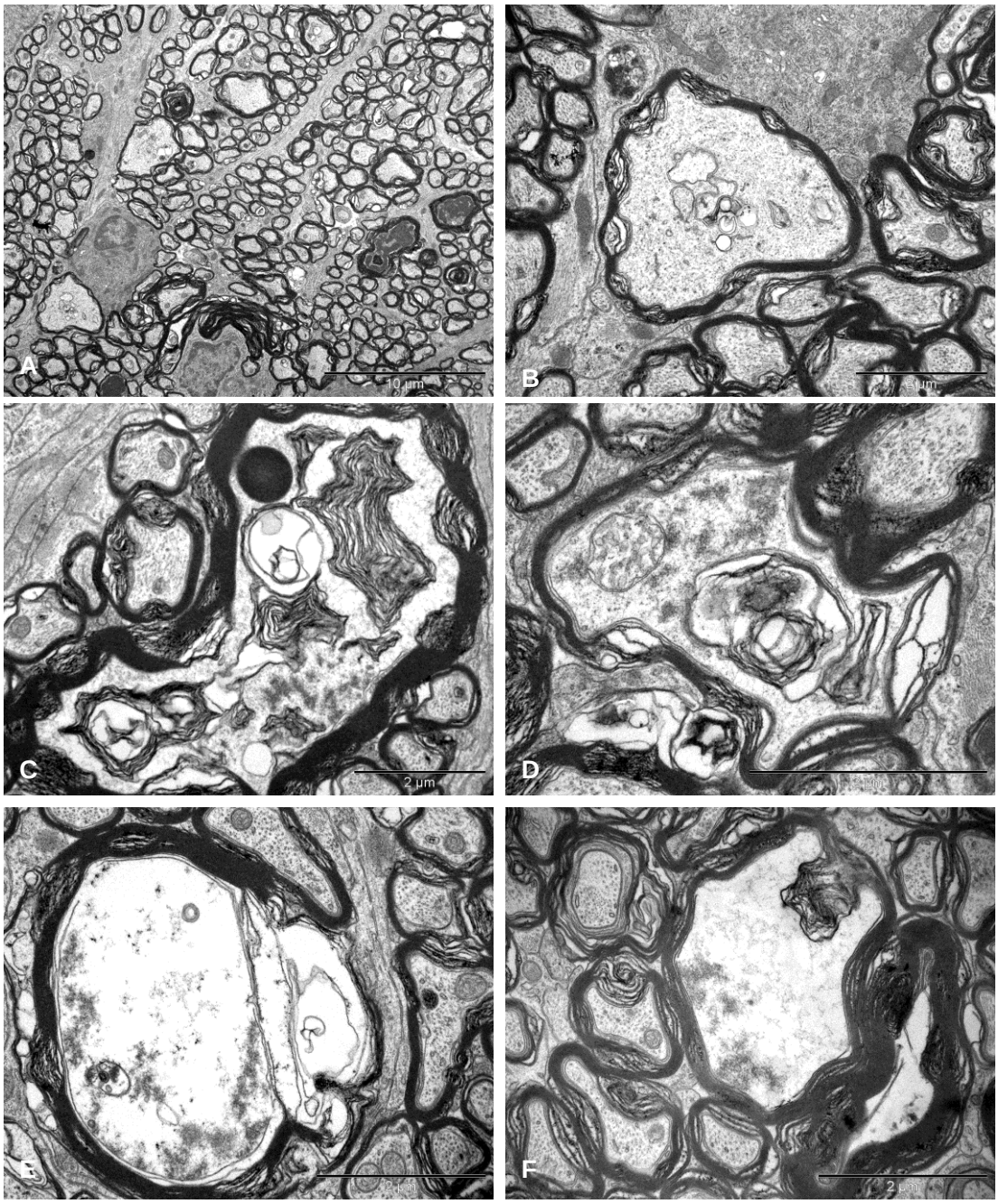

Figure 38. Ultrastructural appearances of axonal swellings in the transverse sections of distal segment of rat optic nerve after 72hrs of NMDA injection. The major change observed is the appearance of swollen axons (A, Bar=10μm). The axoplasm of these axonal swellings show abnormal collection of altered tubulovesicular structures (B-D, Bars=2μm), cytoskeletal disintegration (C-F, Bars=2μm), and multilayered whorled masses (C& F, Bars=2μm), which are seen to be arising from the inner layers of the myelin (F, Bars=2μm).

2) Dense axons- Some small to medium sized axons, which appeared dark under lower magnification, had their axoplasm filled with an amorphous, granular and dark material, thus

portraying what is described as 'dark degeneration'. Although, organelles were visible in some fibres, it was difficult to define the composition of dense axoplasmic material even at very high magnifications. The myelin of dark axons did not show significant alterations. [See Figure 39]

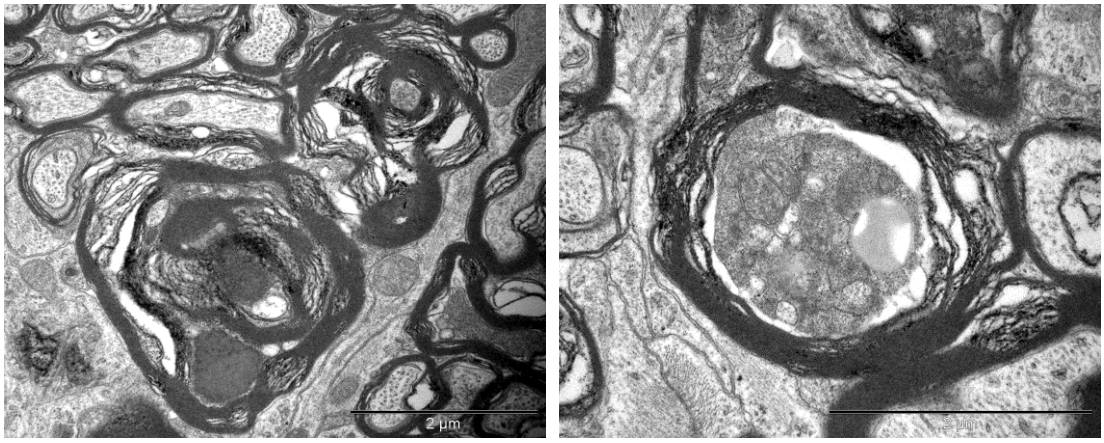

Figure 39. Ultrastructural appearance of hyperdense axons in distal optic nerves in the transverse sections of optic nerves seen 72hrs after NMDA injection (Bars=2μm). Note that despite the extent of the changes some adjacent axons still appear normal.

3) Demyelination- Occasional fibres showed features of demyelination which included vacuolation and splitting of the myelin sheath. Lamellar separation or widening made the myelin look abnormally thick and dark. These demyelinating changes were mainly seen around abnormally dense/dark axons. Partial or complete loss of axon transformed the myelin into collapsed structures which appeared as 'myelin bodies' in the extracellular space. [Figure 40 A & B]

Longitudinal sections displayed abnormal focal swellings and dense axons scattered between numerous normal fibres. Magnified images revealed some pathological changes even in fibres which appeared healthy under lower magnifications. The main abnormal features were abnormal accumulation of tubulo-vesicular structures including organelles in the nodal and

paranodal region, formation of nodal blebs, and intermittent myelin proliferation where the fibres showed splitting and proliferation of inner layers of myelin in the internode. The myelin proliferations formed whorls and loops, which protruded into the axon carrying the axolemmal covering around them. The proliferation was so pronounced that the mesaxonal loops occupied the entire diameter of axon. The axoplasm around the myelin whorls looked normal. The later finding was strictly restricted to the distal segments. No disturbance in the axon-myelin relationship was observed in the paranodal regions and the myelin terminal loops maintained normal relationships to the axons. No myelin debris was seen inside the astrocytes and microglial cells. [See Figure 40]

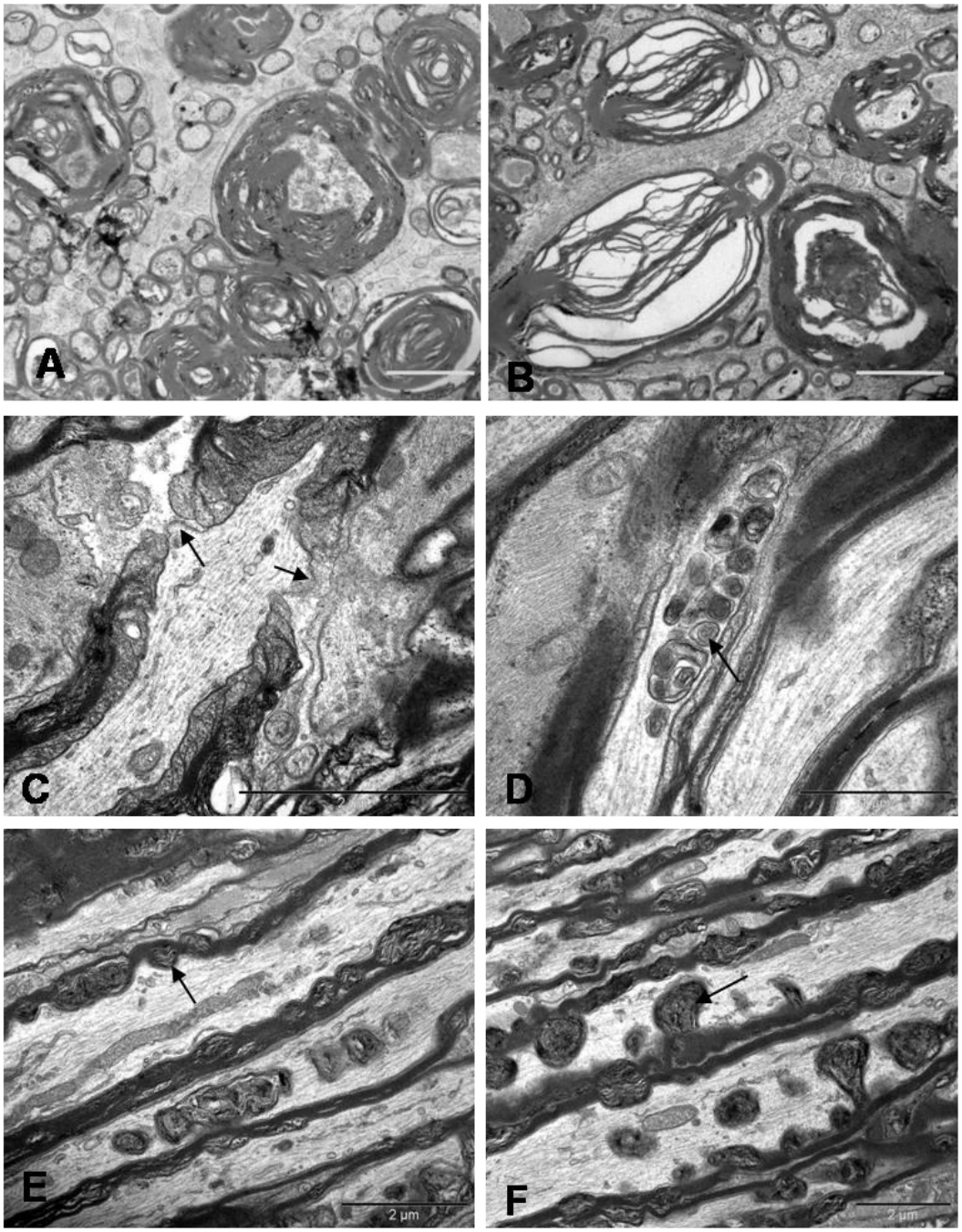

Figure 40. Ultrastructure appearances of the longitudinal sections of the rat optic nerve after 72hrs of NMDA injection showed nodal blebs (A, arrows), abnormal accumulation of altered organelles (B), myelin whorls (C) arising from the inner myelin and forming mesaxon (D). The cytoskeleton surrounding the myelin whorls appears normal at this stage (C & D). Bars=2μm

The degenerative changes at 7 days were clearly more intense than the previous stage. Extensive invasion by the filamentous astrocytic processes completely disorganized the nerve structure. Almost all fibres were altered and only a few scattered fibres showed a normal

appearance. A remarkable feature at this stage was the predominance of dark fibres, as compared to watery fibres. These dark axons appeared shrunken on longitudinal sections to create a gap between the atrophic axon and the inner layers of myelin. The myelin with lamellar separation could maintain the fibre outline. Moreover, demyelinating changes such as myelin breakdown, detached and vacuolated lamellae and formation of myelin bodies were frequently seen. Phagocytosing cells including microglia, astrocytes and oligodendroglial cells were enormously present throughout and myelin debris was mostly an extracellular feature. The most striking finding on longitudinal sections where a substantial length of axon was seen, was that the same axon showed features of watery degeneration (axonal swelling) and dark degeneration (hyperdense axoplasm). [See Figure 41]

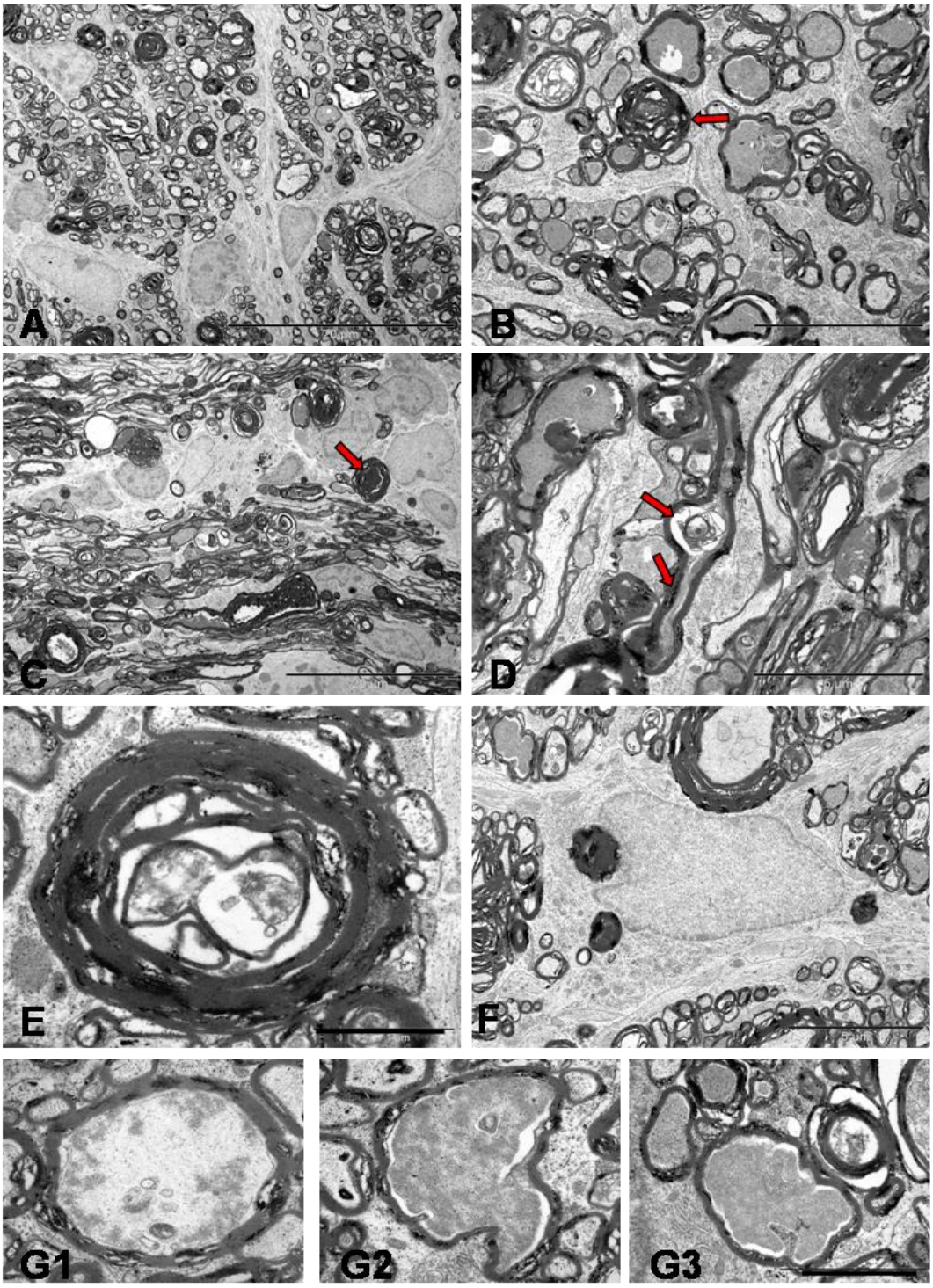

Figure 41. TEM of distal segment of rat optic nerve after 7 days of NMDA injection. Transverse (A, Bar=20μm & B, Bar=5μm) and longitudinal sections (C, Bar=20μm & D, Bar=5μm) show the fibres undergoing dark degeneration with most axons showing hyperdense axoplasm (red arrows). Longitudinal profiles show the focal axonal swelling and hyperdense axoplasm in the same axon (D, arrows). Axon towards the end stage of degeneration (E, Bar=1μm) show nearly collapsed axon structure and the myelin debris phagocytosed by the glial cells (F, Bar=5μm). Last series of photographs (G1, G2, G3, Bar=2μm) represent axoplasm in various stages of dissolution.

8.3 Discussion

Most of the information about the pathology of axonal degeneration is derived from the experimental nerve transection model which causes classic Wallerian degeneration of axons [537] and a reactive gliosis.[535, 536] As described in the chapter 6, NMDA induced excitotoxic injury to the retina causes significant reduction in thickness of inner retina at 72hrs (posterior retina, $p=0.002$ and peripheral retina, $p= 0.012$) with thickness reducing further to 68% and 76% in both regions compared to the control eyes at 7 days ($p< 0.05$). This implies loss of RGCs and their dendrites. Light microscopy also showed that damage to RGC somata is characterized by a well-ordered sequence of organelle changes along with a dying-back-like degeneration of the axons (the optic nerve fibres).

There is paucity of literature regarding degenerative changes in the optic nerve at the ultrastructural level. To our knowledge, this is the first study to report the pathological changes in the optic nerve at ultrastructural level after excitototxic retinal damage. To characterize the events leading to neuronal cell death after isolated injury to the perikaryon, this morphologic study in rats describes the time-dependent pathological sequelae in the RGCs and optic nerve after NMDA-induced retinal damage. TEM analysis showed that the effects of excitotoxic stimuli begin in the retina within 24hrs where RGCs undergo progressive necrosis, and the optic nerve degeneration mimics classic Wallerian degeneration. Studies have shown that Wallerian degeneration mutation rescues axons but not cell bodies in a rat model of glaucoma and that axonal degeneration can be delayed for weeks in the presence of the slow Wallerian degeneration gene (WldS), suggesting that Wallerian degeneration is an active, regulated process.[538] Recent research suggests that the more long-lived, functionally related WldS

protein, a variant of Nmnat1, substitutes for endogenous Nmnat2 loss after axon injury, which is actually considered to prevent spontaneous degeneration of healthy axon.[539]

NMDA induced retinal changes

Previous studies showed that the excitotoxic injury could lead to apoptotic, autophagic or necrotic cell death.[269, 463, 464, 504, 518-521] Evidence is also available that excitotoxic injury can produce hybrids forms existing on a continuum between the classically defined apoptosis and necrosis,[462-464] and is likely to depend on the degree of insult and the sensitivity of exposed neurons. Time-dependent studies of glutamate exposure to cultured neuronal population showed that the excitotoxins induce early necrosis and delayed apoptosis.[269, 540] There is also evidence that the necrotic neurons may completely recover to undergo apoptotic transformation later.[540] Electron microscopic evaluation of the retina in the present study is consistent with the previously reported early neuronal vacuolization and subsequent necrosis.[541, 542] Although, the development of vacuolation prior to emergence of necrotic features and cell loss explain that the vacuolated neurons underwent necrosis later, the possibility of vacuolated neurons recovering completely and non-vacuolated neurons undergoing necrosis cannot be ruled out.

The early neuronal vacuolation, where the RGCs displayed features of somato-dendritic swellings, represented neuronal stress before any morphological evidences of injury. The dendritic swelling is believed to be due to influx of Na^+ through NMDA receptor channels, which in turn causes internalization of another type of ionotropic glutaminergic receptors, AMPA receptors.[543] Because excessive stimulation of AMPA receptors is associated with delayed excitotoxic neuronal damage,[544, 545] the dendritic response can be considered as an early defensive action against excitotoxic insult. The early somal events, seen as cytosolic

and diffuse organelle swelling, represented stress-induced perturbations in cell volume homeostasis and mitochondrial function [546], Here, excessive Ca^{+} influx through NMDA receptor mediated Na^{+}/ Ca^{+} exchanger,[543, 547, 548] causes activation of endogenous phospholipases to produce damage to membrane-bound cytoplasmic organelles.[549] The buffering action of mitochondria in response to excessive free cytosolic Ca^{2+} causes sequestration of Ca^{2+},[293, 550, 551] which builds up oxidative stress and opens up mitochondrial permeability transition pores (MPTPs) causing mitochondria to swell.[293, 550-554] Swelling of mitochondria is characterisctic of early excitotoxic events.[555, 556] Although mitochondrial Ca^{2+} accumulation and MPT (mitochondrial permeability transition) are common denominators in excitotoxin-induced neuronal death,[557, 558] whether the cell will die by necrosis or apoptosis depends on mitochondrial ATP generation.[559] Generally, if ATP synthesis is adversely affected, the cell dies by necrosis; while if mitochondria do not undergo major MPT, the cell undergoes apoptosis.[559, 560]

Cell death seen 72hrs after excitotoxic insult, exhibited the essential features of ‘necrosis’, [462, 561-564] characterized by progressive organelle swelling, cytolysis and karyolysis (lysis of the cell and the nucleus). Similar to the description of a necrotic cell provided by Isaev et al. [558] and Kato et. al.,[565] the cells showed mitochondrial swelling, dilated endoplasmic reticulum, dissolution of ribosomes in early stages and disintegration of cytoplasmic organelles, change in nuclear morphology and mild chromatin aggregation in advanced stages. Because it is believed that the apoptosis requires functional mitochondria,[566] the presence of swollen and disrupting mitochondria suggested that the event was non-apoptotic. In the presence of whorl-like multi-laminated ‘myelin figures’ or ‘myelin-like bodies’[567] in severely damaged RGCs, and in the absence of highly specific features of apoptosis (heterochromatin segregation, nucleolar disintegration or apoptotic bodies) as well as

autophagocytosis (presence of typical autophagosomes) [567-570], cellular events were labelled as necrotic.

EM morphologic features at 7 days showed axon-like process growing in the inner retina.[571, 572] Whether the process represent surviving intraocular part of optic nerve axon or the regrowth of axons indicating regenerating capacity of RGCs remains to be determined. Evidence exists that nerve processes regenerate from the RGCs remaining in the retina post-axotomy.[571, 573, 574] Most research in the field of retinal regeneration done using optic nerve axotomy and crush injury models demonstrate that the axons can regrow not just from the proximal stump of the severed axons, as was previously believed, but also from other parts of the neurons including dendrites, soma or intraretinal axons.[573] If this represents axonal regrowth, raise the question about the origin of the regenerating cells. The possible sources could be the surviving RGCs or the glial cells. These regenerating RGCs are morphologically different from normal RGCs and based on their appearance, are classified into five categories- RI, RII, RIII, Rdelta and displaced RGCs.[574] The surviving RGCs after 7 days of injury looked indistinguishable from the normal RGCs and no specific cells were identified lying in the vicinity of dendritic sprouting. Fischer and Hey demonstrated that after acute neurotoxic injury to the retina, Müller glial cells can also dedifferentiate into retinal progenitor cells which in the presence of some unidentified signals transform into amacrine and bipolar cells.[575] A similar study by Ooto et al showed transformation of Müller glial cells into bipolar and rod photoreceptor cells with retinoic acid as a specific promoter for the growth bipolar cells.[576] Although these studies showed the regeneration of retinal neurons from Müller cells, none of them report Müller cell transformation into RGCs growing out nerve processes. Because there is no convincing evidence available to show transformation of glial cells into RGCs, the possibility of surviving RGCs regenerating new neurons remains high.

Alternatively, it is possible that the neurons may regenerate from the quiescent sparsely distributed neural stem cells, similar to those seen in mouse retina.[577]

Multiple factors are likely to influence the survival and regenerative ability of RGCs in the retina. One major factor can be difference in the cell susceptibility due to difference in subtype and concentration of NMDA receptors between cell populations. Studies have identified that small-sized RGCs are least vulnerable to excitotoxicity.[483, 507] Although, no effort was made to distinguish RGCs based on their size, it seems reasonable that the least injured cells have better chances of survival and regeneration. Another important factor which can affect the regenerative capacity of neurons is the release of neurotrophic factors. Although, it is believed that neurotrophins increase the expression of growth-related genes,[578] their mechanism of action is not firmly established. Despite unclear function, previous work has firmly established their protective role in nerve degeneration.[579-582] Protective effect on retinal neurons (RGCs) is ascertained in optic nerve transection model where intravitreal injection of trophic factors such as GDNF,[583] BDNF or CNTF,[584, 585] intravitreal application of neurotrophin producing genetically modified neural progenitor cells [586] and direct delivery of neurotrophin genes (electroporation) into RGCs [587, 588] have shown a protective effect on RGCs, thereby, increasing their chance of survival and regeneration. Intravitreal injection of NMDA or kainite is known to induce CNTF expression in reactive Müller cells.[469] Also, experiments using optic nerve transaction,[589] experimental glaucoma models [590, 591] have suggested that these factors are released by reactive retinal Müller cells [581, 590, 592] in sufficient amount to impart endogenous neuroprotection to retina. Because the current study demonstrates the appearance of regenerating neurons from surviving RGCs, the possibility of release of neuroprotective factors from retinal glial cells, including Müller cells, astrocytes and microglial cells, should be considered.[593, 594] Though

this regeneration may be a transient phenomenon, it is possible that this axons can regrow up to their full length in the presence of nerve grafts.[572]

NMDA-induced optic nerve changes

This part of the study was a qualitative ultrastructural analysis of the main alterations in the rat's optic nerve after excitotoxin induced pathological neuronal (RGC) activation. In comparison to the popular models of immediate (axotomy) or delayed (stretch) disruptive injuries, where the axons and myelin are simultaneously and directly damaged at the site of lesion, optic nerve fibres in the current model do not suffer any form of direct injury. As axons form a link between the neuronal cell body and the myelin surrounding them, any change in the myelin are secondary to the axonal damage. Because the optic nerve is physically isolated from the eyeball, retro-orbital axonal changes seen in the present study are most likely the result of direct injury to RGCs or indirect damage to the intraretinal axons. Several early physiological studies suggest that the axons lack excitatory amino acid receptors and they respond to excitatory amino acids indirectly by the change in extracellular ion composition associated with neuronal depolarization.[595-597]

The initial sequence of events resulting in axonal degeneration depends upon the type of injury. With the fibres undergoing Wallerian degeneration after axotomyin frog optic nerve, Ishise J et al showed that the asymmetric paranodal myelin retraction is the initial event, which is followed by the formation of nodal blebs and accumulation of abnormal organelles in nodal axolemma.[598] In response to excitotoxic perikaryal injury, this study found nodal changes in the form of bleb formation and abnormal accumulation of organelles in the paranodal region

with no obvious myelin terminal loop retraction as early changes. These changes resembled the response observed after non-disruptive stretch injury, where accumulation of membranous organelles in the paranodal and internodal regions preceeded the nodal bleb formation related with loss of axolemmal undercoating.[599]

Nodal changes seen in the present study indicate the role of disrupted ionic equilibrium in initiating axonal damage following excitotoxic perikaryal injury. It can be suggested that the decreased ATP and mitochondrial formation, usually seen with necrotic cell death, results in energy-dependent pump failure at active nodal sites causing ionic imbalance, focal cytoskeletal dissolution and neurofilament compaction; loss of membranous Ca^{2+}-ATPase pump causing Ca^{2+} influx induce calpain-mediated proteolysis of the subaxolemmal proteins which results in the formation of nodal blebs.[600, 601] This proteolytic activity spreads to involve the entire nodal axoplasm [600] results in focal axonal swellings with variable amount of cytoskeletal disruption. Studies have also shown that proteolyic degradation of sidearms of neurofilaments results in their axoplasmic aggregation.[602] These cytoskeletal changes are likely to affect the axonal transport system leading to the accumulation of transport material including vesicles, organelles, proteins and enzymes in the paranodal and internodal regions.[603]

Unlike the stretch injury model, axons form the only link between the myelin and the cell body in the current study. The selective perikaryal insult is unlikely to result in myelin changes without producing axonal damage at any level. Therefore, it still remains unclear why myelin proliferation and separation occurred intermittently in the internodes in the absence of evident cytoskeletal damage.

Similar to the study using optic nerve crush injury,[452] this study has identified watery and dark degeneration in the axons. Both patterns were observed at 72hrs and 7 days of injury. Although there was no apparent predominant form at 72hrs, there was a clear increment of fibres undergoing dark degeneration and demyelination at 7 days. These changes precedes the onset of focal axonal swelling.[604] The demyelination in the absence of axonal changes was comparable to the general axonal response to trauma. It is unclear whether the same axon displays different type of axoplasmic degeneration at variable distance from RGC at the same time or individual axons undergoes a specific type of degeneration throughout its length. It is possible there is a cause and effect relationship between both types of degeneration, but evidence is circumstantial. Unlike the stretch injury model, axons form the only link between the myelin and the cell body in the current study. It was presumed that perikaryal insult is unlikely to damage myelin without producing axonal changes. However, myelin showed proliferation and intermittent separation at internodes in the absence of cytoskeletal damage.

Glial cells in the optic nerve also reacted to excitotoxic-induced axonal degeneration in a manner similar to that seen during Wallerian degeneration.[605] Although, there are evidences for the expression of NMDA receptors on oligodendrocyte processes in white matter,[460] oligodendrocytes in retro-orbital optic nerve axons remained normal. But astrocytes underwent reactive changes with the development of extensive filament-rich processes. Studies have shown that astrocytes and microglial cells invade the myelin sheath at the intraperiod line and phagocytose the peeled off outer lamellae.[536] No such glial invasion was seen in this study. Myelin debris was seen scattered in the extracellular space. Phagocytosed myelin which is initially in the form of the paired electron-dense curvilinear lines decompose and form a

homogeneous or heterogeneous osmophilic layered structure, the myelin body, which, in the final stages, disintegrate and transform into globoid lipid droplets and needle shaped cholesterol crystal.[536]

In conclusion, selective perikaryal excitotoxic injury causes a predominantly necrotic form of somal death with simultaneous nodal-paranodal changes in axons culminating later to Wallerian-like degeneration in the form of dark and watery degeneration with demyelination. The Wallerian-like degeneration noted in this model, after primary perikaryal injury, raises the possibility that excitotoxicity-induced axonopathy is an active, regulated event. This hypothesis could be tested by using the current model and comparing the axonal degeneration in slow Wallerian degeneration (WldS) rats with the degeneration in control rats.

Chapter 9: EFFECTS OF EXCITOTOXIC PERIKARYAL INJURY ON THE AXON TRANSPORT SYSTEM

9.1 Introduction

Neurons rely on their transport system for their differentiation and survival. Because neuronal processes lack the ability to synthesize proteins, lipids, organelles or synaptic neurotransmitters, transport system plays a crucial role in maintaining their structural integrity and functional viability. Two transport systems responsible for anterograde and retrograde transport of various structural elements are- fast and slow. Fast axonal transport moves membranous organelles such as, synaptic proteins, enzymes, neurotransmitters, mitochondria and other vesicles to the axon terminal [See Section 2.5.1]. Slow axonal transport is responsible for the movement of cytoskeletal proteins such as, neurofilament heteropolymers and microtubule oligomers for incorporation into the major cytoskeletal elements, neurofilaments and microtubules respectively [See Section 2.5.2]. A recent study demonstrated decline in the motor protein, kinesin-1, preceding the axon degeneration.[466] Because decline in the transport of proteins required for the maintenance of the distal axon may be a contributing factor in nerve degeneration, it is pertinent to consider the contribution made by the axon transport system in nerve pathology.

Previous sections of the study demonstrated that NMDA-induced retinal injury produces inner retinal damage and RGC necrosis resulting in dying-back optic nerve degeneration. This section of the study will explore the role of axon transport in somagenic nerve degeneration process, where axon injury is the indirect result of nearly isolated excitotoxic somal death. As most axon transport studies were conducted using direct axon injury models where systemically injected toxins in *in-vivo* neuropathy models,[397, 606, 607] penetrate the blood-

nerve barrier and bind to the cytoskeletal elements or transport motor proteins.[22, 608-610] causing rapid, non-reversible reduction in bidirectional axonal transport, [611] this research will elucidate the role of soma in maintainence of axons and will provide a mechanism of excitotoxic somagenic nerve degeneration and thus, glaucomatous optic neuropathy.

Neurofilaments, transported by slow axonal transport using the motor protein, kinesin, maintain the neuronal growth, size and shape and decline in their synthesis or disturbance in their transport may cause decrease in the axon calibre. Mice with mutant Kinesin heavy chain, KIF5A, accumulate NH-H, NF-M and NF-L in the cell bodies of peripheral sensory neurons causing reduction the axon calibre.[612] Marked but selective acceleration of the neurofilament transport shifting a large amount of neurofilaments towards the distal axon is noted in toxin-induced neuropathy.[390] Hastened transfer with defective 'turnaround' and abnormal proteolysis causes pathological accumulation of NFs in the axonal swellings.[389, 492, 611, 613-617] Taniguchi et al have noted a loss of neurofilament subunit in the optic nerve in ocular hypertension and kainite-induced retinal excitotoxicity models.[618] With an *in-vitro* study using a cortical neuron culture, Chung et al demonstrated loss of NF-H and beaded staining with NF-M and NF-L in neurons following kainite and NMDA exposure.[619] Although studies have suggested the role of neurofilaments in many neurodegenerative disorders,[198, 620, 621] the role of neurofilaments in excitotoxic somagenic nerve degeneration remains unclear. This part of the study demonstrates changes in the distribution of neurofilament subunit, NF-L which forms an obligatory component for basic NF assembly. As NF-L is a marker of slow axonal transport, this study will demonstrate the effect of excitotoxic somal injury on slow axonal transport. Also, NF-L antibody has higher sensitivity and specificity than the antibodies for other subunits.[618]

β-APP is an integral membrane glycoprotein present in the axolemma and synaptic regions of neurons.[622, 623] Synthesized by RGCs, glycosylated β-APP protein molecules are internalized into membrane bound vesicles, which are transported to the nerve terminals by fast anterograde axonal transport.[624, 625] During this active intraneuronal movement, cytoplasmic C-terminal of β-APP in membrane bound vesicles binds to the light chain of the microtubule-dependent motor protein, kinesin.[626-631] Therefore, it serves as a cargo for the translocation of pre-synaptic proteins destined for nerve terminus.[625] Any injury to the axons causes impairment of the fast axonal transport resulting in accumulation of β-APP molecules in injured axons.[632] Because β-APP is an important participant in fast axonal transport and is an excellent marker of axon damage, its immunohistochemical detection forms a very sensitive and reliable method of assessing functional injury/ fast axonal transport injury in the axons.[633-637] Therefore, this part of the study also aimed to assess temporal changes in the expression of β-APP in the retina and optic nerve following excitotoxic perikaryal injury. This precursor molecule is also strongly related with the formation of amyloid fibrils in Alzheimer's disease.[458]

9.2 Results

9.2.1 NF-L immunostaining in the retina

Immunostaining of the saline-injected control retinas showed NF-L localization within the inner retina and to a lesser extent in IPL. Immunostaining was observed in RGCs and also in the axons running in INFL. RGC nuclei counterstained by haematoxylin appeared blue in colour. Within the OPL also, a faint immunoreactivity was observed probably corresponding to horizontal cells. Negative and positive controls showed no damage at any time point. No change in NF-L staining was observed in the saline-injected eye balls at any time point. [See Figure 42]

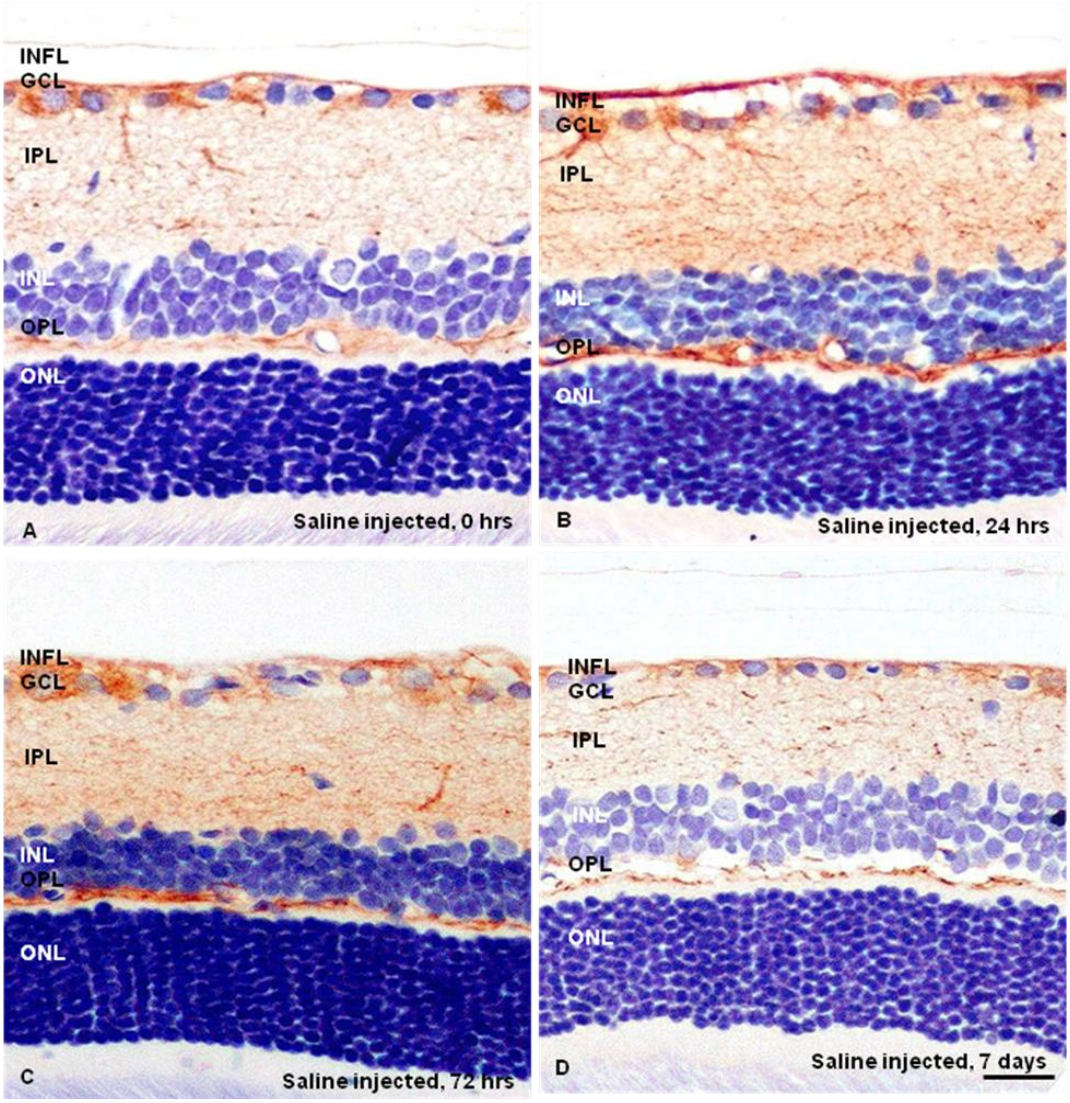

Figure 42. NF-L immunostaining in the retina after intravitreal saline injection in rat. All images shown here are taken from the posterior retina (200μm from the optic disc). Retina at 0 hrs after saline injection shows staining of the INFL, IPL, OPL and faint cytoplasmic cytoplasmic staining of RGCs. No change in immunoreactivity is seen in the retina at 24hrs (B), 72 hrs (C) and 7 days (D). X200 magnification. Bar= 50μm. INFL=inner nerve fibre layer; GCL=ganglion cell layer; IPL=inner plexiform layer; INL=inner nuclear layer; OPL=outer plexiform layer; ONL=outer nuclear layer.

NF-L immunostaining after NMDA injection revealed no significant changes in the NF-L immunoreactivity in the retina upto 24hrs. Light microscopy of retina at day 3 post NMDA injection revealed no changes in the intensity of NF-L staining in the INFL, IPL and OPL. Decrease in ganglion cell counts was reconfirmed. Some RGCs showed NF-L

immunoreactivity similar to that seen in saline control eyes. Rounded spheroidal structures were often encountered with very intense NF-L immunostaining. An attempt was made to distinguish these intensely staining rounded structures as RGCs or axonal swellings in INFL based on their profile, location and presence of nuclei. However, it was very difficult to distinguish them as RGCs or axonal swellings in intraretinal optic nerve axon fibres. At day 7, the RGC count decreased further and the IPL reduced in thickness. Number of NF-L immunostained spheroids also decreased. No change was observed in NF-L immunostaining in the IPL and OPL. [See Figure 43]

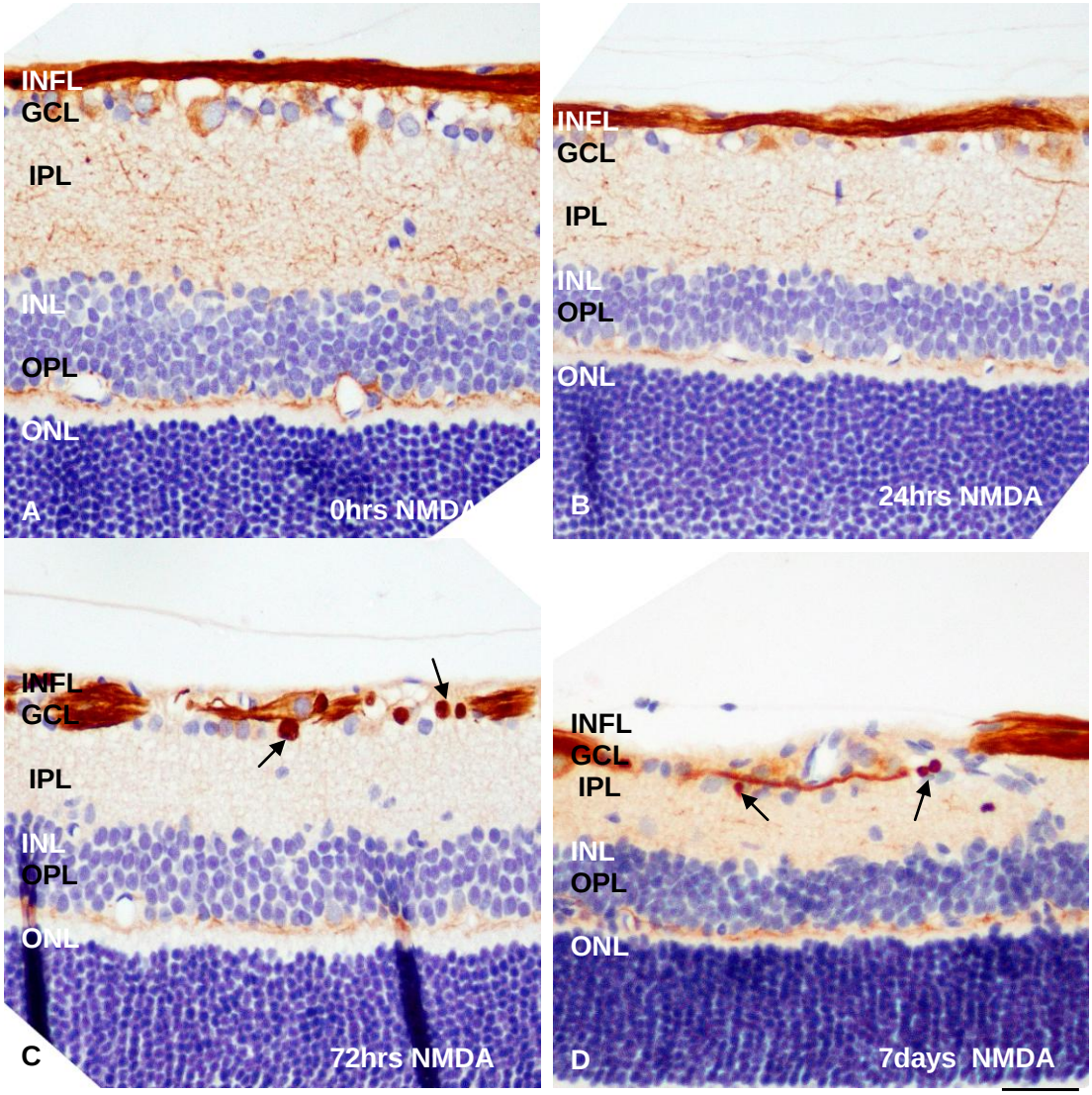

Figure 43. Progressive changes in NF-L immunostaining in the retina after NMDA injection in rat. All images shown here were taken from the posterior retina (200μm from the optic disc). Normal immunoreactivity is seen in the retina at 0 hrs (A) and upto 24hrs after NMDA injection (B). At 72hrs post NMDA injection (C), along with RGC loss, most retinal layers maintain normal NF-L staining except the INFL which shows intensely stained axonal swellings (arrows). 7days after NMDA injection (D), further RGC loss and thinning of the retina was seen with axonal swellings still seen in the INFL. Not many difference are seen in the NF-L immunostaining in the other retinal layers at this stage. X200 magnification. Bar= 50μm. INFL=inner nerve fibre layer; GCL=ganglion cell layer; IPL=inner plexiform layer; INL=inner nuclear layer; OPL=outer plexiform layer; ONL=outer nuclear layer.

9.2.2 NF-L immunostaining in the optic nerve

Longitudinal and transverse sections of the saline-injected optic nerves showed densely packed immunoreactive axons of variable diameter spread uniformaly across the whole optic nerve cross-section. Negative and positive controls showed no damage at any time point. No difference was observed in NF-L immunostaining intensity and profile between the saline injected optic nerves at any time point. [See Figure 44]

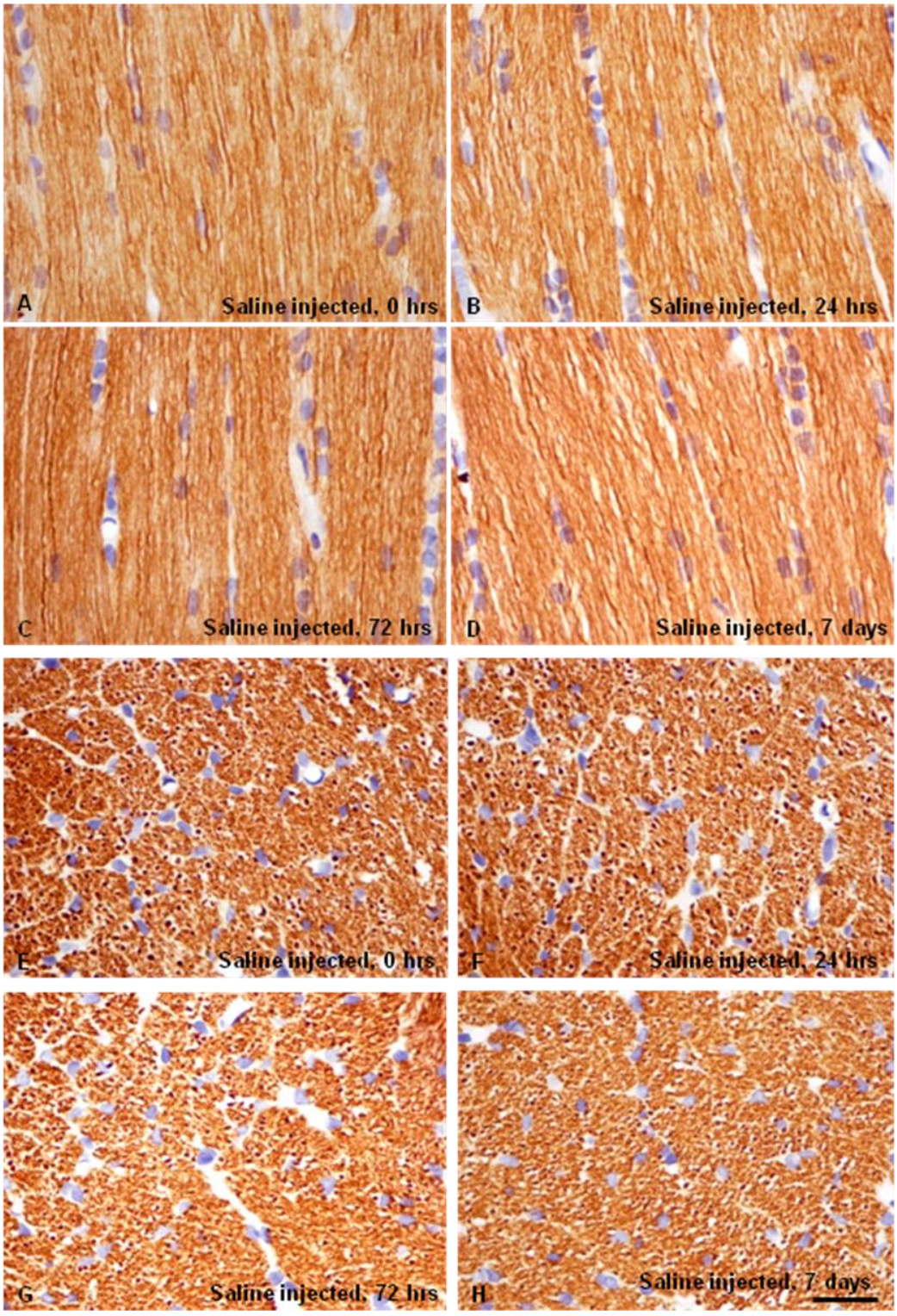

Figure 44. NF-L immunoreactivity in the longitudinal and transverse sections of the saline injected optic nerves at various time points.All photographs are taken from the distal optic nerve segments. Here NF-L stained optic nerve axons are seen compactly packed and running longitudinally parallel to each other in A (0 hrs), B (24 hrs), C (72 hrs) and D (7 days). Similarly compactly packed transverse sections of distal optic nerve segments are seen in E (0 hrs), F(24 hrs), G(72 hrs) and H (7 days). Bar=25μm

Normal axonal NF-L immunoreactivity was detected in the optic nerves immediately and 24hrs after NMDA injection. At day 3, many round unstained empty spaces were seen spread randomly between the NF-L stained axons, which still maintained normal NF-L immunoreactivity. Overall, total immunostaining of NF-L reduced at day 7 in both longitudinal and transverse sections. It appeares to be due to reduced number and calibre of axons. No marked differences were observed between the proximal and distal optic nerve segments. [See Figure 45]

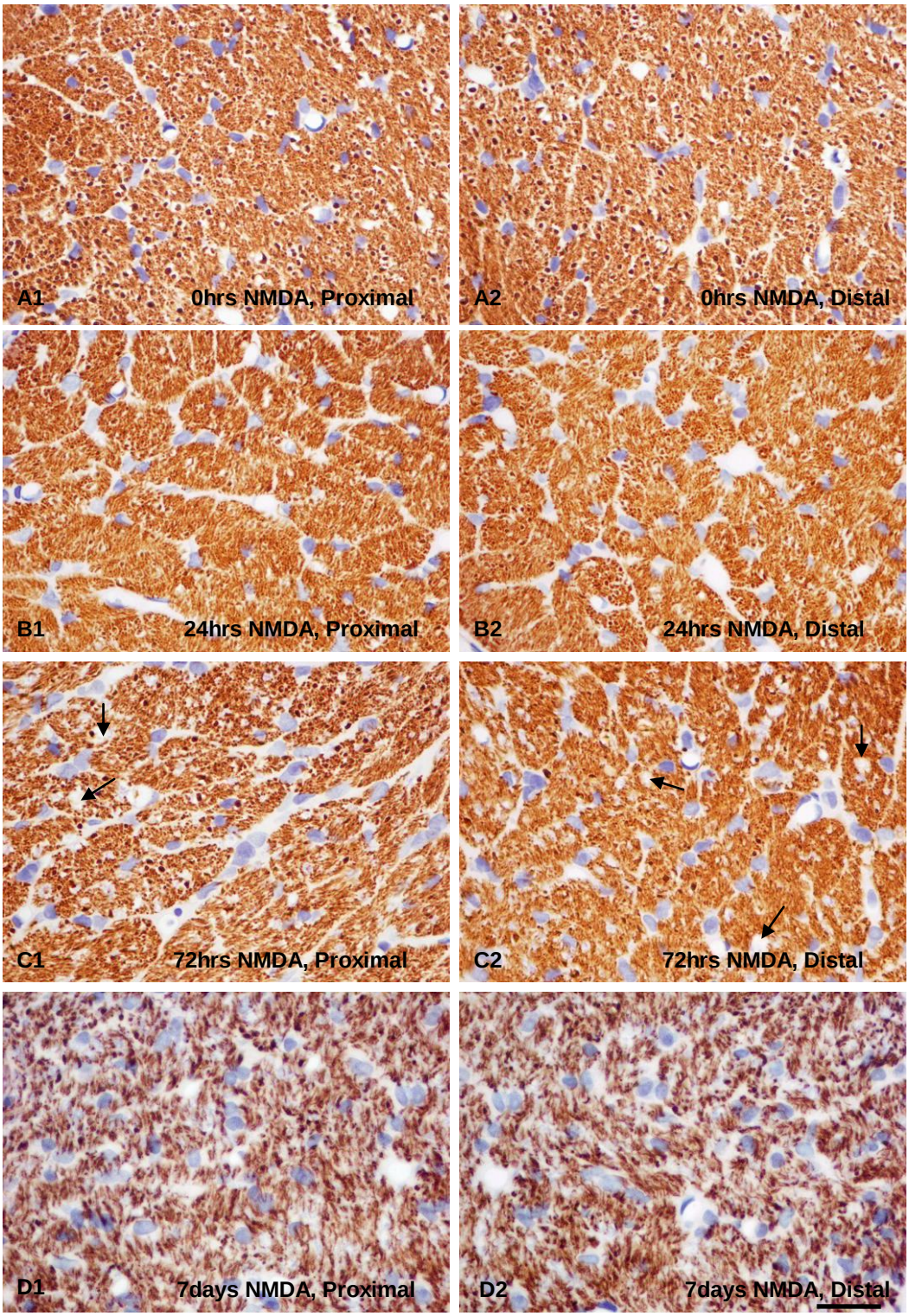

Figure 45. NF-L immunorectivity in the transverse sections of the optic nerve of the NMDA injected rat. Proximal optic nerve sections (A1, B1, C1, D1) showed similar immunostaining as the distal optic nerves (A2, B2, C2, D2). Normal immunostaining is seen at 0hrs (A1, A2) and 24hrs (B1, B2). 72hrs after NMDA injection (C1, C2), unstained round spaces (arrows) are seen between the densely packed axons which still maintain normal NF-L intensity and profile. At day 7 post NMDA injection, the density of NF-L staining is decreased. Bar=25μm

Normal immunostaining intensity and profile was seen in the optic nerve segments after NMDA injection at day 1 and 3 after NMDA injection. A few round clear spaces lied between the axons, the centre of which sometime showed irregular NF-L immunoreactive fibrous structure. At day 7 post NMDA injection, NF-L immunoreactivity reduced as axons numbers reduced. Similar to transverse sections, longitudinal sections did not display any difference between the proximal and distal optic nerve segments.[See Figure 46]

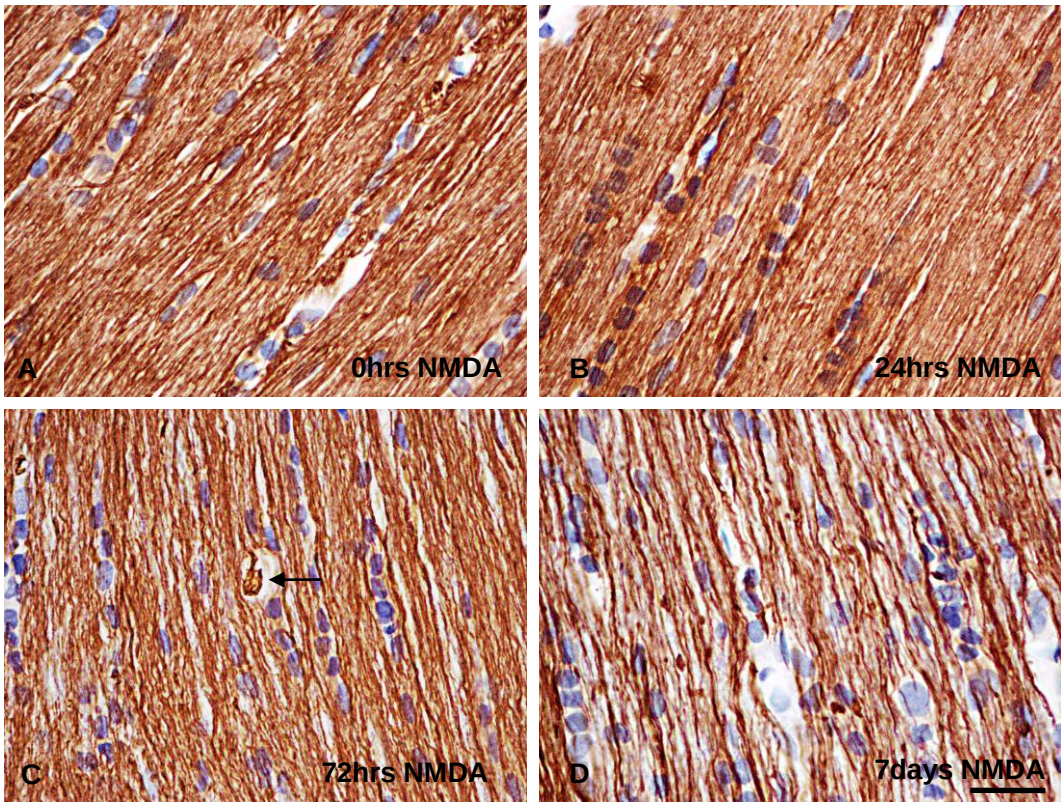

Figure 46. NF-L immunoreactivity in the longitudinal sections of the NMDA-injected optic nerves. All photographs are taken from the distal optic nerve segments. Here NF-L stained optic nerve axons are seen compactly packed and running longitudinally parallel to each other at 0hrs (A), 24hrs (B) and 72hrs (C). At 72hrs after NMDA injection (C), empty spaces are seen occupied by a NF-L stained irregularly structure (arrow). At day 7 (D), the density of axons is much reduced. Bar=25μm

9.2.3 β-APP immunostaining in the retina

Retinal sections of the saline-injected control eyes showed diffuse low level β-APP immunoreactivity in RGCs and INFL at all time points examined. [See Figure 47] Faint axonal staining was also seen in the optic nerve head, which extended into the optic nerve for a short distance from the lamina cribrosa. Most caudal portion of the optic nerve attached to the globe showed no axonal staining; however, weakly stained glial cells were observed in the interfascicular region of this part of the nerve. Negative and positive controls showed no damage at any time point.

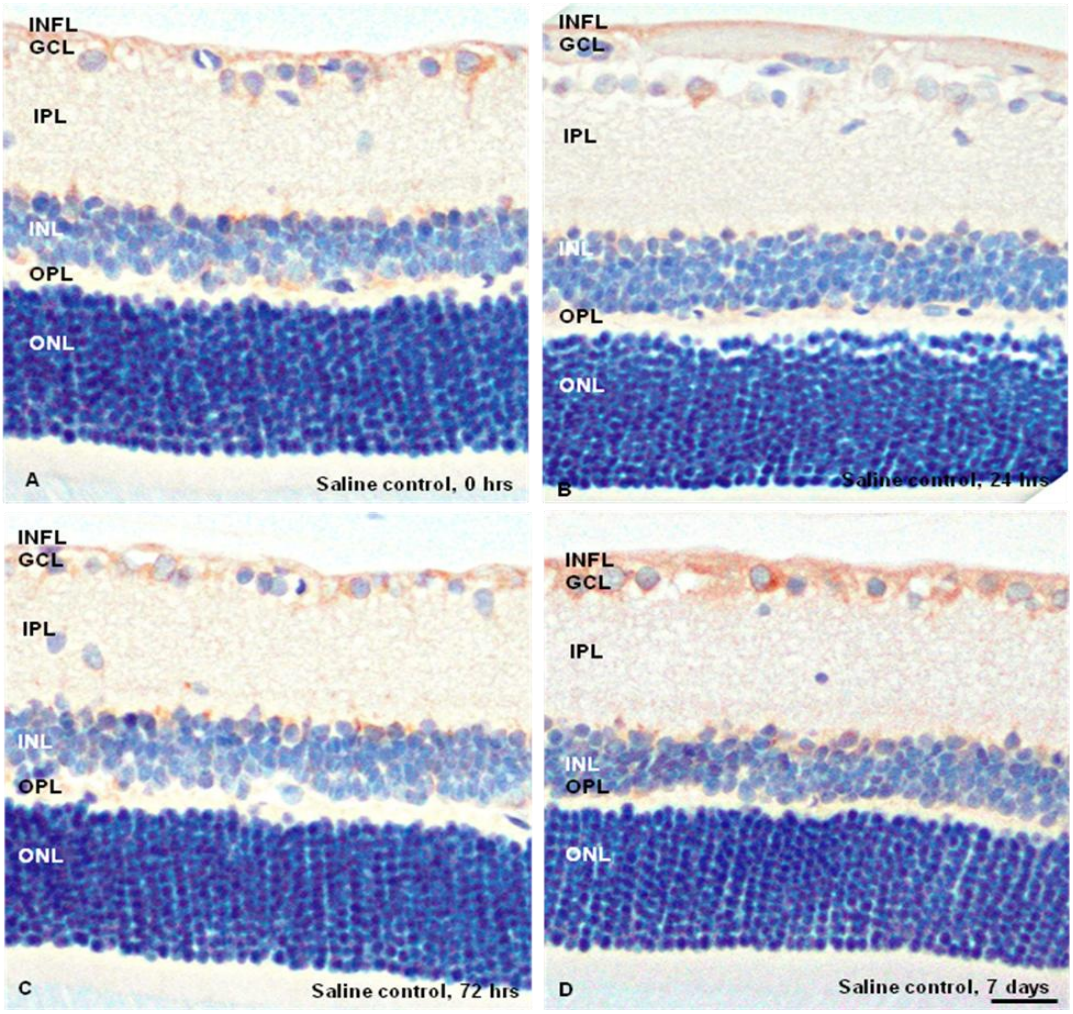

Figure 47. β-APP immunoreactivity in saline-injected rat retinas. Diffuse low level β-APP immunoreactivity noted in INFL in all retinas at all time points. X20, magnification. Bar=50μm

No change in β-APP immunoreactivity was observed in the NMDA exposed retina immediately, day 1, day 3 and day 7 after injection. Although the number RGCs decreased at 3 and 7 days after NMDA injection, intensity of β-APP immunostaining in the RGCs, INFL and optic nerve head of NMDA-injected eyes appeared similar to the saline-injected control eyes at all time points.[See Figure 48]

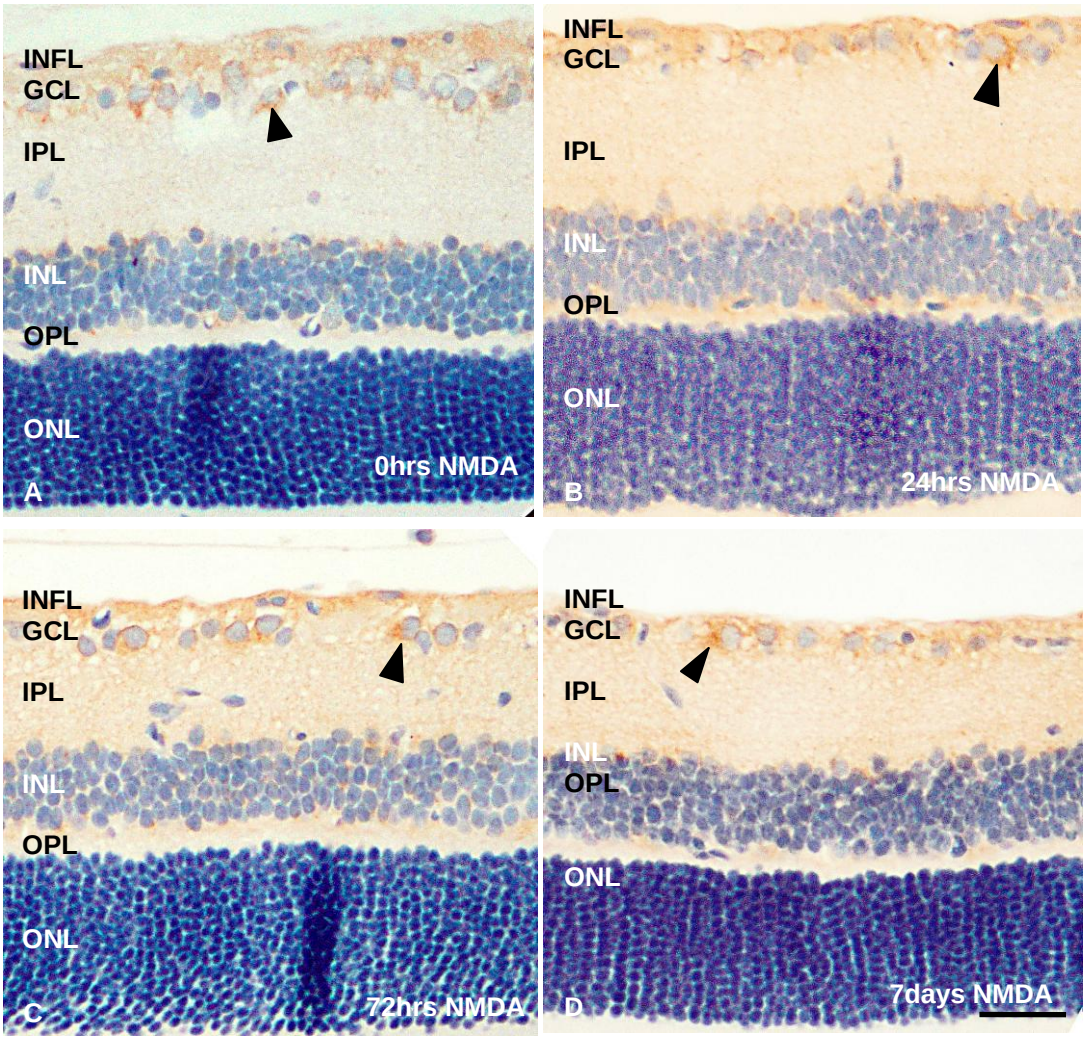

Figure 48. β-APP immunoreactivity in NMDA-injected rat retinas. Note the faint cytoplasmic immunostaining in RGCs as well as INFL. No change in β-APP immunorectivity was observed in the ganglion cells and axons running in the nerve fibre layer soon after injection (A), at day 1 (B), day 3 (C) and day 7 (D) after NMDA injection. magnification, X20. Bar=50μm

9.2.4 β-APP immunostaining in the optic nerve

Longitudinal sections of the saline-injected control proximal and distal optic nerve segments at all time points showed very faint cytoplasmic β-APP immunoreactivity in the interfascicular glial cells. [See Figure 49] Negative and positive controls showed no damage at any time point.

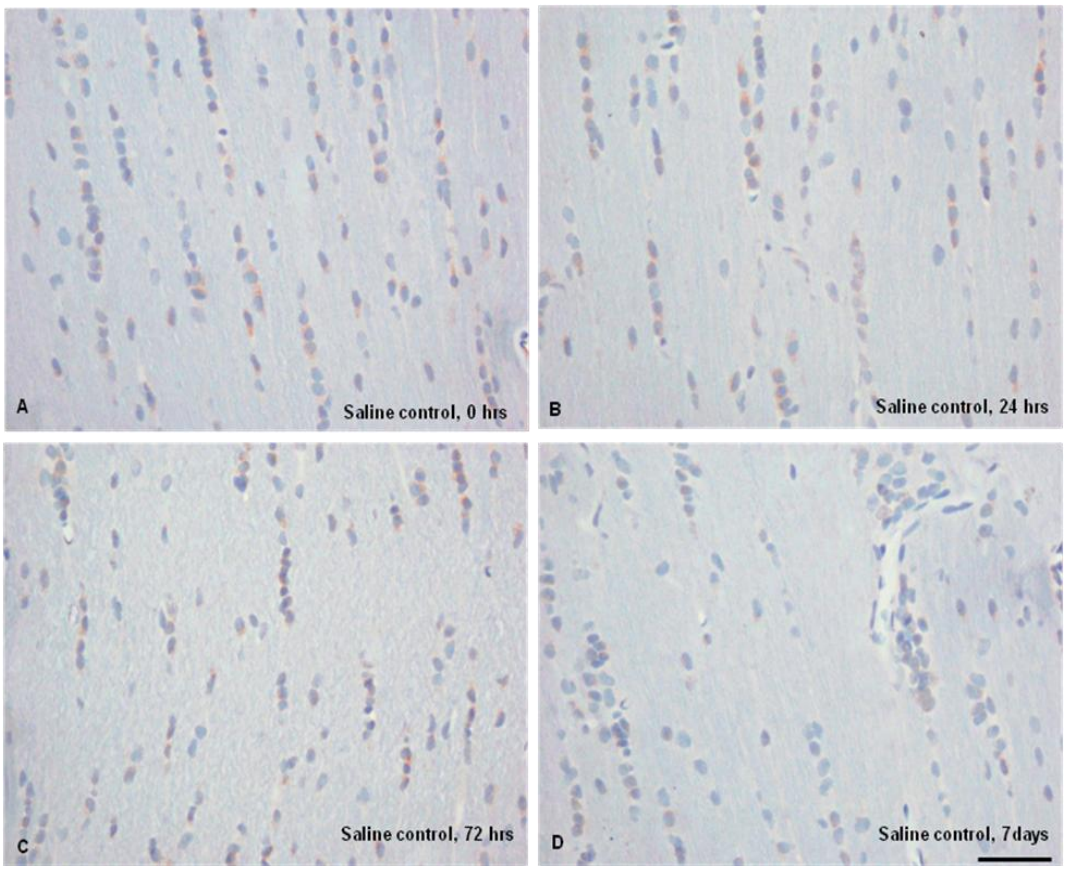

Figure 49. β-APP immunoreactivity in the longitudinal sections of the distal segments of the saline-injected rats. Very faint cytoplasmic β-APP immunoreactivity in the interfascicular glial cells at all time points. X200 magnification, Bar=50μm

Normal β-APP immunological staining was demonstrated in the NMDA injected optic nerves immediately and 24hrs after injection. At 72 hrs post-injection, slight increase in the intensity of β-APP staining was observed in the glial cells of the NMDA-injected optic nerves. At day 7, glial cells immunoreactivity increased further alongwith the appearance of β-APP background

staining. This faint staining emerged out as punctate immunostaining of the optic nerve under higher magnification (400X). [See Figure 50 & 51]

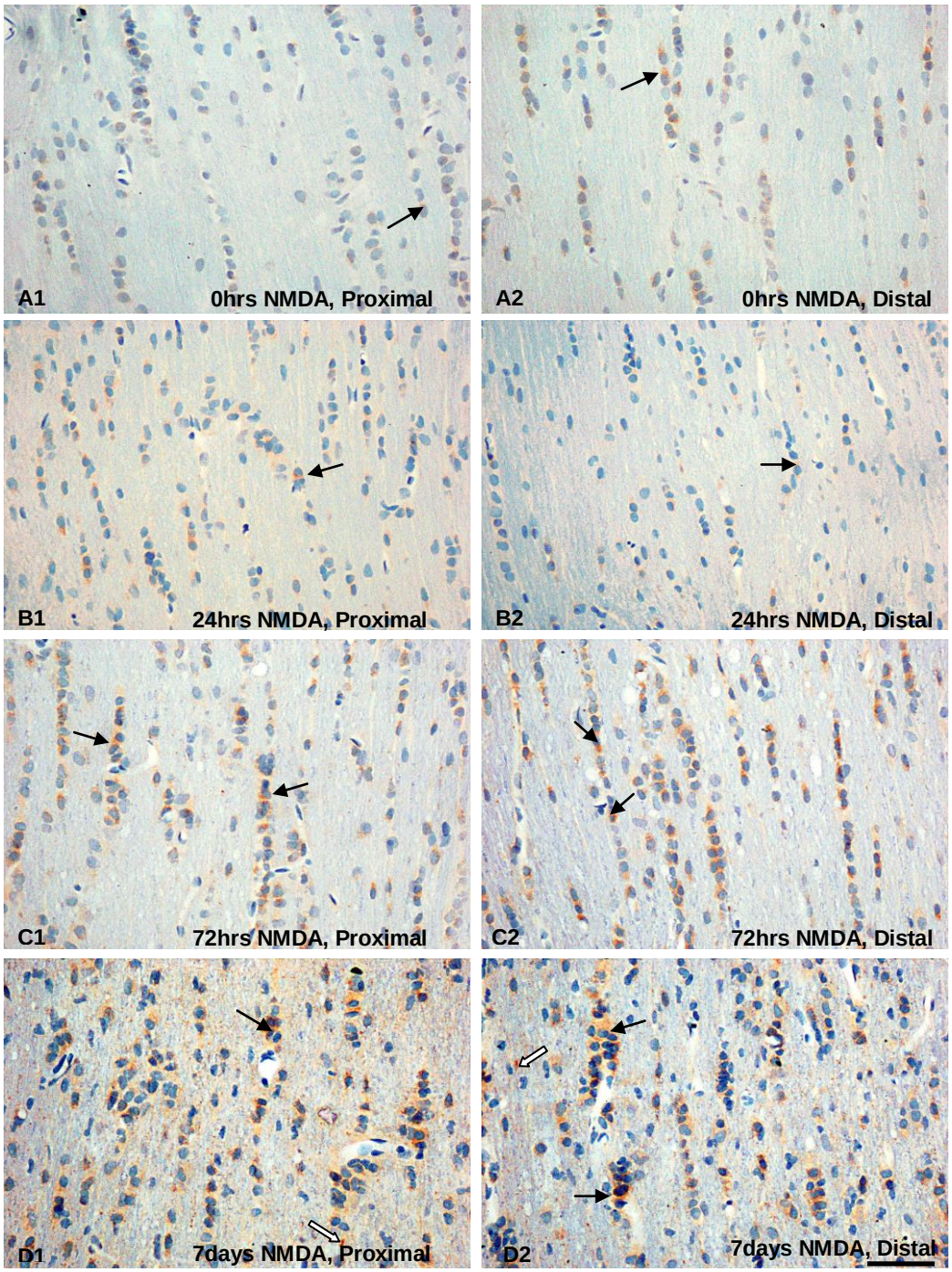

Figure 50. β-APP immunoreactivity in the longitudinal sections of NMDA injected proximal (A1, B1, C1, D1) and distal optic nerves (A2, B2, C2, D2). Faint β-APP immunoreactivity is seen in glial cells of NMDA injected optic nerves at 0hrs (A1, A2, arrows) and 24hrs (B1, B2, arrow) after injection. Slight increase in glial cell immunostaining in seen at 72hrs of NMDA injection (C1, C2, black arrows). Punctate β-APP immunostaining appeared in the axons (white arrows) at day 7 (D1, D2) along with glial immunostaining (black arrows). No difference is seen in the immunostaining between the proximal and distal optic nerve segements at any time point. magnification, X200. Bar=50μm

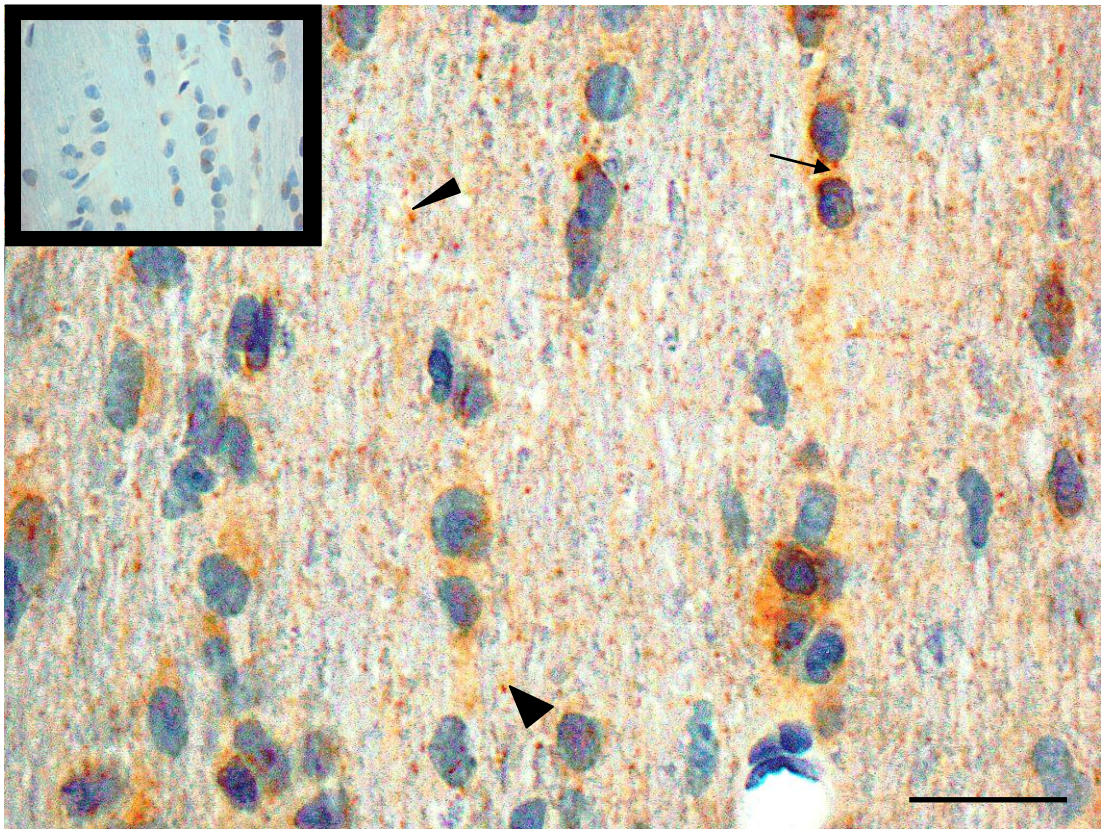

Figure 51. β-APP immunoreactivity in the longitudinal sections of NMDA injected distal optic nerves at day 7. Punctate β-APP immunostaining is seen in the axons (arrowheads) at day 7 along with glial immunostaining (arrows) in comparison to the axons of the control optic nerve (insert box, X400), where the axons in the background show no staining. Bar=25μm

9.3 Discussion

Neurodegenerative disorders are characterized by neuronal death and glial cell activation. Intra-axonal changes, such as axonal swellings and cytoskeletal disarrangement, seen with traumatic axonal degeneration are believed to be due to the impairment of axonal transport.[602, 638, 639] Decline in the fast anterograde transport hinders the rate and quantity of protein delivery required for the maintenance of the axon terminal [609] and the defective fast retrograde transport system hampers the translocation of the used up material from the axon terminal to cell body.[640-642][666-668] This part of the research was aimed to

study changes in the axon transport in optic nerve degeneration following excitotoxic RGC injury.

The major finding of this section is enhanced NF-L expression in the proximal neurons seen in the form of spheroids from day 3 with diminished NF-L staining in the retro-orbital optic nerve at day 7. Such spheroids in INFL have been shown to be due to abnormal accumulations of neurofilaments as well as other cytoskeletal proteins such as perpherin.[643] Altered NF-L immunoreactivity seen in the retina and optic nerve indicates altered anterograde slow axon transport after somagenic excitotoxic injury caused by NMDA. Punctate β-APP immunoreactivity in the optic nerve axons at day 7 implies interruption in the fast axonal transport. Also, glial cells in the optic nerve demonstrate moderate increase in β-APP immunostaining after NMDA indeced retinal injury.

With SOD1G93A transgenic mice, Sasaki et al demonstrated abnormal cord-like accumulation of neurofilaments in proximal axonal swellings in the early stages of dying back degeneration in motor neuron disease.[644] NF-L rich axonal spheroids in proximal axons are also demonstrated in ALS and MND.[643, 645-647] Studies with IDPN (beta,beta'-Iminodipropionitrile) toxin induced neuropathy model also showed similar swellings developing in proximal motor axons along with decrease in the distal axon calibre producing electrophysiological disturbances such as abnormal motor neuron discharge and disturbed neuromuscular response.[648, 649] In the present study, similar spheroidal structures with intense NF-L immunostaining are seen in the proximal intraretinal optic neurons in INFL from day 3 post excitotoxic insult without causing any alteration in the NF-L uptake in the other layers of retina. These retinal changes are associated with reduced NF-L immunostaining of retro-orbital optic nerve at day 7 suggestive of neurofilament cytoskeletal loss, seen as

significant decrease in axon counts as demonstrated with histomorphometric analysis described in the previous chapter [Chapter 6]. These results indicate impairment of slow axonal transport in excitotoxic somagenic insult. This is in contrast to a carbon disulphide induced neuropathy model, which showed reduced amount of NFs in the proximal regions decreasing the calibre of proximal axons by almost 50%, associated with characteristic NFs rich axonal swellings developing in the distal axon indicating a rapid increase in the slow transport of NFs to the distal axon.[491, 492]

Many factors can impair slow axonal transport. This may be the result of reduced synthesis of NFs, their abnormal phosphorylation, damage to the microtubules or molecular motors or damage to the ATP fuel supply. If the process of cell injury is slow, affected turnover of NFs in the stationary pool decreases the axon calibre.[649] However, rapid cell death provides little or no chance to the stationary NFs to get affected and thus, axon maintains calibre until the whole cytoskeleton disintegrates. [649] It can be hypothesized that on exposure to NMDA, accumulation of labile pool of NFs in the soma and proximal axons form axonal spheroids due to impaired slow axonal transport. Distal axonal changes seen in the form of reduced NF-L immunoreactivity in the retro-orbital optic nerve may be the result of reduced cell turnover of NFs in the stationary pool. Chidlow et al showed, a substantial fall in NF-L mRNA in RGCs within 8hrs of intravitreal injection of 20nM NMDA.[650] Also a study has demonstrated that glutamate impairs slow axonal transport by increased phosphorylation of NF-M and NF-H subunits through protein kinases.[651]

Various isoforms of β-APP protein containing different number of amino acids are distributed in neurons and glial cells. In-vitro studies using cell cultures have shown that the rat neurons predominantly contain APP695 isoform.[652] Astroglial cells mainly express two large Kunitz

family of serine protease inhibitors, APP751 and APP770.[652-654] Microglial cells also contain β-APP molecule,[655] but to the best of the knowledge, its exact isoform remains unidentified. In response to different forms of neuronal injury, β-APP isoforms behave differently in neuronal and non-neuronal glial tissues. Using facial and hypoglossal nerve axotomy models, Sola C et al also observed an increased expression of β-APP molecules in neurons and reactive astroglial cells.[656] In contrast, kainite-induced neurotoxic injury produced an increase in the expression of β-APP proteins in reactive astrocytes and reduction in levels of β-APP in neurons.[657] In the present study, increased immunoexpression of β-APP in the interfascicular optic nerve glial cells from day 3 and delayed punctuate B-APP immunostaining in the optic nerve axons at day 7 was seen after NMDA-induced excitotoxic perikaryal damage.

Glycosylated β-APP protein molecules are transported to the nerve terminals by the microtubule-dependent fast anterograde axonal transport.[624, 625] While its active rapid transport across the axon, some β-APP molecules are rapidly processed in transport vesicles to produce amyloidogenic and non-amyloidogenic Aβ (Beta-amyloid) fragments.[658] Remaining molecules reaching the axon are incorporated into the axolemma and synaptic regions of neurons as integral membrane glycoprotein.[622, 623] Although, its precise function is unclear, it is thought to regulate axonal growth. Studies have shown that disintegration of cytoskeletal material result in impairment of axoplasmic flow leading to accumulation of β-APP in the axons within minutes.[633-637] Stokin et. al. showed that disrupted microtubule dependent fast axonal transport due to mutation of kinesin light chain gene also causes increased accumulation of Aβ in axons and increased formation of amyloid deposits, the hallmark of Alzheimer's disease pathology.[458] With NMDA model of retinal damage, β-APP expression observed in the optic nerve axons at day 7 indicates cessation of microtubule-

based fast transport. Because increased β-APP accumulation results in formation of amyloid deposits,[458] it is not unreasonable to speculate that focal accumulation of β-APP molecules observed in optic nerve axons after intravitreal NMDA injection could transform later into amyloid deposits.

Rapid accumulation of β-APP in direct axonal damage denotes the early axonal cytoskeletal injury in the presence of the functionally intact neuronal cell body capable of swiftly translocating this protein to the site of accumulation. Delayed and sparse build up of axonal β-APP in the NMDA model could be due to rapid neuronal death or damaged axonal cytoskeleton. If reduced ATP generation in the cell body had been exclusively responsible for adversely affecting this energy-dependent transport, β-APP would have accumulated in the axons early at day 3, when cell death was obvious. On the other hand, slight accumulation of β-APP at day 7 did not point to the cytoskeletal damage as the sole underlying cause. Based on this pathological finding, it can be assumed that both early neuronal cell death and delayed cytoskeletal damage are responsible for the impairment of fast axonal transport.

Increased expression of β-APP in glial cells along with axons in the optic nerve suggests strong mechanistic ties between these events. Abnormally accumulated β-APP molecules in the neurons activate microglial cells without the addition of pro-inflammatory cytokines.[659] Activation of microglial cells, causes upregulation of all β-APP mRNA and protein.[655] TNF-α released from the activated microglia causes further axonal damage and β-APP accumulation.[660] Neurotoxicity is further enhanced by the release of glutamate and activation of NMDA receptor subtype by activated microglial cells.[661, 662] Inflammatory cytokine, IL-1α, released from the activated microglial cells [663] trigger the astrocytes also to overexpress β-APP.[664] Aβ released by proteolytic processing of β-APP from activated

astrocytes adds to the amyloid generated from neurons.[665] Although no co-immunolabelling was done with GFAP or ED-1 to identify changes in β-APP expression in astrocytes or microglial cells, a generalised increase in glial cell and neuronal β-APP immunolabelling after NMDA injection verifies the existence of a complex interaction between damaged axons and activated glial cells, which is seen as enhanced β-APP expression in these two types of cells. This suggests a probable similarity between the NMDA model of optic neuropathy and Alzheimer's disease.

Several different pathways are proposed for disruption of the axonal transport system in various conditions. Mutant SOD1 induces disruption of the slow and fast axonal transport with mitochondrial dysfunction, oxidative stress, protein misfolding, excitotoxicity, insufficient growth factor signaling, and inflammation, to cause MND and ALS.[666-669] Genetic mutations in kinesin 1, spastin (protein that sever microtubules) and mitochondrial ATPase cause defect in axonal transport resulting in HSP.[670-673] Expression of these mutant genes is a primary determinant of disease onset; however, the primary site of insult in these conditions is not limited to neurons. They do not elucidate the role played by the neurons or glia in the axon transport damage. Use of current NMDA model establishes the primary site of insult and limits it to the soma of optic neurons thereby, providing an opportunity to study the role played by the somal excitotoxic insult in the damage to axon transport system. It is hypothesised the initial insult to the axon transport in NMDA induced somagenic injury is the result of perikaryal excitotoxicity causing mitochondrial damage, oxidative stress and downregulation of microtubule, molecular motors and neurofilaments. Once established, the axon transport injury self-propagates due to axon- glia interplay to cause nerve degeneration.

In conclusion, early impairment of slow axonal transport results in formation of NF-L rich spheroids in proximal neurons with NF-L loss in axons within 72 hrs. However, fast axonal transport damage is evident as appearance of axonal β-APP at the 7th day. Although, the study shows that excitotoxic somal injury results in downstream changes in the axonal cytoskeleton, it still remains unclear whether damage to the axon transport system contributes to the sequence of nerve degeneration or whether the cytoskeletal damage during the axonal degeneration causes interruption of the transport.